Title
Protonic Devices From A Cephalopod Structural Protein

Permalink
https://escholarship.org/uc/item/9b28b7d5

Author
Ordinario, David Diaz

Publication Date
2016

Peer reviewed|Thesis/dissertation

UNIVERSITY OF CALIFORNIA,
IRVINE

Protonic Devices From A Cephalopod Structural Protein

DISSERTATION

submitted in partial satisfaction of the requirements
for the full degree of

DOCTOR OF PHILOSOPHY

in Materials Science and Engineering

by

David Diaz Ordinario

Dissertation Committee:
Professor Alon A. Gorodetsky, Chair
Professor Nancy Da Silva
Professor Vasan Venugopalan

2016

TABLE OF CONTENTS

(where $n_{H+} = n_{H+}^o$ is the proton concentration at an arbitrary gate bias and n_{H+}^o is the experimentally observed proton concentration at $V_{GS} = 0$ V). There is agreement between the observed and expected modulations of the charge-carrier density.

LIST OF TABLES

ACKNOWLEDGEMENTS

I would first like to thank my advisor, Professor Alon A. Gorodetsky, for the continued guidance and support he has provided over the past seven years. He has provided me a thorough education in the skills necessary for a research career, and I will forever be indebted to him for the time and effort he has spent on me. I would also like to thank Professor Nancy Da Silva and Professor Vasan Venugopalan for giving their time to be members of both my qualification exam committee and my doctoral dissertation committee.

I would next like to thank my family for supporting me throughout school and helping me pursue my goals. The work contained in this dissertation would not have been possible without them.

I especially wish to thank Long Phan and Amir Mazaheripour for their continued professional and personal assistance, as well as their continued unconditional friendship, over the past nine years.

I would additionally like to thank the many people that I have had the pleasure of working with during my time in the Gorodetsky Group. In particular, I would first like to thank Jonah Jocson for all of the time and effort he devoted to the work contained in this dissertation. I would also like to thank Tam N. Nguyen for her efforts in improving many of the experimental procedures described in Chapters 3, 4, 5, and 6. I would next like to thank Emil Karshalev and Nina Hüsken for their help and collaboration during the early stages of the reflectin characterization work described in Chapter 2. I would like to thank Dr. Anthony Burke and Dr. D. Joshua Dibble for their general guidance during the early stages of establishing the laboratory. I would like to thank Mehran J. Umerani for this work on acquiring mass spectrometry data of the reflectin. I would also like to thank Rylan Kautz and Priyam Patel for their plans to continue the protonic device work after my departure from the laboratory. I would like to thank the undergraduate students that have contributed to supporting the protonic device project, including Amanda G. Smith, Michael Nguyen, MyAnh Kaylee Dao, Justin P. Kerr, Mahan Naeim, Nikka Mofid, and Mercedeez Aquino. I would like to acknowledge Erica M. Leung for her assistance with reflectin production and data simulation, as well as her efforts at moral support. I would finally like to express many thanks to the many collaborators that have played a role in advancing our work at the Gorodetsky Group.

I would like to acknowledge and thank the Sheehan Group at the Naval Research Laboratory (NRL) for hosting me as a visiting researcher for over a year to complete the artificial iridophore work described in Chapter 6. I wish to thank Dr. Paul E. Sheehan for the guidance he graciously provided during my time at the NRL, Dr. Woo Kyung Lee, Dr. Stanislav Tsoi, Dr. Rory Stine, and Dr. Cy Tamanaha for the technical assistance they provided, Dr. Keith Whitener, Dr. David Kidwell, and Dr. Shawn P. Mulvaney for their general assistance and feedback.

I would like to thank Professor Albert Yee's Laboratory for the use of their optical microscope, Professor Matthew Law's Laboratory for the use of their atomic force microscope, Professor Allon Hochbaum's Laboratory for the use of their fluorescence microscope, and Professor Ioannis Kymissis' Laboratory for the use of their impedance analyzer.

I would like to thank Dr. Jesse P. Angle for his insight and help with electrochemical impedance spectroscopy.

CURRICULUM VITAE

David D. Ordinario
67411 Verano Place **·** Irvine, CA 92617
(845) 598-6914 **·** dordinar@uci.edu

Education

University of California, Irvine, Henry Samueli School of Engineering	**Irvine, CA**
PhD in Materials Science and Engineering	June 2013 – Oct. 2016
M.S. in Materials Science and Engineering	Sept. 2011 – June 2013
Columbia University, Fu Foundation School of Engineering and Applied Science	**New York, NY**
B.S. in Materials Science and Engineering	Aug. 2007 – May 2011
Princeton University, Department of East Asian Studies	**Kanazawa, Japan**
Princeton in Ishikawa Study Abroad Program	May 2009 – Aug. 2009

Research Experience

Gorodetsky Research Group, Department of Chemical Engineering and Materials Science, University of California, Irvine   **Irvine, CA**

Ph.D. Candidate   Sept. 2011 – Sept. 2016

- Advisor: Dr. Alon A. Gorodetsky
- Research protonic conduction in biomaterials for the purpose of expanding current understanding of their properties and developing new technologies.

Nuckolls Research Group, Department of Chemistry, Columbia University   **New York, NY**

Research Assistant   Jan. 2010 – Aug. 2011

- Advisor: Dr. Colin Nuckolls
- Researched fabrication of carbon nanotube/DNA biosensors for the purpose of developing early stage disease detection systems.

Professional Experience

Surface Nanoscience and Sensor Technology Section, Surface Chemistry Branch, United States Naval Research Laboratory   **Washington, D.C.**

Visiting Research Scientist   April 2015 – Nov. 2015
  July 2013 – Oct. 2013

- Supervisor: Dr. Paul E. Sheehan
- Investigated new kinds of biomaterials in close Collaboration with Navy scientists in order to both determine their optical and electronic properties, and

to examine any potential for real-world applications.

Awards and Honors

- Postdoctoral Fellow, Japan Society for the Promotion of Science — Nov. 2016
- ISACS15 Poster Presentation Competition, First Place, Royal Society of Chemistry — Aug. 2014
- Honorable Mention, NSF Graduate Research Fellows Program — April 2013
- Henry Samueli School of Engineering Graduate Fellowship — Sept. 2011 – May 2013
- Dean's List, Columbia University School of Engineering and Applied Science — May 2010, Dec. 2008
- New York State Scholarship for Academic Excellence — Aug. 2007 – May 2011

Publications

10. D. D. Ordinario, L. Phan, A. A. Gorodetsky. "The Cephalopod Electric: Unusual Inspiration for Conducting Materials." *J. Polym. Sci. Part B Polym. Phys.* Invited Review, *In Preparation*

9. D. D. Ordinario, E. M. Leung, L. Phan, P. E. Sheehan, A. A. Gorodetsky. "Protochromic Devices from a Cephalopod Structural Protein". *Submitted.*

8. D. D. Ordinario, L. Phan, Y. Van Dyke, E. M. Leung, M. Nguyen, A. G. Smith, J. Kerr, M. Naeim, W. G. Walkup IV, I. Kymissis, A. A. Gorodetsky. "Production and Electrical Characterization of the Reflectin A2 Isoform from *Doryteuthis* (*Loligo*) *pealeii*". *RSC Adv.* **2016**, *6*, 57103.

7. D. D. Ordinario, L. Phan, Y. Van Dyke, T. Nguyen, A. G. Smith, M. Nguyen, N. M. Mofid, M. K. Dao, A. A. Gorodetsky. "Photochemical Doping of Protonic Transistors from a Cephalopod Protein". *Chem. Mater.* **2016**, *28*, 3703–3710.

6. L. Phan, D. D. Ordinario, E. Karshalev, M. Shenk, A. A. Gorodetsky. "Infrared Invisibility Stickers Inspired by Cephalopods". J. Mater. Chem. C. **2015,** *3,* 6493–6498. *Cover Feature.*

5. D. D. Ordinario, L. Phan, J-M. Jocson, T. Nguyen, A. A. Gorodetsky. "Protonic Transistors from Thin Reflectin Films". *APL. Mat.* **2015,** *3,* 014907/1–014907/5.

4. D. D. Ordinario, A. M. Burke, L. Phan, J-M. Jocson, H. Wang, M. N. Dickson, A. A. Gorodetsky. "Sequence Specific Detection of Restriction Enzymes at DNA-Modified Carbon Nanotube Field Effect Transistors". *Anal. Chem.* **2014,** *86,* 8628–8633.

3. D. D. Ordinario, L. Phan, W. G. Walkup IV, J-M. Jocson, E. Karshalev, N. Hüsken, A. A. Gorodetsky. "Bulk Protonic Conductivity in a Cephalopod Structural Protein". *Nat. Chem.* **2014,** *6,* 596–602.

2. L. Phan, W. G. Walkup IV, D. D. Ordinario, E. Karshalev, J-M. Jocson, A. M. Burke, A. A. Gorodetsky. "Reconfigurable Infrared Camouflage Coatings from a Cephalopod Protein". *Adv. Mater.* **2013,** *25,* 5621–5625. *Cover Feature*.

1. H. Wang, N. B. Muren, D. Ordinario, A. A. Gorodetsky, J. K. Barton, and C. Nuckolls. "Transducing Methyltransferase Activity into Electrical Signals in a Carbon Nanotube-DNA Device". *Chem. Sci.* **2012,** *3,* 62–65.

Patent Applications

6. L. Phan, D. D. Ordinario, W. G. Walkup IV, E. Karshalev, M. Shenk, A. A. Gorodetsky. "Dynamic Infrared-Reflective Materials Based on Reflectin Films." U. S. Patent Application, Number 14723772, May 28, 2015.

5. L. Phan, D. D. Ordinario, M. A. Shenk, W. G. Walkup IV, A. A. Gorodetsky. "Infrared Invisibility Stickers Inspired by Cephalopods." Patent Application, United States U.C. Case No. 2015-217-1, September 3, 2014.

4. L. Phan, D. D. Ordinario, W. G. Walkup IV, A. A. Gorodetsky. "Building Materials Having Dynamically Controlled IR Reflectance." Patent Application, Number 62024771, July 15, 2014.

3. L. Phan, D. D. Ordinario, W. G. Walkup IV, A. A. Gorodetsky. "Textiles Having Dynamically Controlled IR Reflectance." Patent Application, Number 62007713, June 4, 2014.

2. L. Phan, D. D. Ordinario, W. G. Walkup IV, A. A. Gorodetsky. "Reflectin Thin Film Compositions and Methods." Patent Application, Number 62003915, May 28, 2014.

1. D. D. Ordinario, L. Phan, W. G. Walkup IV, A. A. Gorodetsky. "Reflectin-Based Transistors and Related Applications." Patent Application, Number 61911314, December 3, 2013.

Peer-Reviewed Conference Proceedings
- D. D. Ordinario, L. Phan, W. G. Walkup IV, J.-M. Jocson, E. Karshalev, N. Hüsken, A. A. Gorodetsky. "Proton Conduction in a Cephalopod Structural Protein." 2016 MRS Spring Meeting and Exhibit, Materials Research Society, Phoenix, AZ, March 2016.
- D. D. Ordinario, L. Phan, J.-M. Jocson, T. Nguyen, A. A. Gorodetsky. "Protein-Based Protonic Transistors." 2016 MRS Spring Meeting and Exhibit, Materials Research Society, Phoenix, AZ, March 2016.
- L. Phan, D. D. Ordinario, E. Karshalev, W. G. Walkup IV, M. Shenk, A. A. Gorodetsky. "Infrared Invisibility Stickers Inspired by Cephalopods." 2016 MRS Spring Meeting and Exhibit, Materials Research Society, Phoenix, AZ, March 2016.
- D. D. Ordinario, L. Phan, T. Nguyen, J.-M. Jocson, A. A. Gorodetsky. "Protein-Based Protonic Transistors." 251st ACS National Meeting and Exposition, American Chemical Society, San Diego, CA, March 2016.
- D. D. Ordinario, L. Phan, W. G. Walkup IV, J.-M. Jocson, N. Hüsken, A. A. Gorodetsky. "Proton Conduction in a Cephalopod Structural Protein." 251st ACS National Meeting and Exposition, American Chemical Society, San Diego, CA, March 2016.
- L. Phan, D. D. Ordinario, E. Leung, W. G. Walkup IV, A. A. Gorodetsky. "Biophysical and Electrical Characterization of Reflectin Isoforms from Squid and Cuttlefish." 251st ACS National Meeting and Exposition, American Chemical Society, San Diego, CA, March 2016.
- L. Phan, D. D. Ordinario, E. Karshalev, W. G. Walkup IV, M. Shenk, A. A. Gorodetsky. "Infrared Invisibility Stickers Inspired by Cephalopods." 251st ACS National Meeting and Exposition, American Chemical Society, San Diego, CA, March 2016.
- L. Phan, D. D. Ordinario, E. Karshalev, W. G. Walkup IV, A. A. Gorodetsky. "Infrared Invisibility Stickers Inspired by Cephalopods." Pacifichem 2015, International Chemical Congress of Pacific Basin Societies, Honolulu, HI, December 2015.
- L. Phan, W. G. Walkup IV, D. D. Ordinario, A. A. Gorodetsky. "Biophysical and Electrical Characterization of Reflectin Isoforms from Squid and Cuttlefish." Pacifichem 2015,

International Chemical Congress of Pacific Basin Societies, Honolulu, HI, December 2015.

- D. D. Ordinario, L. Phan, W. G. Walkup IV, J.-M. Jocson, E. Karshalev, N. Hüsken, A. A. Gorodetsky. "Proton Conduction in a Cephalopod Structural Protein." Pacifichem 2015, International Chemical Congress of Pacific Basin Societies, Honolulu, HI, December 2015.
- L. Phan, D. D. Ordinario, E. Karshalev, W. G. Walkup IV, M. Shenk, A. A. Gorodetsky. "Infrared Invisibility Stickers Inspired by Cephalopods." 2015 MRS Fall Meeting and Exhibit, Materials Research Society, Boston, MA, December 2015.
- L. Phan, W. G. Walkup IV, D. D. Ordinario, A. A. Gorodetsky. "Biophysical and Electrical Characterization of Reflectin Isoforms from Squid and Cuttlefish." 2015 MRS Fall Meeting and Exhibit, Materials Research Society, Boston, MA, December 2015.
- D. D. Ordinario, L. Phan, W. G. Walkup IV, J.-M. Jocson, E. Karshalev, N. Hüsken, A. A. Gorodetsky. "Proton Conduction in a Cephalopod Structural Protein." 2015 MRS Fall Meeting and Exhibit, Materials Research Society, Boston, MA, December 2015.
- D. D. Ordinario, L. Phan, J.-M. Jocson, T. Nguyen, Y. Van Dyke, E. Karshalev, A. A. Gorodetsky. "Protein-Based Protonic Transistors." 2015 MRS Spring Meeting and Exhibit, Materials Research Society, San Francisco, CA, April 2015.
- D. D. Ordinario, L. Phan, W. G. Walkup IV, J.-M. Jocson, E. Karshalev, N. Hüsken, A. A. Gorodetsky. "Proton Conduction in a Cephalopod Structural Protein." 249th ACS National Meeting and Exposition, American Chemical Society, Denver, CO, March 2015.
- L. Phan, D. D. Ordinario, E. Karshalev, M. Shenk, A. A. Gorodetsky. "Infrared Invisibility Stickers Inspired by Cephalopods." 249th ACS National Meeting and Exposition, American Chemical Society, Denver, CO, March 2015.
- D. D. Ordinario, L. Phan, J.-M. Jocson, T. Nguyen, A. A. Gorodetsky. "Protein-Based Protonic Transistors." 249th ACS National Meeting and Exposition, American Chemical Society, Denver, CO, March 2015.
- L. Phan, W. G. Walkup IV, D. D. Ordinario, A. A. Gorodetsky. "Biophysical Characterization of Reflectin Isoforms From Squid and Cuttlefish." 249th ACS National Meeting and Exposition, American Chemical Society, Denver, CO, March 2015.
- D. D. Ordinario, A. M. Burke, L. Phan, J.-M. Jocson, H. Wang, M. N. Dickson, A. A. Gorodetsky. "Sequence Specific Detection of Restriction Enzymes at DNA-Modified Carbon Nanotube Field Effect Transistors." 249th ACS National Meeting and Exposition, American Chemical Society, Denver, CO, March 2015.
- D. D. Ordinario, L. Phan, W. G. Walkup IV, A. A. Gorodetsky. "Proton Conduction in a Cephalopod Structural Protein." BioEL 2015 International Winterschool on Bioelectronics, Johannes Kepler University Linz, Kirchberg in Tirol, Austria, February 2015.
- W. G. Walkup IV, L. Phan, D. D. Ordinario, A. A. Gorodetsky. "Biophysical Characterization of Reflectin Isoforms from *L. Pealei* and *E. Scolopes*." 248th ACS National Meeting and Exposition, American Chemical Society, San Francisco, CA, August 2014.
- L. Phan, W. G. Walkup, D. D. Ordinario, E. Karshalev, J.-M. Jocson, A. M. Burke, A. A. Gorodetsky. "Cephalopod-Inspired Tunable Infrared Camouflage." 2014 MRS Spring Meeting and Exhibit, Materials Research Society, San Francisco, CA, April 2014.
- D. D. Ordinario, L. Phan, W. G. Walkup, J.-M. Jocson, E. Karshalev, N. Hüsken, A. A. Gorodetsky. "Bulk Proton Conduction in a Structural Protein." 2014 MRS Spring Meeting and Exhibit, Materials Research Society, San Francisco, CA, April 2014.
- L. Phan, W. G. Walkup, D. Ordinario, E. Karshalev, J.-M. Jocson, A. M. Burke, A. A.

Gorodetsky. "Cephalopod-Inspired Tunable Infrared Camouflage." 247th ACS National Meeting and Exposition, American Chemical Society, Dallas, TX, March 2014.

- D. D. Ordinario, L. Phan, W. G. Walkup, J.-M. Jocson, E. Karshalev, N. Hüsken, A. A. Gorodetsky. "Bulk Protonic Conduction in a Cephalopod Structural Protein." 247th ACS National Meeting and Exposition, American Chemical Society, Dallas, TX, March 2014.
- D. D. Ordinario, L. Phan, W. G. Walkup, A. A. Gorodetsky. "Structural Proteins as Proton Conductive Materials." 2013 MRS Fall Meeting and Exhibit, Materials Research Society, Boston, MA, December 2013.
- L. Phan, W. G. Walkup, D. D. Ordinario, E. Karshalev, J. Jocson, A. A. Gorodetsky. "Reconfigurable Infrared Camouflage Coatings from Cephalopod Protein." 2013 MRS Fall Meeting and Exhibit, Materials Research Society, Boston, MA, December 2013.
- D. D. Ordinario, M. N. Dickson, A. M. Burke, J. Jocson, A. A. Gorodetsky. "Microfluidic-Encapsulated Carbon Nanotube Field Effect Transistors for the Detection and Monitoring of Protein/DNA Interactions." 245th ACS National Meeting and Exposition, American Chemical Society, New Orleans, LA, April 2013.
- D. D. Ordinario, M. N. Dickson, A. M. Burke, J. Jocson, A. A. Gorodetsky. "Microfluidic-Encapsulated Carbon Nanotube Field Effect Transistors for the Detection and Monitoring of Protein/DNA Interactions." 2013 MRS Spring Meeting and Exhibit, Materials Research Society, San Francisco, CA, April 2013.
- L. Phan, W. G. Walkup, D. D. Ordinario, E. Karshalev, A. A. Gorodetsky. "Biomimetic Camouflage Inspired by Cephalopods." 2013 MRS Spring Meeting and Exhibit, Materials Research Society, San Francisco, CA, April 2013.
- A. A. Gorodetsky, L. Phan, D. Ordinario, A. Burke. "Integrating Biological and Organic Nanowires into Devices." Department of Chemistry Seminar, Stonehill College, North Easton, MA, November 2012.
- A. A. Gorodetsky, L. Phan, D. Ordinario, A. Burke. "Biologically-Inspired Materials for Renewable Energy." SPIE Optics + Photonics, San Diego, CA, August 2012.
- A. A. Gorodetsky, D. Ordinario, H. Wang, N. Muren, J. K. Barton, C. Nuckolls. "Electrical Detection of DNA-Binding Enzymes at DNA-Modified Carbon Nanotubes." Materials Research Society Spring Meeting, Materials Research Society, San Francisco, CA, April 2012.
- D. Ordinario, H. Wang, N. Muren, A. A. Gorodetsky, J. K. Barton, C. Nuckolls. "Electrical Detection of DNA Methyltransferases at Single DNA Molecules Bridging a Carbon Nanotube Gap." 243rd ACS National Meeting and Exposition, American Chemical Society, San Diego, CA, March 2012.
- A. A. Gorodetsky, H. Wang, D. Ordinario, N. Muren, J. K. Barton, C. Nuckolls. "Electrical Detection of DNA-Binding Enzymes at DNA Bridging a Single Walled Carbon Nanotube Gap." Materials Research Society Fall Meeting, Materials Research Society, Boston, MA, November 2011.

Certifications

- Japanese Language Proficiency Test (JLPT) – Level N2

Professional Memberships

- American Chemical Society (ACS)
- Materials Research Society (MRS)

- Royal Society of Chemistry (RSC)

<u>Other Activities</u>

Symphony Irvine	**Irvine, CA**
First Violinist	May 2013 – Sept. 2016
Columbia University Orchestra	**New York, NY**
Second Violinist	Sept. 2007 – May 2010
Rockland Symphony Orchestra	**Nyack, NY**
First Violinist	Oct. 2003 – June 2007
Freelance Photographer	July 2014 – Sept. 2016

ABSTRACT OF THE DISSERTATION

Protonic Devices From A Cephalopod Structural Protein

By

David Diaz Ordinario

Doctor of Philosophy in Materials Science and Engineering

University of California, Irvine, 2016

Professor Alon A. Gorodetsky, Chair

The field of bioelectronics has the potential to revolutionize both fundamental biology and personalized medicine. As such, much research effort has been devoted to the development of devices and materials that are intrinsically compatible with biological systems. Within this context, several recent studies have focused on protonic transistors from naturally occurring materials, such as squid-derived polysaccharides and proteins. Herein, we report the rational design, fabrication, and characterization of protonic devices, for which the active material consists of a cephalopod protein-based proton conducting material known as reflectin. We first characterize the proton-conducting capabilities of reflectin, demonstrate reflectin-based two- and three-terminal protonic devices, and then investigate strategies for optimizing their performance. Next, we investigate the conductive properties of a reflectin isoform and then proceed to fabricate and characterize protonic devices where it serves as the active layer. We then investigate the properties of protonic devices featuring reflectin films doped with a small molecular photoacid, and show the selective enhancement of their electrical properties through an exogenous photophysical stimulus. Finally, we demonstrate reflectin-based protonic devices that mimic the color-changing functionality of natural iridophores in cephalopod skin. Altogether, our findings underscore the potential of

reflectins as functional materials and hold significance for both developing novel color-changing

technologies and the understanding and control of proton transport in both biological systems and

bioelectronic platforms.

CHAPTER 1   Introduction

1.1: Overview of the Dissertation

This dissertation aims to outline the development of various protonic devices based on the cephalopod structural protein known as reflectin. Reflectin is a protein found in the skin cells (i.e. chromatophores, iridophores, and leucophores) of cephalopods, and has been shown to play important roles in cephalopod adaptive coloration by serving as components of optically-active structures in each of these cell types.[1-10] These cells are hierarchically controlled by a network of nerve fibers, which directly interfaces the cells with the central nervous system.[10,11] Inspired by the role that cephalopods have played in the facilitation of fundamental neurobiological research[12-19] as well as the fact that cephalopod coloration is activated by neuronal signaling,[5,6] we investigate the electrical properties of reflectins and sought to fabricate artificial devices which utilize it as the active material.

We begin our investigation of reflectin in Chapter 2 by first characterizing the electrical properties of reflectin A1 and proving that protonic conductivity as the conduction mechanism. This is followed by a demonstration of various two- and three-terminal devices where reflectin serves as the active layer, including the world's first protein-based protonic transistor. In Chapter 3, we discuss and validate a strategy for increasing the performance of the reflectin-based transistors fabricated in the previous chapter. This strategy is straightforward and should be applicable to all protonic transistor devices. In Chapter 4, we investigate methods for the production of reflectins in quantities significant for materials applications. We demonstrate and validate these methods on a "model" system based on the reflectin A2 isoform, and also demonstrate protonic devices based on the reflectin A2 isoform. In Chapter 5, we report the design, fabrication, and characterization of two- and three-terminal reflectin A1-based protonic devices

where the reflectin layer is doped with a small molecular photoacid. We show the selective enhancement of these devices' electrical properties using a non-destructive, illumination-based stimulus. In Chapter 6, we design color-changing devices that emulate aspects of optically-active structures found in squid skin cells. These devices, which consist of a proton-transporting reflectin A1 active layer contacted by a proton-conducting actuating electrode, show distinct and quantifiable shifts in reflectance and coloration. Finally, in Chapter 7 a brief summary of the dissertation is provided.

1.2: References

1. W. J. Crookes, L. L. Ding, Q. L. Huang, J. R. Kimbell, J. Horowitz, M. J. McFall-Ngai, *Science* **2004**, *303*, 235– 238.

2. R. M. Kramer, W. J. Crookes-Goodson, R. R. Naik, *Nat. Mater.* **2007**, *6*, 533– 538.

3. A. R. Tao, D. G. DeMartini, M. Izumi, A. M. Sweeney, A. L. Holt, D. E. Morse, *Biomaterials* **2010**, *31*, 793– 801.

4. D. G. DeMartini, M. Izumi, A. T. Weaver, E. Pandolfi, D. E. Morse, *J. Biol. Chem.* **2015**, *290*, 15238– 15249.

5. D. G. DeMartini, D. V. Krogstad, D. E. Morse, *Proc. Natl. Acad. Sci. U. S. A.* **2013**, *110*, 2552–2556.

6. D. G. DeMartini, M. Izumi, A. T. Weaver, E. Pandolfi, D. E. Morse, *J. Biol. Chem.* **2015**, *290*, 15238–15249.

7. D. G. DeMartini, A. Ghoshal, E. Pandolfi, A. T. Weaver, M. Baum, D. E. Morse, J. *Exp. Biol.* **2013**, *216*, 3733–3741.

8. L. Mäthger, S. L. Senft, M. Gao, S. Karaveli, G. R. R. Bell, R. Zia, A. M. Kuzirian, P. B. Dennis, W. J. Crookes-Goodson, R. R. Naik, G. W. Kattawar, R. T. Hanlon, *Adv. Funct. Mater.* **2013**, *23*, 3980–3989.

9. L. F. Deravi, A. P. Magyar, S. P. Sheehy, G. R. R. Bell, L. M. Mäthger, S. L. Senft, T. J. Wardill, W. S. Lane, A. M. Kuzirian, R. T. Hanlon, E. L. Hu, K. K. Parker, *J. R. Soc., Interface* **2014**, *11*, 20130942.

10. J. B. Messenger, *Biol. Rev. Cambridge Philos. Soc.* **2001**, *76*, 473–528.

11. T. J. Wardill, P. T. Gonzalez-Bellido, R. J. Crook, R. T. Hanlon, *Proc. R. Soc. B* **2012**, *279*, 4243.

12. L. W. Williams, in *The Anatomy of the Common Squid, Loligo pealii*, Lesueur; The Library and Printing Office of E. J. Brill, Leiden, **1910**.

13. J. Z. Young, *J. Physiol.* **1935**, *83*, 27.

14. T. H. Bullock, *J. Neurophysiol.* **1948**, *11*, 343.

15. E. Sereni, J. Z. Young, *Pubbl. Staz. Zool. Napoli* **1932**, *12*, 173.

16. A. L. Hodgkin, A. F. Huxley, A. F. *J. Physiol.* **1952**, *117*, 500.

17. J. Bloedel, P. W. Gage, R. Llinás, D. M. Quastel, *Nature* **1966**, *212*, 49.

18. B. Katz, R. Miledi, *Nature* **1966**, *212*, 1242.

19. E. Florey, F. Dubas, R. T. Hanlon, R. T. *Comp. Biochem. Physiol., C: Comp. Pharmacol.* **1985**, *82*, 259.

CHAPTER 2　　　Bulk Protonic Conductivity in Reflectin

2.1: Abstract

Proton-conducting materials play a central role in many renewable energy and bioelectronics technologies, including fuel cells, batteries and sensors. Thus, much research effort has been expended to develop improved proton-conducting materials, such as ceramic oxides, solid acids, polymers and metal–organic frameworks. Within this context, bulk proton conductors from naturally occurring proteins have received somewhat less attention than other materials, which is surprising given the potential modularity, tunability and processability of protein-based materials. Here, we report proton conductivity for thin films composed of reflectin, a cephalopod structural protein. Bulk reflectin has a proton conductivity of $\sim 2.6 \times 10^{-3}$ S cm^{-1} at 65 °C, a proton transport activation energy of ~ 0.2 eV and a proton mobility of $\sim 7 \times 10^{-3}$ cm^2 V^{-1} s^{-1}. These figures of merit are similar to those reported for state-of-the-art artificial proton conductors and make it possible to use reflectin in protein-based protonic transistors. Our findings may hold implications for the next generation of biocompatible proton-conducting materials and protonic devices.

2.2: Introduction

Proton conduction is a ubiquitous and extensively studied fundamental phenomenon.[1-20] For example, a variety of chemical processes, including redox reactions and acid/base catalysis, are coupled to proton transfer.[1-5] In addition, numerous biomolecules, such as electrochemically driven proton pumps in mitochondria and voltage-gated proton channels in phagocytes, have evolved specific structural motifs that facilitate proton translocation.[6-10] Moreover, the function of

an increasingly diverse array of technologically relevant devices, which include fuel cells, electrolyzers, batteries and sensors, crucially relies on proton transport.[11-17] The study of proton conduction has therefore captured the attention of chemists, biologists and materials scientists for over 200 years.[18-20]

Owing to the technological importance of proton conduction, solid-state proton-conducting materials, such as ceramic oxides, solid acids, polymers and metal–organic frameworks, remain the focus of much research effort.[11-17] Within this context, naturally occurring proteins have received less attention than other materials,[11-17, 21-26] which is surprising given the prevalence of proton translocation in biology.[6-10] Indeed, protein-based materials possess particular advantages as candidate proton conductors, including structural modularity, tunable physical properties, ease and specificity of functionalization, generalized expression/purification protocols and intrinsic biocompatibility.[27-31] Thus, naturally occurring proteins constitute a promising class of proton-conducting materials with a potential yet to be fully realized.

From an applications perspective, protein-based proton-conducting materials are uniquely positioned to contribute to the next generation of bioelectronics.[32-36] For example, given the importance of protons (and ions in general) for electrical signaling in biology,[32-36] protonic transistors represent a natural choice for interfacing rugged traditional electronics and biological systems that are decidedly more fragile. One can envision the direct and robust transduction of biochemical events into electrical signals with such devices.[32-36] However, in spite of this potential for biological applications, there are few examples in the literature of protonic transistors (which include recent reports by Rolandi and co-workers of devices based on maleic chitosan).[37-42] Protonic transistors from biological materials are therefore exciting targets for further research and development.[32-36, 40, 41]

6

Given the significance of biologically compatible proton conductors, we chose to develop a new class of these materials from reflectin, a cephalopod structural protein.[43-47] Reflectins contain a large number of charged amino acid residues, consist of one to six highly conserved repeating subdomains separated by variable linker regions and possess little-to-no organized secondary structure.[43-47] Reflectins are also remarkably robust, even when exposed to acidic conditions, heated up to 80 °C or processed into films with standard lithographic protocols.[47] Moreover, within cephalopod skin cells (iridocytes), reflectins aggregate to form platelets, which play a crucial role in cephalopod structural coloration as part of modular Bragg reflector-like structures.[48, 49] Our current studies were inspired not only by the favorable physical characteristics of reflectins, but also by the demonstration of electrical control over cephalopod skin iridescence, which hinted at the possibility of unique electrical behavior for iridocyte proteins.[50]

Herein, we describe the characterization of the conductive properties of platelet-like thin films from a *Doryteuthis* (formerly *Loligo*) *pealeii* reflectin A1 isoform.[45-47] Our studies show that bulk reflectin is an effective proton-conducting material. The protonic conductivities measured for reflectin's aggregated thin-film form (referred to hereafter as the solid state) are among the highest reported for naturally occurring proteins and are even comparable to those found for many state-of-the-art artificial proton conductors. Moreover, reflectin shows behavior consistent with the Grotthuss mechanism of proton conduction and effectively exhibits the same electrical characteristics as a dilute acidic solution. Such favorable properties enable the demonstration of protonic transistors in which a protein (reflectin) serves as the active material. Our measurements indicate that reflectins may represent a promising new class of modular proton-conducting materials for bioelectronics and other applications.

7

2.3: Experimental Section

2.3.1: Design and Cloning of Wild Type Reflectin A1 Genes

An *E. coli* codon optimized gene coding for 6x histidine tagged wild type reflectin A1 protein from *Doryteuthis* (formerly *Loligo*) *pealeii* (Genbank: ACZ57764.1) was synthesized and cloned into pJExpress414 vector (DNA2.0). The wild type sequence is shown in Figures 2.1 and 2.2.

2.3.2: Design and Cloning of Mutant Reflectin A1 Genes - DE->A Mutant

The DE->A mutant reflectin A1 protein was designed using Gene Designer 2.0 software (DNA2.0). To generate the DE->A mutant reflectin A1, all aspartic acid (GAT/GAC) and glutamic acid (GAA/GAG) codons in wild type reflectin A1 were replaced with alanine codons (GCA/GCC/GCG/GCT), resulting in a total of 34 DE->A mutations. The DE->A reflectin A1 mutant gene was then synthesized (GeneArt) and restriction cloned into a pJExpress414 plasmid in frame with an N-terminal 6x histidine tag. The DE->A sequence is shown in Figure 2.3.

2.3.3: Design and Cloning of Mutant Reflectin A1 Genes - Random Mutant

A scrambled mutant reflectin A1 protein was designed using the Emboss shuffleseq and Needle algorithms. The wild type reflectin A1 amino acid sequence was input into Emboss shuffleseq and run for 20 shufflings. The resulting sequences were then force aligned in pairwise alignments with wild type reflectin A1 using the Emboss Needle algorithm (BLOSUM62 matrix,
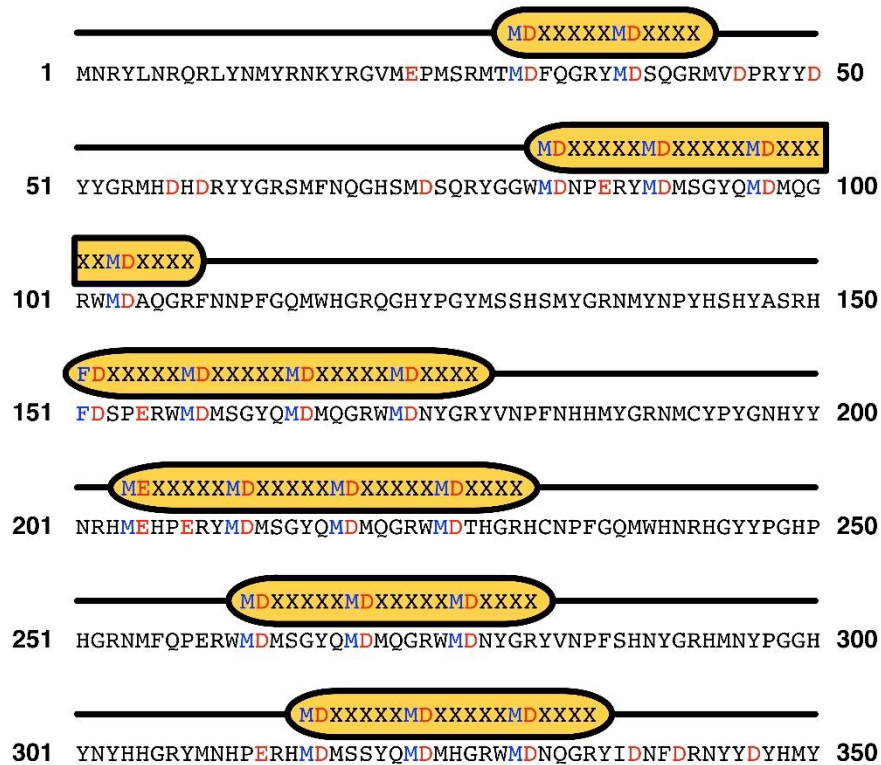
Figure 2.1: The primary sequence of reflectin A1 from *Doryteuthis* (formerly *Loligo*) *pealeii* contains six repeating subdomains with the (M/F-D-X$_5$)(M-D-X$_5$)$_n$(M-D-X$_{3-4}$) sequence motif.[43-46] The subdomains are outlined by orange ovals. Aspartic and glutamic amino acid residues present in both the subdomains and linker regions are highlighted in red. Methionine and phenylalanine residues confined only to subdomains are highlighted in blue. Reflectin is comprised of ~30% hydrophilic charged residues and ~20% hydrophobic aromatic residues.[43-46]

Figure 2.2: A tryptic peptide sequence coverage map of the wild type reflectin A1 protein obtained after mass spectrometry analysis of the porcine trypsin-digested protein. Bolded amino acids with a yellow background correspond to amino acids comprising tryptic peptides. Bolded amino acids with a green background correspond to oxidized amino acids comprising tryptic peptides. The total sequence coverage of 94% definitively confirmed the purified protein's identity as wild type reflectin A1 (the ExPASy Peptide Mass program predicted a theoretical coverage of 98.3%).

DE_to_A_reflectin (100%), 43,010.6 Da
Mutant reflectin-like protein A1 Doryteuthis pealeii
34 exclusive unique peptides, 65 exclusive unique spectra, 157 total spectra, 335/357 amino acids (94% coverage)

Figure 2.3: A tryptic peptide sequence coverage map of the DE->A mutant reflectin A1 protein obtained after mass spectrometry analysis of the porcine trypsin-digested protein. Bolded amino acids with a yellow background correspond to amino acids comprising tryptic peptides. Bolded amino acids with a green background correspond to oxidized amino acids comprising tryptic peptides. The total sequence coverage of 94% definitively confirmed the purified protein's identity as the DE->A mutant reflectin A1 (the ExPASy Peptide Mass program predicted a theoretical coverage of 98.3%).

100 Gap Open, 10 Gap Extend, End Gap Penalty True, 10 End Gap Open, 10 End Gap Extend).

The alignments were examined to select a Random reflectin A1 protein sequence that lacked any

$(M/F-D-X_5)(M-DX_5)_n(M-D-X_{3-4})$ repeats and exhibited minimal global pairwise sequence identity

(7.4%) to wild type reflectin A1. The scrambled sequence is shown in Figure 2.4.

2.3.4: Expression and Purification of Wild Type and Mutant Reflectin A1

A general protocol was used for the expression and purification of wild type and mutant reflectin A1.[47] In brief, the pJExpress414 expression vectors containing wild type or mutant reflectin were transformed into BL21(DE3) cells (Novagen). Reflectins were expressed at 37 °C

Randomized_reflectin (100%), 44,605.3 Da
reflectin-like protein A1 Doryteuthis pealeii
18 exclusive unique peptides, 28 exclusive unique spectra, 42 total spectra, 121/357 amino acids (34% coverage)

Figure 2.4: A tryptic peptide sequence coverage map of the Random mutant reflectin A1 protein obtained after mass spectrometry analysis of the porcine trypsin-digested protein. Bolded amino acids with a yellow background correspond to amino acids comprising tryptic peptides. Bolded amino acids with a green background correspond to oxidized amino acids comprising tryptic peptides. The total sequence coverage of 34% definitively confirmed the purified protein's identity as the Random mutant reflectin A1 (the ExPASy Peptide Mass program predicted a theoretical coverage of 50.7%).

using Overnight Express Instant Terrific Broth (TB) media (Novagen) supplemented with 100 μg mL^{-1} Carbenicillin. Reflectin was completely insoluble when expressed at 37 °C and was sequestered in inclusion bodies prepared using Novagen BugBuster® according to the manufacturer's suggested protocol. Reflectin inclusion bodies were then solubilized in denaturing buffer (pH 7.4, 50 mM Sodium Phosphate, 300 mM NaCl, 6M guanidine hydrochloride) and purified under denaturing conditions on HisPur Cobalt Resin (Thermo Scientific) immobilized metal affinity chromatography (IMAC) gravity columns according to the manufacturer's protocols. The protein was eluted by using denaturing buffer supplemented with 250 mM imidazole. The fractions containing reflectin were pooled and concentrated on Millipore Amicon Concentrators before further purification with high-performance liquid chromatography (HPLC) on an Agilent 1260 Infinity system using an Agilent reverse phase C18 column with a gradient evolved from 95% Buffer A:5% Buffer B to 5% Buffer A:95% Buffer B at a flow rate of 1 mL min^{-1} over 30 minutes (Buffer A: 99.9% H2O, 0.1% TFA; Buffer B: 95% acetonitrile, 4.9% H2O, 0.1% TFA). The pure reflectin fractions were pooled, flash frozen in liquid nitrogen, and lyophilized. Protein concentrations and yields were quantified *via* a Bradford protein assay with bovine serum albumin (BSA) as a standard (BioRad).

2.3.5: Characterization of Wild Type and Mutant Reflectin A1

A general protocol was used for assaying the purity and confirming the sequence of both wild type and mutant reflectin A1. In brief, purified and unpurified reflectin samples were analyzed by SDS-PAGE and GelCode Blue Staining (Thermo) using an Invitrogen XCell *SureLock* Mini using NuPAGE Novex 4-12% Bis-Tris gels, with NuPAGE MOPS as the running buffer under reducing conditions. Stained protein bands were subjected to in-gel tryptic digestion, performed according to literature procedures.[51] After digestion, the peptides were separated on a C18

chromatography column and analyzed by mass spectrometry on a Thermo Orbitrap instrument outfitted with an electrospray ionization source. The resulting sequence coverage was 94% for the wild type reflectin A1 (Figure 2.2), 94% for the DE->A mutant reflectin A1 (Figure 2.3), and 34% for the Random mutant reflectin A1 (Figure 2.4).

2.3.6: Fabrication of Reflectin Devices - Preparation of Substrates

For two- and three-terminal direct current measurements, the devices were fabricated on SiO_2/Si substrates. The substrates were cut from 4 inch, 405 to 455 μm thick, p-type Boron doped wafers, with a <100> crystallographic orientation and a 3000 Å oxide layer on both sides (International Wafer Service). The wafers were sectioned into individual 1.5 cm^2 chips using standard lithographic techniques. For three-terminal transistor measurements, the chips were etched to reduce the thickness of the oxide layer to ~900 Å, as confirmed by ellipsometry. Prior to deposition of the electrodes, the substrates were cleaned in Piranha solution (1:3 hydrogen peroxide to sulfuric acid). For electrochemical impedance spectroscopy measurements, the devices were fabricated on glass slides (Fisher Scientific). The glass substrates were cleaned by sequential sonication in acetone and isopropanol prior to deposition of the electrodes.

2.3.7: Fabrication of Reflectin Devices - Deposition of Electrical Contacts

The electrodes consisted of a 4 nm chromium layer overlaid with either a 40 nm gold layer or a 40 nm palladium layer. The metals were deposited onto the clean SiO_2/Si or glass substrates *via* shadow mask lithography with a CV-8 Electron Beam Deposition System (Temescal). To fabricate completed devices, reflectin solutions were drop cast onto the electrodes, with the solvent allowed to evaporate in ambient overnight. The resulting films were mechanically scribed with a probe station needle to leave a rectangular reflectin square spanning each electrode pair (Figures
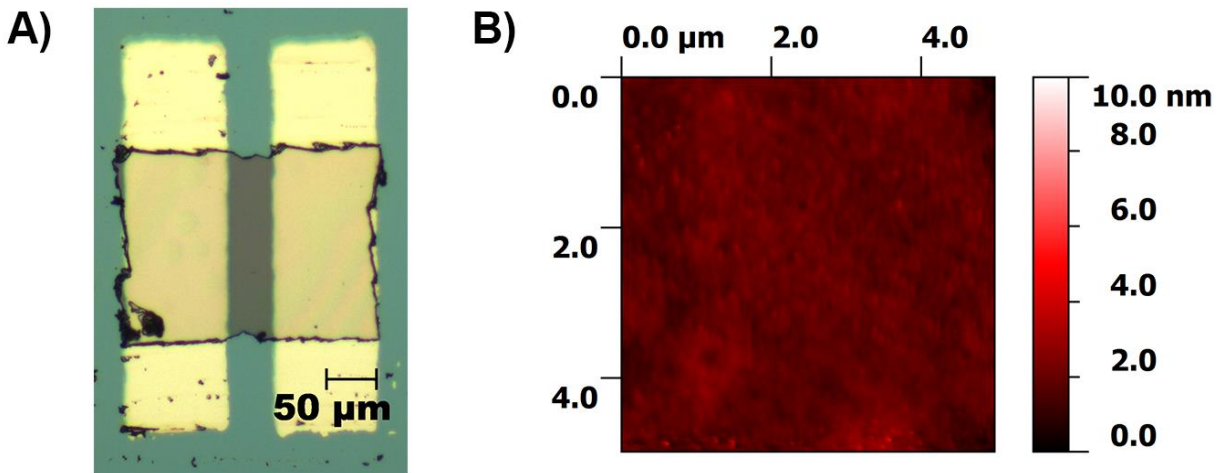
Figure 2.5: (A) A typical optical image of a reflectin device with a wild type reflectin film bridging two gold electrodes. The dimensions of the electrodes were 100 μm wide by 400 μm long, with a separation of 50 μm. **(B)** Representative atomic force microscopy (AFM) image of a wild type reflectin film. The films are smooth and featureless over large areas.

2.5 and 2.6). Reflectin films fabricated in this fashion were smooth and featureless, as determined by AFM (Figure 2.5).

2.3.8: Optical Microscopy of Reflectin Films

Each completed reflectin device was imaged with an Axio Imager A1 Microscope (Carl Zeiss) outfitted with an Epiplan 20X, NA = 0.4 lens (Carl Zeiss). The image data was processed with AxioVision AC Release 4.5 (Carl Zeiss), and the device dimensions (length and width) were extracted from analysis of these images. A typical optical image of a reflectin device is shown in Figure 2.5.

2.3.9: Atomic Force Microscopy of Reflectin Films

The thickness of all reflectin films was measured with atomic force microscopy (AFM) by examining trenches scribed directly into the films. Iridium coated silicon probes (Asylum Research
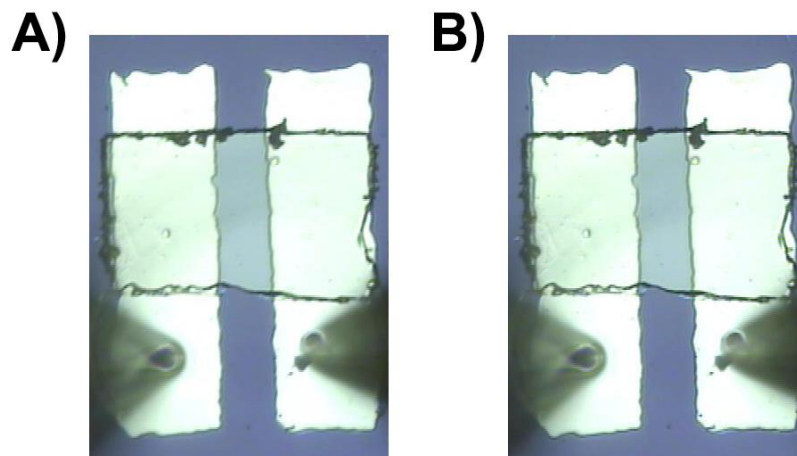
Figure 2.6: (A) Typical optical image of a reflectin device, where a wild type reflectin film bridges the two PdH$_x$ electrodes, prior to any electrical experiments. **(B)** Typical optical image of a reflectin device, where a wild type reflectin film bridges the two PdH$_x$ electrodes, after repeated electrical biasing (more than ten scans). Note that there is no change in the coloration of the film after electrical biasing. The reflectin film is continuing to perform its function (the reflection of light) and no obvious degradation has occurred due to the electrical measurements. The dark triangles at the bottom are the probe station needles used to electrically contact the electrodes.

ASYELEC-01) were used to record the images. The films were examined *in situ* at different relative humidities with a MFP-3D AFM (Asylum Research) outfitted with a Humidity Sensing Cell (Asylum Research). The images were collected by using iridium coated silicon probes (Asylum Research ASYELEC-01) with a spring constant of 2 N m^{-1}, resonance frequency of 70 kHz, and tip radius of 28 nm. The scans were rastered either at 0.17 Hz or at 1.0 Hz and normalized using polynomial subtraction for improved image quality; a typical AFM topography scan of a reflectin film is shown in Figure 2.5. The thickness of the films was found to increase by ~40% upon going from dry conditions (< 50% relative humidity) to 90% relative humidity. The swollen thicknesses of the reflectin films under appropriate humidified conditions were reported for the device dimensions in all instances and were used for the relevant calculations. All AFM data and parameters were processed/extracted with the Gwyddion software package.

2.3.10: Electrical Characterization of Reflectin Devices - Two-Terminal Measurements with Gold or Palladium Electrodes

Current as a function of voltage was recorded at various relative humidities on a PM-5 Probe Station (Cascade Microtech) outfitted with a 4156C Semiconductor Parameter Analyzer (Agilent). The electrical measurements were performed in ambient atmosphere under controlled-humidity conditions, with the humidity constantly monitored *via* a hygrometer (Fisher Scientific). The sweep rate was 0.2 V μs^{-1} and the hold time was 0.5 s. The dimensions of the paired electrodes were 100 μm wide by 400 μm long, with an inter-electrode separation of 50 μm.

2.3.11: Electrical Characterization of Reflectin Devices - Three-Terminal Measurements with Palladium Hydride Electrodes

Current was recorded as a function of source-drain voltage (at different gate voltages) in a humidified environment on a PM-5 Probe Station (Cascade Microtech) outfitted with a 4156C Semiconductor Parameter Analyzer (Agilent). The electrical measurements were performed under a 5% hydrogen/95% argon atmosphere, with the humidity carefully controlled and constantly monitored *via* a hygrometer (Fisher Scientific). The sweep rate was 0.2 V μs^{-1} and the hold time was 0.5 s. The dimensions of the paired electrodes were 100 μm wide by 400 μm long with a channel length of 50 μm.

2.3.12: Electrical Characterization of Reflectin Devices - Electrochemical Impedance Spectroscopy Measurements with Gold Electrodes

Impedance data was recorded with a 4192A LF Impedance Analyzer (Hewlett Packard) or a 4294A Impedance Analyzer (Agilent). The electrical measurements were performed in a humidified environment at various frequencies with a constant applied voltage of 500 mV. The

data was collected at temperatures between 25 °C to 65 °C, with the humidity constantly monitored *via* a hygrometer. Before each measurement, a 30-minute dwell at each temperature was used to ensure thermal stability. The dimensions of the paired electrodes were 2.5 cm wide by 3 cm long with an inter-electrode separation of 100 μm.

2.3.13: Electrochemistry of Reflectin Thin Films - Preparation of Reflectin-modified Electrodes

Electrochemical experiments were performed with gold working electrodes with a diameter of 2 mm (CH Instruments). The electrodes were sequentially polished with 0.3 μm and 0.05 μm wet alumina slurries on microcloth (Buehler) and then thoroughly rinsed and sonicated in Milli-Q water to remove remaining adsorbed alumina traces. The electrodes were subsequently electrochemically etched in 1 M H_2SO_4 to expose a clean gold surface and rinsed again with Milli-Q water. Reflectin films were formed by directly depositing reflectin solutions onto clean electrodes and allowing the solvent to evaporate overnight.

2.3.14: Electrochemistry of Reflectin Thin Films - Cyclic Voltammetry of Reflectin Thin Films

Cyclic voltammetry (CV) experiments were performed in a three-electrode electrochemical cell on a CHI832C Electrochemical Analyzer (CH Instruments). The reflectin-coated gold electrode served as the working electrode, a platinum wire served as the auxiliary electrode, and a silver/silver chloride electrode served as the reference electrode. The measurements were performed in 10X BupH Phosphate Buffered Saline (pH 7.2, 1 M phosphate, 1.5 M sodium chloride), which was purged with argon (Thermo Scientific). The high salt content

of this buffer ensured that the reflectin remained insoluble and bound to the electrode during the electrochemical measurements.

2.3.15: Water Uptake of Reflectin and Reflectin Mutants - Preparation of Reflectin Samples

A small amount (~1–5 mg) of either wild type or mutant reflectin was weighed out onto a clean platinum pan. The sample was then hydrated in either water or deuterium oxide vapor at a relative humidity of 90% immediately prior to analysis.

2.3.16: Water Uptake of Reflectin and Reflectin Mutants - Analysis of Reflectin Samples

Thermogravimetric analysis of solvent mass loss was performed on a TGA Q500 instrument (TA Instruments). Sample pans containing either wild type or mutant reflectin were loaded into the instrument and heated under a nitrogen atmosphere at a ramp rate of 20 °C per minute, from room temperature to 350 °C.

2.3.17: Calculation of Conductivity from Three-Terminal Measurements with Palladium Hydride Electrodes

The conductivity of reflectin films was obtained from the current versus voltage characteristics of the reflectin transistors. The slope of the source-drain current (I_{DS}) versus source-drain voltage (V_{DS}) curves at a gate voltage $V_{GS} = 0$ V yielded the device conductance, i.e. slope $= 1/R_o = G$.[40, 52, 53] The conductivity was calculated according to the equation:

$$\sigma = \frac{Gd}{A} \quad (1)$$

where σ is the conductivity, G is the conductance, d is the channel length, and A is the cross-sectional area of the film.[52, 53] As an example, for $1/R_o = G = 6.76 \times 10^{-8} \ \Omega^{-1}$, $d = 50$ μm, and $A = 315$ μm^2, the equation above yielded $\sigma = 1.07 \times 10^{-4}$ S cm^{-1}.

2.3.18: Calculation of Conductivity from Electrochemical Impedance Spectroscopy Measurements with Gold Electrodes

The impedance spectra were analyzed with ZView version 3.2c (Scribner Associates). The software was used to generate Nyquist plots and to fit the data to a simple equivalent circuit consisting of a capacitor (C_i) in series with a resistor (R_b) and a capacitor (Cb). In the equivalent circuit, C_i corresponds to the capacitance of the film/electrode interface, R_b corresponds to the bulk resistance of the film, and C_b corresponds to the bulk capacitance of the film.[54-58] The film resistance was extracted from this model and used in equation 1 to calculate the conductivity. The calculations were performed for measurements taken in 5 °C increments at temperatures between 30 °C and 65 °C. As an example, at a temperature of 30 °C, R = 6.54 x 10^4 Ω, G = 1.53 x 10^{-5} S, d = 100 μm, and A = 47,250 μm^2, the equation above yielded σ = 3.24 x 10^{-4} S cm^{-1}.

2.3.19: Calculation of the Activation Energy

The activation energy of proton hopping/transport was determined from impedance measurements obtained at different temperatures. For proton hopping, the conductivity follows a simplified temperature dependence of the form:[59]

$$\sigma = \sigma_o e^{\frac{-E_a}{RT}} \quad (2)$$

where σ is the conductivity, σ_o is a constant, E_a is the activation energy, R is the gas constant, and T is the temperature.[59] The resistance was extracted from the impedance measurements and converted to the conductivity at temperatures between 30 °C and 65 °C. The log of the conductivity was then plotted as a function of the temperature. The slope of a linear fit of this plot was equal to $-E_a/R$, enabling calculation of the activation energy.

2.3.20: Calculation of Gate Capacitance Per Unit Area

The gate capacitance per unit area was calculated according to the equation:

$$C_{GS} = \frac{3.9 \cdot \varepsilon_o}{t_o} \quad (3)$$

where ε_o is the permittivity of free space and t_o is the thickness of the gate oxide.[52, 53] As an example, for a gate oxide thickness of approximately $t_o = 9.1$ x 10^{-6} cm, the equation above yielded a gate capacitance per unit area of $C_{GS} = 3.79$ x 10^{-8} F cm^{-2}.

2.3.21: Calculation of the Proton Mobility

The proton mobility was extracted from the transistor transfer characteristics by using the gradual channel approximation.[41] The slope of the I_{DS} versus V_{DS} curves obtained at different V_{GS} yielded the conductivity of reflectin at different gate voltages. A plot of the conductivity as a function of the gate voltage was then fit with the following equation:

$$\mu_{H^+} = \pm \frac{\partial \sigma}{\partial V_{GS}} \cdot \frac{t}{C_{GS}} \quad (4)$$

where $\frac{\partial \sigma}{\partial V_{GS}}$ is the slope of the linear fit, t is the thickness of the reflectin film, and C_{GS} is the gate capacitance per unit area (*41*). As an example, for a slope with a value of -1.75 x 10^{-4} Ω^{-1}, a film thickness of $t = 1.26$ μm, and a gate capacitance per unit area of $C_{GS} = 3.79$ x 10^{-8} F cm^{-2}, the equation above yielded a mobility of $\mu_{H^+} = 5.82$ x 10^{-3} cm^2 V^{-1} s^{-1}.

2.3.22: Calculation of the Experimental Proton Concentration at Different Gate Voltages

The charge-carrier density (proton concentration) in reflectin-based devices was calculated by using the mobility derived from the device transfer characteristics. The charge-carrier density was calculated according to the following equation:

$$n_{H^+} = \frac{\sigma_{H^+}}{\mu_{H^+}e} \quad (5)$$

where σ_{H^+} is the conductivity evaluated at an arbitrary V_{GS}, e is the elementary charge, and μ_{H^+} is the mobility. As an example, for a conductivity of $\sigma = 7.52$ x 10^{-5} S cm^{-1} at $V_{GS} = 0$ V and a mobility of $\mu_{H^+} = 5.82$ x 10^{-3} cm^2 V^{-1}s^{-1}, the equation yielded a value of $n_{H^+} = 8.07$ x 10^{16} cm^{-3} for the charge-carrier density.

2.3.23: Calculation of the Theoretical Proton Concentration at Different Gate Voltages

The theoretically predicted charge-carrier density (proton concentration) under different applied gate voltages was calculated according to the following equation:[40, 41]

$$n_{H^+} = n_{H^+}^0 - \frac{C_{GS} \cdot V_{GS}}{e \cdot t} \quad (6)$$

where n_{H^+} is the theoretically predicted proton concentration at an arbitrary gate bias, $n_{H^+}^0$ is the experimentally observed proton concentration at $V_{GS} = 0$ V, C_{GS} is the gate capacitance per unit area, e is the elementary charge, and t is the film thickness. As an example, for an experimentally observed proton concentration of $n_{H^+}^0 = 8.07$ x 10^{16} cm^{-3}, a gate capacitance per unit area of C_{GS} = 3.79 x 10^{-8} F cm^{-2}, and a film thickness of $t = 1.26$ μm, the equation yielded n_{H^+} values of 9.96 x 10^{16} cm^{-3} at −10 V, 8.07 x 10^{16} cm^{-3} at 0 V, and 6.19 x 10^{16} cm^{-3} at 10 V.

2.4: Results and Discussion

We began our studies by heterologously expressing a histidine-tagged *D. pealeii* reflectin A1 isoform in *Escherichia coli* (Figure 2.1). Reflectin A1 inclusion bodies were first prepared according to standard protocols.[47] The protein was then sequentially purified with immobilized

metal-affinity chromatography under denaturing conditions and high-performance liquid chromatography (Figure 2.7).[47] The identity of the purified reflectin was definitively confirmed by in-gel tryptic digestion and mass spectrometry (Figure 2.2).[47] Our optimized protocol yielded >800 mg pure protein per liter of cell culture, which facilitated the preparation of reflectin films and subsequent electrical experiments.[47]

For the electrical measurements, we fabricated two- and three-terminal bottom-contact devices, wherein reflectin served as the active material (Figure 2.8 and Figure 2.5). In brief, we used shadow mask lithography to electron-beam evaporate arrays of paired gold (or palladium) electrodes onto either silicon dioxide/silicon (SiO_2/Si) or glass substrates. Subsequently, we drop-cast smooth and featureless thin films of reflectin directly onto these electrodes from aqueous solution and mechanically scribed away excess material, taking great care to avoid damaging the
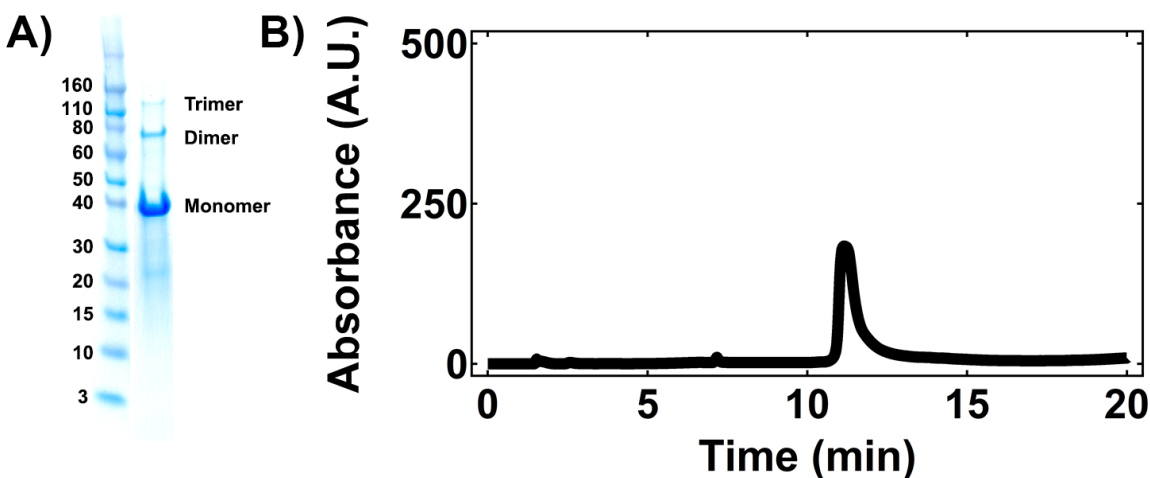
Figure 2.7: **(A)** GelCode Blue stained SDS-PAGE gel of purified wild type reflectin A1. The left lane contains the Novex Sharp Unstained Protein Standard covering molecular weights from 3.5 kDa to 260 kDa. The right lane contains eluate from a HisPur Cobalt IMAC gravity column used to purify reflectin A1. The prominent band at 40 kDa corresponds to the wild type reflectin A1 monomer. **(B)** Typical reverse phase HPLC chromatogram (C18 column) of wild type reflectin A1 following elution from the HisPur Cobalt IMAC gravity column and concentration on a Millipore Amicon Concentrator. The single, large peak at ~11 minutes indicates excellent purity.

electrodes (Figure 2.5). The completed devices were then subjected to systematic electrical interrogation.
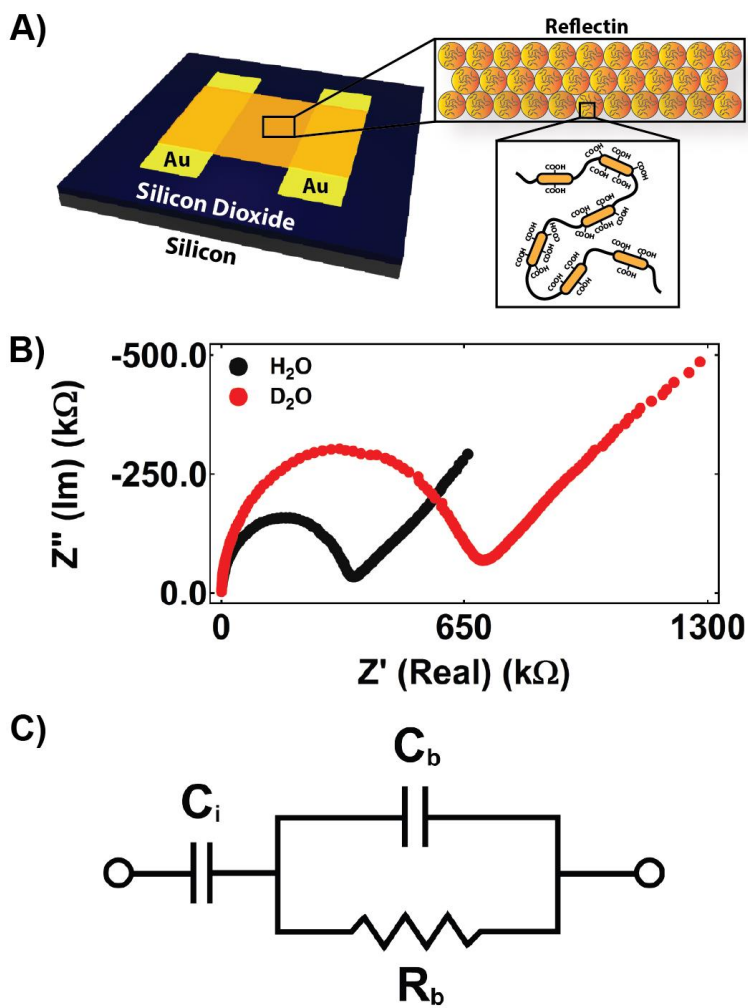
Figure 2.8: (**A**) Illustration of a two-terminal device in which a film composed of aggregated reflectin protein bridges two gold electrodes. Wild-type reflectin contains six repeating subdomains (orange) connected by variable linker regions (black). The carboxylic acid portions of the aspartic and glutamic acid residues in the repeating subdomains are labelled as COOH. The aliphatic portions of the labelled aspartic and glutamic acid residues are omitted for simplicity. (**B**) A typical Nyquist plot for a reflectin-bridged two-terminal device in the presence of water vapor (black) and in the presence of deuterium oxide vapor (red), both at a RH of 90%. There is a change in the effective film resistance (the size of the semicircle increases) on switching from H_2O to D_2O. The device had a length of 50 µm, a width of 25,000 µm and a thickness of 4.6 µm. (**C**) Diagram of the equivalent circuit used to analyze the impedance data. The circuit consists of a capacitor (C_i) in series with both a resistor (R_b) and a capacitor (C_b), which correspond to the film/electrode interface capacitance, the film bulk resistance and the film bulk capacitance, respectively.
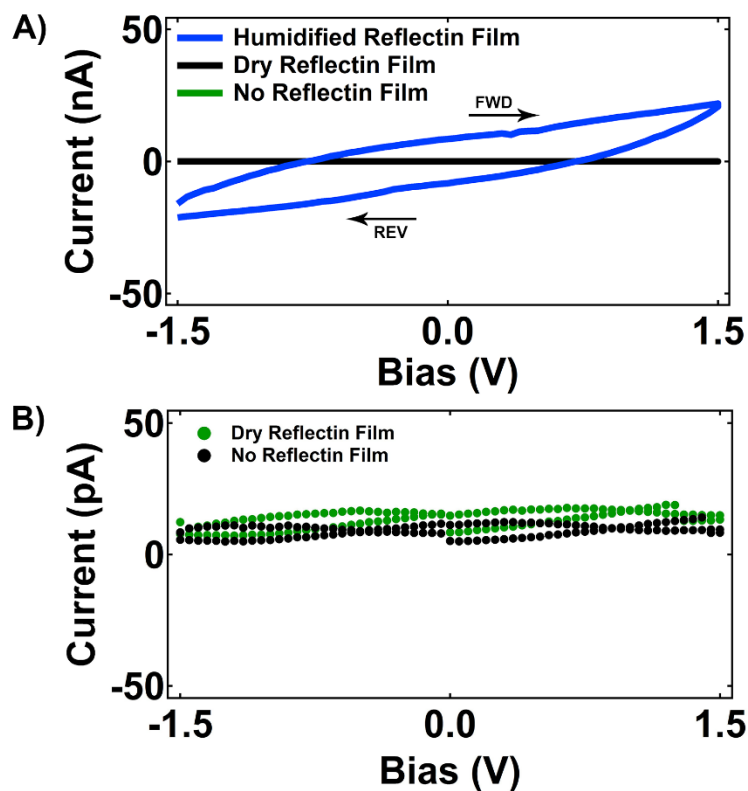
Figure 2.9: (A) Current versus voltage measurements of a wild type reflectin film taken under dry conditions (black) and with a film at a relative humidity of 90% (blue). Note the hysteresis between the forward and reverse scans (the arrows indicate the scan direction). The identical measurement for a device without any bridging material at a relative humidity of 90% is also plotted (green). **(B)** Close-up of the black and green curves from **A** which demonstrate that dry films (measured at a relative humidity of <50%) show no conductivity. For dry films, the current levels were on the order of picoamps (black), similar to those found in devices lacking bridging material (green). The device had a length of 50 μm, a width of 250 μm, and a thickness of 1.3 μm.

We first investigated the electrical properties of reflectin in a two-terminal configuration by recording current as a function of voltage, with gold electrodes serving as the electrical contacts on SiO_2/Si substrates. To avoid contributions from water electrolysis, we limited the maximum applied biases to ~1.5 V, which is the thermoneutral voltage for this reaction, and observed no evidence of gas formation for our devices; electrolysis would require even larger biases because of the probable presence of an overpotential.[60, 61] Here, completely dry reflectin films at relative humidities (RHs) of <50% revealed current levels on the order of a few picoamps, which were

23

similar to the current levels found in the absence of bridging material (Figure 2.9). However, at a high RH (90%), reflectin devices exhibited a marked increase in the current density to 0.6 (± 0.2) $\times 10^{-2}$ A cm^{-2} at 1.5 V across a set of 16 independent films (Figure 2.9). The resulting current-versus-voltage characteristics displayed a clear deviation from linearity and hysteresis between the forward and reverse scans; this behavior qualitatively resembled that found for maleic chitosan proton conductors contacted by blocking gold electrodes.[40] Such non-ideal characteristics indicated the presence of capacitive effects and/or charge-carrier blocking at the electrical contacts, consistent with protonic (and ionic) conductivity.[53]

We sought to gain insight into whether reflectin's conductivity was protonic[6, 10, 36] or electronic[36, 62-65] in origin (both types of mechanisms are well known for proteins). Long-range electronic conduction in proteins often occurs through hopping or tunneling of charge carriers between suitably oriented peptides or cofactors that are readily oxidized or reduced.[62, 65] Thus, we investigated the electrochemical properties of reflectin films in a standard three-electrode configuration with cyclic voltammetry. Our experiments revealed that reflectin on gold was electrochemically silent over a large potential window, with no distinct oxidation or reduction peaks (Figure 2.10). This lack of electrochemical activity at low potentials suggested that redox-associated electronic conduction might be improbable over long distances (tens of microns) for reflectin films.

To better understand the mechanism of conduction for reflectin, we used electrochemical impedance spectroscopy (EIS) to interrogate reflectin-based devices contacted with gold electrodes on glass substrates. We applied alternating current (a.c.) potentials to our hydrated films and visualized the real and imaginary parts of the impedance in Nyquist plots (Figure 2.8).[54, 55] Our plots displayed a semicircle in the high-frequency region and an inclined spur in the low-

frequency region. Such curves are a fingerprint of proton conductors contacted by blocking electrodes, in which the semicircle corresponds to the bulk protonic impedance and the spur corresponds to the pile-up of protons at the electrodes.[54-58] Thus, the curves were fit with a simple equivalent circuit, which has been shown to model proton-exchange membranes accurately by accounting for the bulk impedance and capacitive effects at the contacts (Figure 2.8).[54-58] The high quality of the fit indicated that this simple model was applicable for our reflectin films, and the equivalent circuit yielded a bulk resistance that translated into an effective conductivity of 1.0 $(\pm 0.5) \times 10^{-4}$ S cm^{-1} across a set of nine independent films. These EIS measurements implied that protonic conductivity was probable for our material.

As additional evidence for proton conduction in reflectin films, we sought to observe the kinetic isotope effect for our two-terminal devices. To this end, we recorded EIS measurements for reflectin films contacted with gold electrodes on glass in the presence of deuterium oxide (D_2O) vapor. At RHs of 90%, the solvent uptake of D_2O was almost identical to that of H_2O for reflectin,
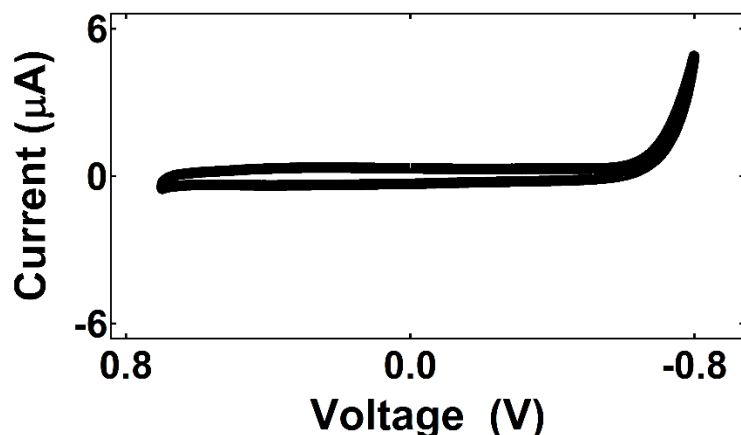
Figure 2.10: A typical cyclic voltammogram for a reflectin thin film on a gold electrode at a scan rate of 100 mV s^{-1} in phosphate buffer. Note that no redox activity was observed for reflectin over a potential window of 0.7 V to –0.8 V (versus a silver/silver chloride reference and a platinum auxiliary electrode).

which ensured a reliable comparison (Table 2.1). Here, we observed a distinct isotope effect, in close agreement with literature observations for other proton-conducting materials;[11-16, 59] on going from H_2O to D_2O *in situ*, the Nyquist plots showed identical characteristic inclined spurs, but the conductivity decreased by 40% from 1.0 ($\pm$0.5) $\times$ 10^{-4} S cm^{-1} to 0.6 ($\pm$0.3) $\times$ 10^{-4} S cm^{-1} across a set of nine independent films (Figure 2.8). This measurement was again consistent with proton conduction in reflectin films.

Protein	Wild Type (H_2O)	Wild Type (D_2O)	DE->A Mutant	Random Mutant
Average	11.4 ($\pm$ 1.5) %	11.8 ($\pm$ 2.4) %	11.5 ($\pm$ 1.0) %	11.7 ($\pm$ 1.6) %

Table 2.1: A comparison of solvent uptake for wild type reflectin (H_2O and D_2O), the DE->A mutant (H_2O), and the Random mutant (H_2O). The solvent uptake was determined by thermogravimetric analysis over a minimum of five independent trials.

We proceeded to investigate the electrical properties of reflectin films when contacted with proton-transparent palladium hydride (PdH_x) electrodes (Figure 2.11). PdH_x facilitates proton injection to yield higher currents for proton-conducting materials (and lower currents for electron-conducting materials).[40, 66] We therefore fabricated two-terminal devices with Pd as the electrode material and exposed these devices to H_2 gas, which enabled the formation of PdH_x electrical contacts *in situ*.[40, 66] At a RH of 90%, electrical measurements for such devices yielded a current density of 8.2 ($\pm$5.9) $\times$ 10^{-2} A cm^{-2} at 1.5 V across a set of 16 independent films (Figure 2.11); the spread in the current densities probably resulted from variability among the non-stoichiometric PdH_x contacts. Although the current densities were over an order of magnitude higher than those found for gold electrodes, the reflectin films did not appear to degrade as a result of electrical

interrogation, as gauged by optical microscopy (Figure 2.6). If significant film degradation had occurred, it might have been accompanied by permanent changes in film coloration. In addition, the current–voltage curves displayed hysteresis consistent with charge accumulation/depletion at the contacts (Figure 2.11),[40, 59] but relative to devices with gold electrodes, the hysteresis was somewhat reduced, presumably as a result of the improved charge injection. These observations supported the notion of proton conduction in reflectin films.
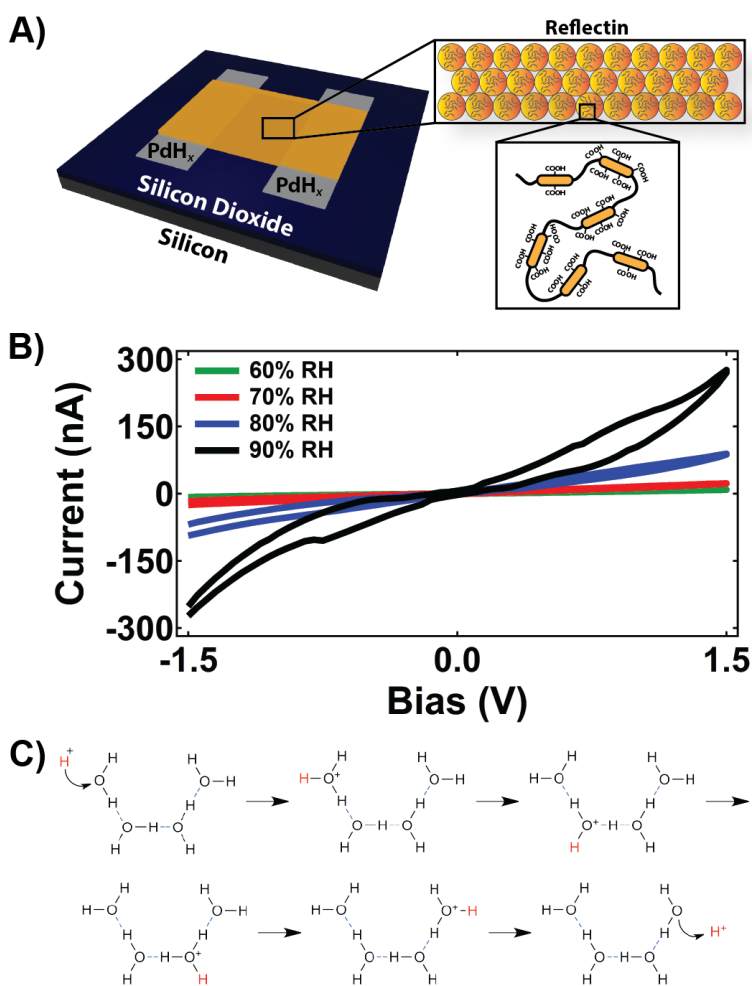
Figure 2.11: (A) Illustration of a two-terminal device in which a film composed of aggregated reflectin protein bridges two PdH$_x$ electrodes. **(B)** The electrical response (current versus voltage) of reflectin films contacted with PdH$_x$ electrodes. The current increases as the RH is raised from 60% to 90%. Both the forward and reverse scans are shown for each measurement. The device had a length of 50 µm, a width of 220 µm and a thickness of 1.3 µm. **(C)** Illustration of proton translocation along a chain of hydrogen-bonded water molecules, as postulated to occur for the Grotthuss mechanism. The mobile proton that moves along the hydrogen-bonded chain is labelled in red.

We also explored the properties of reflectin films contacted with PdH_x electrodes at different levels of hydration. Previous studies have demonstrated that reflectin effectively behaves as a hydrogel, swelling as a function of RH.[44, 45, 47] Here, our reflectin devices displayed a noticeable increase in the current level with increasing humidity (Figure 2.11). For biomolecular proton conductors, water uptake induces the formation of hydrogen-bonded proton-conduction pathways, which facilitate Grotthuss-type proton transfer (Figure 2.11).[10, 18-20, 40] Given the large number of charged and/or hydrophilic residues found in reflectin,[44, 45, 47] the same effect probably accounted for our observed increase in current as a function of RH. Taken together, our measurements with PdH_x contacts suggested that bulk reflectin was a proton-conducting material.

To gain insight into the structural origins of reflectin's conductive properties, we leveraged reflectin's advantages as a protein-based material and introduced targeted mutations within its primary sequence. Reflectin's polar charged amino acid side chains (aspartic acid, glutamic acid, lysine, arginine and histidine) probably play a crucial role in proton transport, as observed for other proteins.[6, 8, 10] For example, the carboxylic acids on its aspartic (D) and glutamic (E) amino acid residues (pK_a values of 3.9 and 4.3, respectively)[67] may either participate in hydrogen bonding or donate the excess protons necessary for conductivity in hydrated reflectin;[6, 8, 10] eliminating the residues that contain carboxylic acid should therefore decrease reflectin's protonic conductivity. To test this hypothesis, we heterologously expressed and purified a reflectin mutant (termed DE->A), in which all of the aspartic acid and glutamic acid residues were substituted with alanine (Figure 2.12 and Figures 2.13 and 2.3). Despite the removal of hydrophilic aspartic and glutamic acid residues, the DE->A mutant exhibited a similar water uptake to that of wild-type reflectin (Table 2.1), presumably because of the overall large percentage of charged residues in reflectin (Figure 2.1). Our PdH_x devices fabricated from the DE->A mutant featured a current density of

$0.9\ (\pm 0.2) \times 10^{-2}$ A cm^{-2} at 1.5 V across a set of 11 independent films, which was approximately

an order of magnitude lower than that found for wild-type reflectin (Figure 2.12). This

measurement further corroborated the notion of protonic conductivity for bulk reflectin.
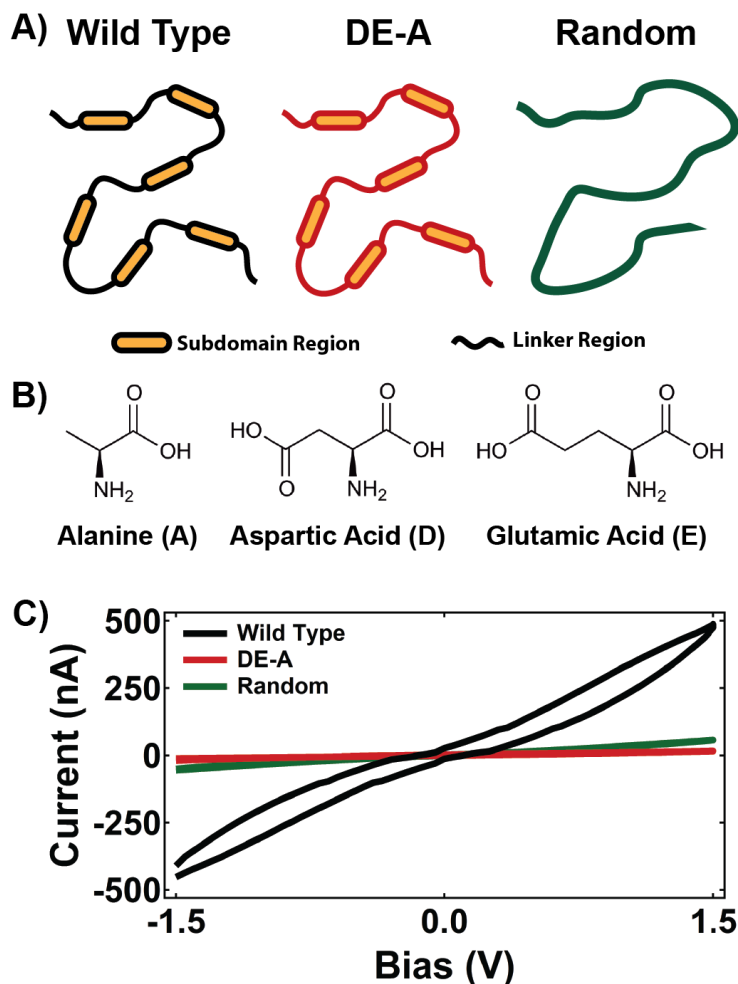
Figure 2.12: (A) Cartoon of the primary structures of wild-type reflectin (left), the DE->A mutant (center) and the Random mutant (right). The wild-type and DE->A mutant reflectin consist of six repeating subdomains (orange) connected by linker regions (colored black for wild type and red for DE->A). For the DE->A mutant, the aspartic and glutamic acids have been replaced by alanine. For the Random mutant (green), the amino acid sequence has been scrambled to eliminate the repeating subdomains. **(B)** Illustration of the chemical structures of alanine (A), aspartic acid (D) and glutamic acid (E). **(C)** Comparison of the typical electrical characteristics (current versus voltage) for PdH$_x$ electrode two-terminal devices fabricated from wild-type reflectin (black), the DE->A mutant (red) and the Random mutant (green). The current for the mutants decreases relative to that for the wild-type protein. Both the forward and reverse scans are shown for each measurement. The RH was 90%. The wild-type, DE->A mutant and Random mutant devices had lengths of 50, 50 and 50 μm, respectively, widths of 265, 210 and 220 μm, respectively, and thicknesses of 0.8, 1.0 and 1.1 μm, respectively.
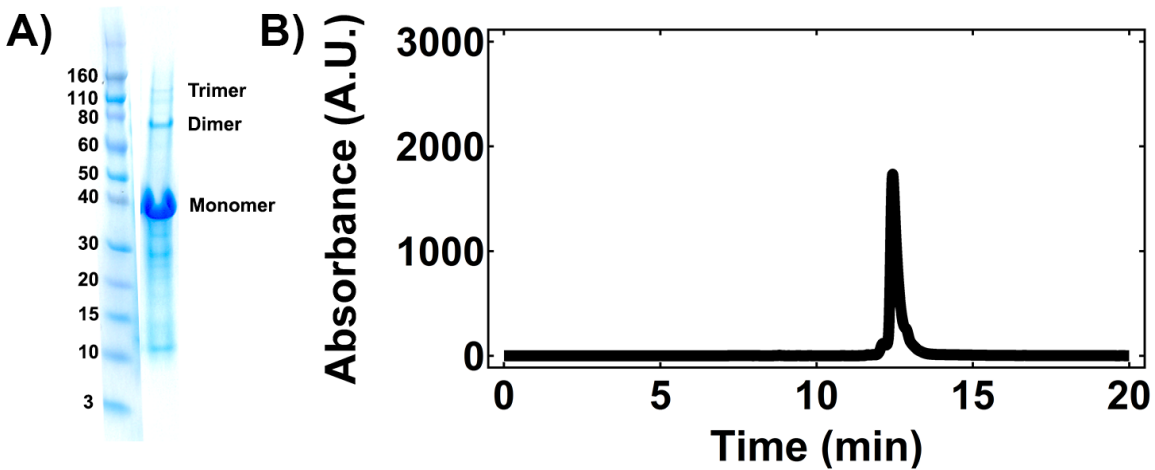
Figure 2.13: (**A**) GelCode Blue stained SDS-PAGE gel of the purified DE->A reflectin A1 mutant. The left lane contains the Novex Sharp Unstained Protein Standard covering molecular weights from 3.5 kDa to 260 kDa. The right lane contains eluate from a HisPur Cobalt IMAC gravity column used to purify the DE->A reflectin A1 mutant. The prominent band at 40 kDa corresponds to the DE->A reflectin A1 mutant monomer. (**B**) Typical reverse phase HPLC chromatogram (C18 column) of the DE->A reflectin A1 mutant following elution from the HisPur Cobalt IMAC gravity column and concentration on a Millipore Amicon Concentrator. The single, large peak at ~12.5 minutes indicates excellent purity.

To better understand the conductive behavior of reflectin, we also altered its amino acid sequence dramatically. Reflectin's multiple conserved repeating subdomains and self-assembly properties suggest that this protein possesses a defined quaternary structure/nanoscale morphology in the solid state.[43-47] We suspect that this potentially unique structure/morphology enables the formation of hydrogen-bonded water networks, which facilitate effective Grotthuss-type proton transfer. Consequently, we postulated that scrambling the primary sequence of reflectin to eliminate the conserved subdomains should disrupt the protein's structure and, in turn, decrease its conductivity by impeding the formation of the requisite hydrogen-bonded water networks.[10, 18-20, 40] To test this hypothesis, we heterologously expressed and purified a reflectin mutant (termed Random) in which the amino acid order was scrambled, but the percentage of the individual amino acids (including the D and E residues) was maintained (Figure 2.12 and Figures 2.14 and 2.4). Although the Random mutant exhibited a similar water uptake to that of wild-type reflectin (Table

2.1), PdH$_x$ devices fabricated from this variant featured a current density of 1.7 ($\pm$0.3) $\times$ 10^{-2} A cm^{-2} at 1.5 V across a set of 11 independent films, which was approximately fivefold lower than that measured for wild-type reflectin (Figure 2.12). Interestingly, the current density of the Random mutant was twofold higher than the current density of the DE->A mutant, potentially a result of the Random mutant's higher aspartic and glutamic amino acid content. Overall, our observations supported the notion that residues containing carboxylic acid play proton-donation or hydrogen-bonding roles for reflectin and underlined the probable importance of reflectin's structural features for its electrical properties.

We sought to characterize further the protonic conductivity in our films by interrogating them with EIS as a function of temperature. We therefore formulated Nyquist plots for reflectin devices contacted with blocking gold electrodes on glass over a temperature range from 30 °C to
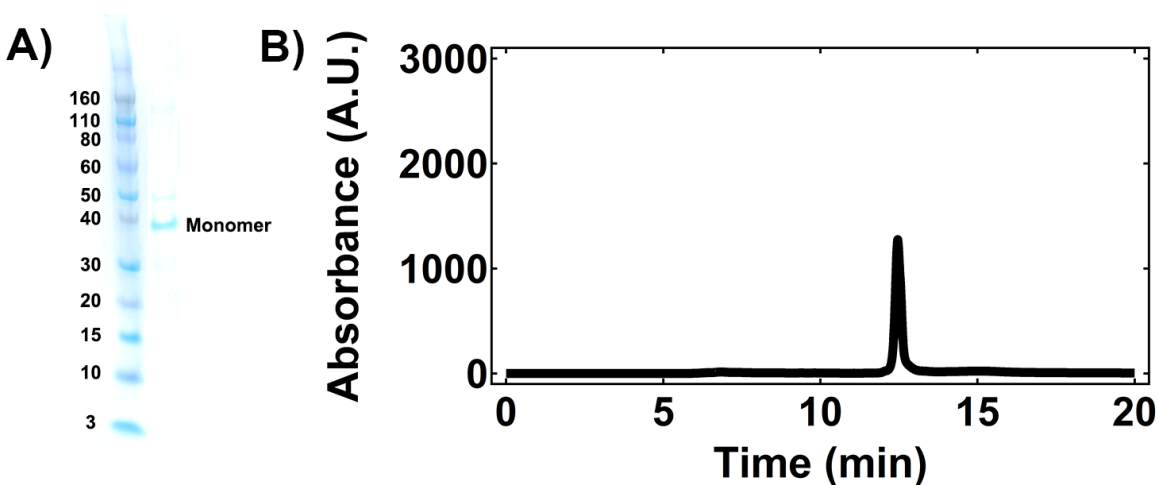
Figure 2.14: **(A)** GelCode Blue stained SDS-PAGE gel of purified the Random reflectin A1 mutant. The left lane contains the Novex Sharp Unstained Protein Standard covering molecular weights from 3.5 kDa to 260 kDa. The right lane contains eluate from a HisPur Cobalt IMAC gravity column used to purify the Random reflectin A1 mutant. The prominent band at 40 kDa corresponds to the Random reflectin A1 mutant monomer. **(B)** Typical reverse phase HPLC chromatogram (C18 column) of the Random reflectin A1 mutant following elution from the HisPur Cobalt IMAC gravity column and concentration on a Millipore Amicon Concentrator. The single, large peak at ~13 minutes indicates excellent purity.

31

65 °C (Figure 2.15); reflectin is expected to be stable across this range because it maintains its functionality even after processing at temperatures as high as 80 °C.[47] By fitting the impedance data with the equivalent circuit depicted in Figure 2.8, we determined the conductivity of our reflectin films at different temperatures (Figure 2.15). At a RH of 90% and a temperature of 65 °C, we measured a peak conductivity of 2.6×10^{-3} S cm^{-1} and an average conductivity of 1.2 $(\pm 1) \times 10^{-3}$ S cm^{-1} across a set of three independent films (Figure 2.15). These values compare favorably to those found for other proton-conducting materials[11-17] and are among the best reported for any bulk solid-state material from a naturally occurring protein.[21-26]

We next constructed Arrhenius-type conductivity plots from our temperature-dependent measurements, which allowed us to determine the activation energy (E_a) of proton conduction for reflectin (Figure 2.15).[12, 59] This activation energy corresponds to the cost of dissociating and/or transporting protons through the hydrogen-bonded water networks that presumably permeate our protein films.[10, 20] The average value of $E_a = 0.22$ (± 0.05) eV calculated from a linear fit of our measurements was characteristic of a Grotthuss-type conduction mechanism (Figure 2.7);[10, 19, 20] similar activation energies have been found for proton conduction in gramicidin channels ($E_a \approx 0.2 \sim 0.3$ eV) and dilute acids ($E_a \approx 0.1$ eV).[10, 19, 20] The low activation energy provided additional confirmation of protonic conductivity for bulk reflectin.

Given that proton conductors are important for a variety of high-technology applications,[11-17] we sought to demonstrate the utility of reflectin in a technologically relevant device. We chose to focus our efforts on the fabrication of protonic transistors because only a handful of these have been reported, none of which used a naturally occurring protein as the active material.[37-42] We therefore fabricated three-terminal reflectin devices that featured PdH$_x$ electrical contacts (formed

in situ) on SiO$_2$/Si substrates; the PdH$_x$ contacts enabled the selective injection of protons into our films.[40, 66]

We proceeded to study the electrical properties of our reflectin-based transistors. Thus, we recorded the protonic current between the source and the drain (I_{DS}) as a function of the applied voltage between the source and the drain (V_{DS}), at the same time as modulating the gate voltage
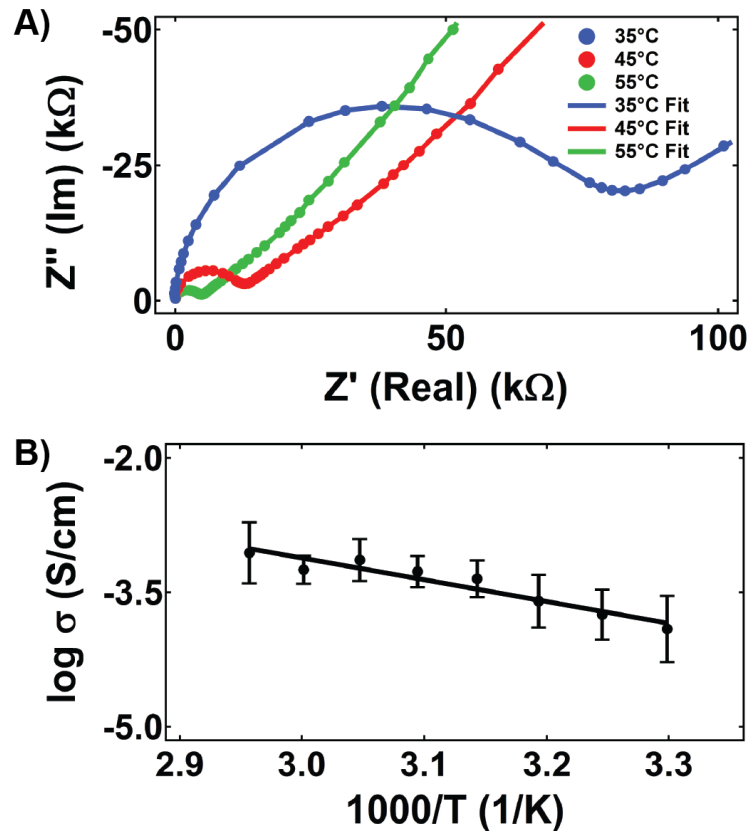
Figure 2.15: (A) Typical Nyquist plots of the imaginary part of the impedance (Z'') versus the real part of the impedance (Z') for a gold electrode two-terminal reflectin device at a RH of 90%. The impedance responses were recorded at temperatures of 35 °C (blue dots), 45 °C (red dots) and 55 °C (green dots). For each temperature, the lines represent a fit of the data with an equivalent circuit model, which accounts for the bulk impedance and capacitive effects at the gold contacts. The device had a length of 100 µm, a width of 25,000 µm and a thickness of 2.6 µm. **(B)** Arrhenius-type plot of the conductivity (σ) as a function of temperature for reflectin devices at a RH of 90%. The measurements were performed at 5 °C intervals over a temperature range of 30 °C to 65 °C, with each data point corresponding to three independent films. The line represents a linear fit of the data. The error bars represent the standard deviation for each data point.
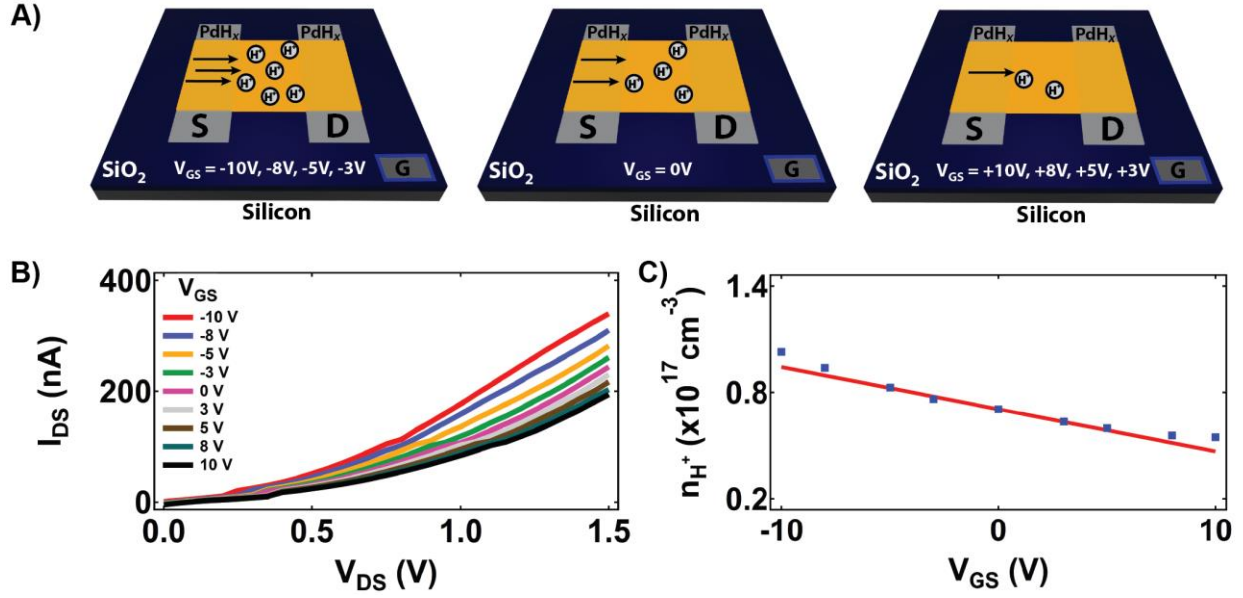
Figure 2.16: (A) Illustration of the proton current for a reflectin-bridged three-terminal protonic transistor under different applied gate voltages (V_{GS}). The current decreases on moving from a negative gate voltage (left) to a gate voltage of zero (middle) to a positive gate voltage (right). The device is fabricated on a SiO_2/Si substrate with PdH_x electrodes as the electrical contacts. **(B)** Typical source–drain current (I_{DS}) as a function of the source–drain voltage (V_{DS}) at different values of V_{GS}. The magnitude of I_{DS} increases as V_{GS} is modulated from positive to negative values. The measurements were performed at a RH of 90%. The device has a length of 50 µm, a width of 267 µm and a thickness of 1.1 µm. **(C)** Plot of the experimentally observed charge-carrier density (proton concentration) as a function of V_{GS} (blue squares). The data are derived from the current–voltage curves in **B** for this specific device. The red line represents the theoretically expected change in the proton concentration, as determined from the equation $n_{H^+} = n_{H^+}^o - V_{GS}C_{GS}/et$ (where $n_{H^+} = n_{H^+}^o$ is the proton concentration at an arbitrary gate bias and $n_{H^+}^o$ is the experimentally observed proton concentration at $V_{GS} = 0$ V). There is agreement between the observed and expected modulations of the charge-carrier density.

(V_{GS}) (Figure 2.16). Our measurements demonstrated electrostatic control over proton conduction:

a negative V_{GS} induced the injection of protons into the channel, which increased the observed

current, and a positive V_{GS} depleted the channel of protons, which decreased the observed current

(Figure 2.16). The electrostatic gating effects were remarkably reproducible, as exemplified by

curves obtained from four representative devices (Figure 2.16). For low source–drain biases, we

observed a small barrier for current flow, probably associated with the activation energy of proton

dissociation/transport. Furthermore, in agreement with previous measurements, the I_{DS} versus V_{DS}

curves exhibited hysteresis, presumably caused by charge accumulation/depletion at the contacts

or an imperfect reflectin/SiO$_2$ interface (Figure 2.17).[40] We also recorded negligible leakage currents, as might be expected for a proton-conducting active material on a proton-insulating substrate (Figure 2.18). Altogether, our findings demonstrated the functionality of reflectin in protonic transistors.

As a consistency check, we compared the conductivities calculated from our transistor measurements with the values determined by EIS. The slope of the I_{DS} versus V_{DS} plot at $V_{GS} = 0$ V yielded an effective resistance for the reflectin films, which translated into a conductivity of 1.1 $(\pm 0.3) \times 10^{-4}$ S cm^{-1} for seven independent devices. This value was similar to the conductivity of 1.0 $(\pm 0.5) \times 10^{-4}$ S cm^{-1} found with EIS (Figure 2.8). Given the substantial experimental differences between the two techniques, this agreement highlights the robustness and reliability of our measurements.
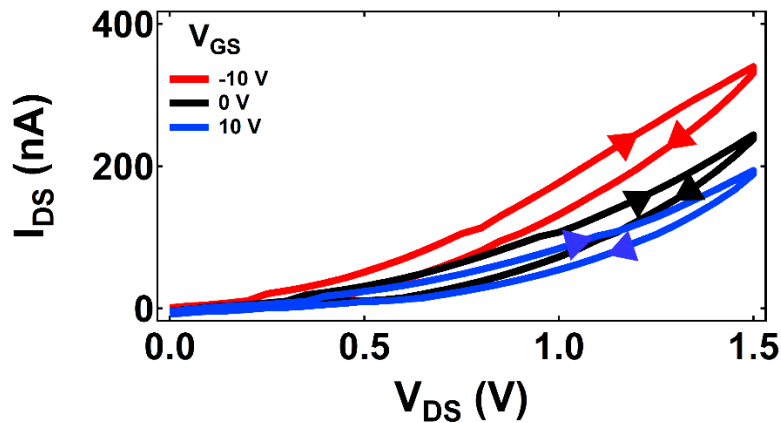
Figure 2.17: Source-drain current (I$_{DS}$) versus source-drain voltage (V$_{DS}$) characteristics for a typical reflectin transistor, showing both the forward and reverse scans at different gate (V$_{GS}$) biases. The forward and reverse scans do not overlap, demonstrating hysteresis (the arrows indicate the scan direction). The device, which corresponds to Figure 2.16, was fabricated on a SiO$_2$/Si substrate with PdH$_x$ electrodes as the electrical contacts. The transistor had a length of 50 μm, a width of 267 μm, and a thickness of 1.1 μm.
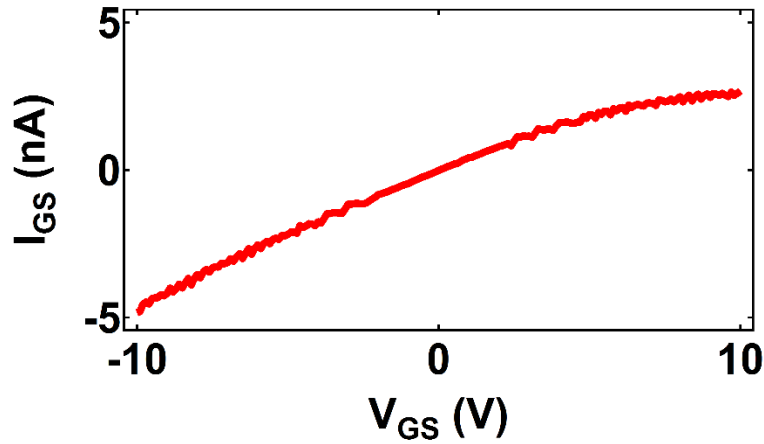
Figure 2.18: Typical gate current (I_{GS}) versus source gate bias (V_{GS}) characteristics where the source-drain bias (V_{DS}) is held at zero. The device was fabricated on a SiO$_2$/Si substrate with PdH$_x$ electrodes as the electrical contacts. The transistor had a length of 50 μm, a width of 250 μm, and a thickness of 1.3 μm.

We next estimated the effective proton mobility from the transfer characteristics of our devices via a literature protocol.[41] Thus, we extracted the conductivity of our films from the I_{DS} versus V_{DS} curves at different V_{GS} biases (Figure 2.16). Linear fits of the dependence of the conductivity on V_{GS} yielded a mobility of $\mu_{H^+} = 7.3$ (± 2.8) $\times 10^{-3}$ cm^2 V^{-1} s^{-1} for seven independent devices. This value is in agreement with mobilities reported for proton conduction in dilute acid solutions (~3 $\times 10^{-3}$ cm^2 V^{-1} s^{-1}),[20] PEDOT:PSS (~3.9 $\times 10^{-3}$ cm^2 V^{-1} s^{-1}),[68] and maleic chitosan proton conductors (~4.9 $\times 10^{-3}$ cm^2 V^{-1} s^{-1}).[40]

Finally, we evaluated the charge-carrier density in our reflectin films. From the equation $\sigma_{H^+} = \mu_{H^+} \cdot n_{H^+} \cdot e$ (where σ_{H^+} is the proton conductivity and e is the elementary charge) and our calculated mobility, the free proton concentration was estimated to be $n_{H^+} = 10.6(\pm 6.1) \times 10^{16}$ cm^{-3} at $V_{GS} = 0$ V for seven independent devices.[40, 41] These excess protons may originate from reflectin's many charged residues, such as the D and E amino acids that contain carboxylic acid. Moreover, from our I_{DS} versus V_{DS} curves, we determined the change

in the number of free protons on the application of different gate biases (Figure 2.16). The experimentally observed proton concentrations were in excellent agreement with those predicted theoretically by the equation $n_{H^+} = n_{H^+}^o - V_{GS}C_{GS}/et$ (where C_{GS} is the gate capacitance per unit area and t is the film thickness), which further underlines the consistency of our measurements (Figure 2.16).[40]

2.5: Conclusion

We have discovered and characterized novel electrical properties for the cephalopod structural protein reflectin. The protein was interrogated by humidity-dependent direct current (d.c.) electrical measurements with both proton-blocking and proton-injecting contacts, a.c. electrical measurements in the presence of water and deuterium oxide, rationally guided mutagenesis experiments and temperature-dependent EIS. Our findings indicate that reflectin functions as an efficient proton-conduction medium.

Based on our measurements, we infer that reflectin exhibits the characteristics of a dilute acid, with an average proton conductivity of $\sim 1 \times 10^{-4}$ S cm^{-1}, a proton transport activation energy of ~ 0.2 eV and a proton mobility of $\sim 7 \times 10^{-3}$ cm^2 V^{-1} s^{-1}. Bulk reflectin is quite unique in this regard; as far as we are aware, no other protein has been shown to mimic a dilute acidic solution so closely. Moreover, reflectin's maximum conductivity of 2.6×10^{-3} S cm^{-1} at 65 °C is among the largest values found for any naturally occurring protein. Within the context of other biological (and even artificial) proton-conducting materials, reflectin's figures of merit are impressive and may represent new benchmarks for proteins in the solid state.[21-26]

Reflectin's physical properties enable the fabrication and characterization of protein-based protonic transistors. The characteristics of our transistors are similar, in terms of mobility, threshold voltage and on/off current ratio, to those reported previously for devices based on maleic chitosan.[40] However, relative to maleic chitosan, reflectin allows protonic transistors to leverage the distinct advantages of protein-based materials, which include structural modularity, tunable physical properties, ease and specificity of functionalization, and generalized expression/purification.[27-31] Indeed, reflectin is simple to produce in high purity and yield, stable under harsh conditions and amenable to modulation of its electrical properties through site-directed mutagenesis. Consequently, given the handful of reported examples of protonic transistors and the possibilities available to functional protein-based materials, our reflectin-based devices may offer exciting new research avenues.

Here, it is important to underline our device reliability and consistency. Electrical measurements are known to be notoriously difficult for delicate protein-based systems, which are often unstable and undergo degradation.[6, 10, 36, 59, 61, 62] However, reflectin films withstand processing and electrical cycling under acidic conditions and at elevated temperatures. Moreover, our electrochemical impedance studies and transistor measurements are in good agreement with one another. Our observations thus highlight the robustness of reflectin as a candidate material for bioelectronic devices.

Reflectin's function as a proton-conducting material is especially fascinating when one considers its unique amino acid sequence, which contains ~30% hydrophilic charged residues and ~20% hydrophobic aromatic residues (Figure 2.1).[43-47] This unusual sequence composition makes reflectin amphipathic and induces its aggregation into nanoparticles both in solution and in thin films.[44, 45, 47] We postulate cautiously that hydrated reflectin films are segregated into distinct

hydrophobic regions and proton-conducting hydrophilic water channels, which probably serve as highly effective conduits for proton transport. Interestingly, this type of segregated structure would be directly analogous to that reported for the sulfonated fluoropolymer Nafion.[14] Our mutagenesis studies and electrical experiments, together with previous characterization of reflectin films,[45] provide compelling evidence that reflectin may possess well-defined and potentially unique morphology/structural features in the hydrated solid state. The exact internal structure of reflectin films probably holds the key to understanding this protein's unexpected electrical properties and certainly represents a fruitful area for further exploration. Our observations thus hint that reflectin may constitute a template for the design and production of the next generation of biologically compatible proton-conducting materials.

2.6: Acknowledgements

2.7: References

1. E. F. Caldin, V. Gold, in *Proton-Transfer Reactions*, Chapman and Hall, **1975**.

2. A. Müller, H. Ratajczak, W. Junge, E. Diemann, in *Electron and Proton Transfer in Chemistry and Biology: Studies in Physical and Theoretical Chemistry Vol. 78*, Elsevier, Amsterdam, **1992**.

3. K. D. Karlin, K. W. Kramarz, J. R. Norton, in *Slow Proton-Transfer Reactions in Organometallic and Bioinorganic Chemistry*, Wiley, Hoboken, **1994**.

4. A. Douhal, F. Lahmani, A. H. Zewail, *Chem. Phys.* **1996**, *207*, 477–498.

5. D. R. Weinberg, C. J Gagliardi, J. F. Hull, C. F. Murphy, C. A. Kent, B. C. Wastlake, A. Paul, D. H. Ess, D. G. McCafferty, T. J. Meyer, *Chem. Rev.* **2012**, *112*, 4016–4093.

6. Z. Schulten, K. Schulten, *Methods Enzymol.* **1986**, *127*, 419–438.

7. T. E. DeCoursey, *Physiol. Rev.* **2003**, *83*, 475–579.

8. T. E. DeCoursey, *J. Physiol.* **2008**, *586*, 5305–5324.

9. T. Gensch, J. Heberle, C. Viappiani, *Photochem. Photobiol.* **2006**, *5*, 529–530.

10. C. A. Wraight, *Biochim. Biophys. Acta* **2006**, *1757*, 886–912.

11. P. Colomban, in *Proton Conductors: Solids, Membranes and Gels – Materials and Devices*, Cambridge Univ. Press, Cambridge, **1992**.

12. K.-D. Kreuer, *Chem. Mater.* **1996**, *8*, 610–641.

13. K.-D. Kreuer, S. J. Paddison, E. Spohr, M. Schuster, *Chem. Rev.* **2004**, *104*, 4637–4678.

14. K. A. Mauritz, R. B. Moore, *Chem. Rev.* **2004**, *104*, 4535–4385.

15. T. Norby, *MRS Bull.* **2009,** *34*, 923–928.

16. E. Fabbri, D. Pergolesi, E. Traversa, *Chem. Soc. Rev.* **2010**, *39*, 4355–4369.

17. M. Yoon, K. Suh, S. Natarajan, K. Kim, *Angew. Chem. Int. Ed.* **2013**, 52, 2688–2700.

18. C. J. T. de Grotthuss, *Ann. Chim.* **1806**, *58*, 54–73.

19. N. Agmon, *Chem. Phys. Lett.* **1995**, *244*, 456–462.

20. S. Cukierman, *Biochim. Biophys. Acta* **2006**, *1757*, 876–885.

21. J. E. Algie, J. G. Downes, B. H. Mackay, *Text. Res. J.* **1960**, *30*, 432–434.

22. G. H. Bardelmeyer, *Biopolymers* **1973**, *12*, 2289–2302.

23. E. J. Murphy, *J. Colloid Interface Sci.* **1976**, *54*, 400–408.

24. R. H. Tredgold, R. C. Sproule, J. McCanny, *J. Chem. Soc. Faraday Trans. 1* **1976**, *72*, 509–512.

25. G. Careri, M. Geraci, A. Giasanti, J. A. Rupley, *Proc. Natl Acad. Sci. U. S. A.* **1985**, *82*, 5342–5346.

26. B. Gabriel, J. Teissie, *Proc. Natl Acad. Sci. U. S. A.* **1996**, *93*, 14521–14525.

27. D. Kaplan, K. McGrath, in *Protein-Based Materials – Bioengineering of Materials*, Birkhäuser, Boston, **1996**.

28. S. A. Maskarinec, D. A. Tirrell, *Curr. Opin. Biotechnol.* **2005**, *16*, 422–426.

29. L. Shen, N. Bao, Z. Zhou, P. E. Prevelige, A. Gupta, *J. Mater. Chem.* **2011**, *21*, 18868–18876.

30. R. L. DiMarco, S. C. Heilshorn, *Adv. Mater.* **2012**, *24*, 3923–3940.

31. T. Z. Grove, L. Regan, *Curr. Opin. Struct. Biol.* **2012**, *22*, 451–456.

32. R. M. Owens, G. G. Malliaras, *MRS Bull.* **2010**, *35*, 449–456.

33. K. Svennersten, K. C. Larsson, M. Berggren, A. Richter–Dahlfors, *Biochim. Biophys. Acta* **2011**, *1810*, 276–285.

34. G. Tarabella, F. M. Mohammadi, N. Coppedè, F. Barbero, S. Iannotta, C. Santato, F. Cicoira, *Chem. Sci.* **2013**, *4*, 1395–1409.

35. E. D. Glowacki, M. Irimia-Vladu, S. Bauer, N. S. Sariciftci, *J. Mater. Chem. B* **2013**, 1, 3742–3753.

36. P. Meredith, C. J. Bettinger, M. Irimia-Vladu, A. B. Mostert, P. E. Schwenn, *Rep. Prog. Phys.* **2013**, *76*, 034501.

37. V. F. Petrenko, N. Maeno, *J. Phys. Colloq.* **1987**, *48*, 115–119.

38. Z. G. Chiragwandi, O. Nur, M. Willander, N. Calander, *Appl. Phys. Lett.* **2003**, *83*, 5310–5312.

39. R. Fan, S. Huh, R. Yan, J. Arnold, P. Yang, *Nature Mater.* **2008**, *7*, 303–307.

40. C. Zhong, Y. Deng, A. F. Roudsari, A. Kapetanovic, M. P. Anatram, M. Rolandi, *Nature Commun.* **2011***, 2*, 476.

41. Y. Deng, E. Josberger, J. Jin, A. F. Roudsari, B. A. Helms, C. Zhong, M. P. Anatram, M. Rolandi, *Sci. Rep.* **2013**, *3*, 2481.

42. A. M. Deml, A. L. Bunge, M. A. Reznikov, A. Kolessov, R. P. O'Hayre, *J. Appl. Phys.* **2012**, *111*, 074511.

43. W. J. Crookes, L.-L. Ding, Q. L. Huang, J. R. Kimbell, J. Horwitz, M. J. McFall-Ngai, *Science* **2004**, *303*, 235–238.

44. R. M. Kramer, W. J. Crookes-Goodson, R. R. Naik, *Nature Mater.* **2007**, *6*, 533–538.

45. A. R. Tao, D. G. DeMartini, M. Izumi, A. M. Sweeney, A. L. Holt, D. E. Morse, *Biomaterials* **2010**, *31*, 793–801.

46. M. Izumi, A. M. Sweeney, D. DeMartini, J. C. Weaver M. L. Powers, A. Tao, T. V. Silvas, R. M. Kramer, W. J. Crookes-Goodson, L. M. Mäthger, R. R. Naik, R. T. Hanlon, D. E. Morse, *J. R. Soc. Interface* **2010**, *7*, 549–560.

47. L. Phan, W. G. Walkup IV, D. D. Ordinario, E. Karshalev, J-M. Jocson, A. M. Burke, A. A. Gorodetsky, *Adv. Mater.* **2013**, *25*, 5621–5625.

48. L. M. Mäthger, E. J. Denton, N. J. Marshall, R. T. Hanlon, *J. R. Soc. Interface* **2009**, *6*, 149–163.

49. D. G. DeMartini, D. V. Krogstad, D. E. Morse, *Proc. Natl Acad. Sci. U. S. A.* **2013**, *110*, 2552–2556.

50. T. J. Wardill, P. T. Gonzalez-Bellido, R. J. Crook, R. T. Hanlon, *Proc. R. Soc. B* **2012**, *279*, 4243–4252.

51. A. Shevchenko, H. Tomas, J. Havlis, J. V. Olsen, M. Mann, *Nat. Protoc.* **2006**, *1*, 2856–2860.

52. S. M. Sze, K. K. Ng, in *Physics of Semiconductor Devices, 3rd edn*, Wiley, Hoboken, **2006**.

53. I. Kymissis, in *Organic Field Effect Transistors: Theory, Fabrication and Characterization (Integrated Circuits and Systems)*, Springer, New York, **2009**.

54. E. Barsoukov, J. R. Macdonald, *Impedance Spectroscopy: Theory, Experiment and Applications 2nd edn*, Wiley, Hoboken, **2005**.

55. X-Z. Yuan, C. Song, H. Wang, J. Zhang, in *Electrochemical Impedance Spectroscopy in PEM Fuel Cells: Fundamentals and Applications*, Springer, New York, **2012**.

56. R. A. Huggins, *Ionics* **2002**, *8*, 300–313.

57. Z. Xie, C. Song, B. Andreaus, T. Navessin, Z. Shi, J. Zhang, S Holdcroft, *J. Electrochem. Soc.* **2006**, *153*, 173–178.

58. T. Soboleva, Z. Xie, Z. Shi, E. Tsang, T. Navessin, S. Holdcroft, *J. Electroanal. Chem.* **2008**, *622*, 145–152.

59. L. Glasser, *Chem. Rev.* **1975**, 75, 21–65.

60. A. Ursúa, L. M. Gandía, P. Sanchis, *Proc. IEEE* **2012**, *100*, 410–426.

61. K. Zeng, D. Zhang, *Prog. Energy Combust. Sci.* **2010**, *36*, 307–326.

62. M. Cordes, B. Giese, *Chem. Soc. Rev.* **2009**, *38*, 892–901.

63. M. W. Shinwari, M. J. Deen, E. B. Starikov, G. Cuniberti, *Adv. Funct. Mater.* **2010**, 20, 1865–1883.

64. I. Ron, I. Pecht, M. Sheves, D. Cahen, *Acc. Chem. Res.* **2010**, *43*, 945–953.

65. J. R. Winkler, H. B. Gray, *J. Am. Chem. Soc.* **2014**, 136, 2930–2939.

66. H. Morgan, R. Pethig, G. T. Stevens, *J. Phys. E* **1986**, *19*, 80–82.

67. T. E. Creighton, in *Proteins: Structures and Molecular Properties 2nd edn*, W. H. Freeman, New York, **1993**.

68. E. Stavrinidou, P. Leleux, H. Rajaona, D. Khodagholy, J. Rivnay, M. Lindau, S. Sanaur, G. G. Malliaras, *Adv. Mater.* **2013**, *25*, 4488–4493.

CHAPTER 3   Protonic Transistors From Thin Reflectin Films

3.1: Abstract

Ionic transistors from organic and biological materials hold great promise for bioelectronics applications. Thus, much research effort has focused on optimizing the performance of these devices. Herein, we experimentally validate a straightforward strategy for enhancing the high to low current ratios of protein-based protonic transistors. Upon reducing the thickness of the transistors' active layers, we increase their high to low current ratios 2-fold while leaving the other figures of merit unchanged. The measured ratio of 3.3 is comparable to the best values found for analogous devices. These findings underscore the importance of the active layer geometry for optimum protonic transistor functionality.

3.2: Introduction

Ionic transistors from organic and biological materials represent an emerging class of devices for bioelectronics applications.[1–9] Indeed, the processing and fabrication techniques required for the preparation of these transistors are simple, convenient, and inexpensive.[1–5] The constituent organic or biological materials are also amenable to chemical modification and functionalization.[1,5–7] In addition, the mechanical properties of organic materials are inherently compatible with those of biological systems.[1,3,8] Moreover, organic and biological ionic conductors are well suited for the transduction of biochemical events into electronic signals.[1,4–7,9] These key advantages have made ionic transistors from organic and biological materials exciting targets for further research and development.

Within the broader ionic transistor class of devices, there have been several reports of protonic transistors,[10–16] including two notable examples from the Rolandi group.[13,14] For these devices, the application of a voltage to the gate modulates the current flow between the source and the drain, in analogy to conventional unipolar field effect transistors.[13,14] The magnitude of the current is determined by the proton charge carrier density in the device channel, as given by the equation $n_{H+} = n_{H+}^0 - V_{GS}C_{GS}/et$, where n_{H+} is the proton concentration at an arbitrary gate voltage, n_{H+}^0 is the proton concentration at a gate bias of 0 V, V_{GS} is the gate voltage, C_{GS} is the gate capacitance, e is the charge of the proton, and t is the thickness of the active layer.[13,14] Thus, a negative gate voltage induces the injection of protons into the channel, leading to an increase in the source-drain current, and a positive gate voltage depletes the channel of protons, leading to a decrease in the source-drain current.[13,14] This operating mechanism enforces limits on the ratio between protonic transistors' high (on) and low (off) currents (I_{HIGH}/I_{LOW}), relative to standard field effect transistors. However, the I_{HIGH}/I_{LOW} ratio, in principle, can be improved by reducing the active layer thickness, thereby increasing the difference between the transistors' high and low current states.

Recently, our group discovered that reflectin, a structural protein that plays a key role in the color-changing abilities of cephalopods,[16–20] is an effective proton conducting material.[21] This finding enabled the fabrication of protein-based protonic transistors with excellent figures of merit, including a proton mobility (μ_{H+}) of $\sim 7.3 \times 10^{-3}$ cm^2 V^{-1} s^{-1}.[21] However, due to active layers with thicknesses between $\sim$1 and $\sim$2 μm, the transistors possessed relatively poor I_{HIGH}/I_{LOW} ratios of $\sim$1.6.[21]

Herein, we build upon our previous work and demonstrate improved I_{HIGH}/I_{LOW} current ratios for reflectin-based protonic transistors. We first fabricate two-terminal devices from thin

reflectin films and characterize their conductivity when contacted with palladium (Pd) and palladium hydride (PdH_x) electrodes. We next describe the electrical interrogation of reflectin films with an average thickness of ~0.30 μm in a three-terminal transistor configuration. We find that the majority of the device metrics, including mobility and proton concentration, are comparable to those previously reported for protonic transistors from reflectin films with a thickness between ~1 and ~2 μm.[21] However, we observe a 2-fold improvement in the thin protonic transistors' I_{HIGH}/I_{LOW} current ratios. Overall, our findings highlight the importance of the active layer geometry for the performance of protein-based (and other) protonic transistors.

3.3: Experimental Section

3.3.1: Preparation of Substrates

For two- and three-terminal measurements, the devices were fabricated on SiO_2/Si substrates. The substrates were cut from 4 inch, 405 to 455 μm thick, p-type Boron doped wafers, with a <100> crystallographic orientation and a 3000 Å oxide layer on both sides (International Wafer Service). The wafers were sectioned into individual 2.25 cm^2 chips using standard lithographic techniques. The chips were etched to reduce the thickness of the oxide layer to ~900 Å. The etching process did not influence the uniformity of the oxide layer, as confirmed by optical profilometry and atomic force microscopy. Prior to deposition of the electrodes, the substrates were cleaned in Piranha solution (1:3 hydrogen peroxide to sulfuric acid).

3.3.2: Deposition of Electrical Contacts

The electrodes consisted of a 4 nm chromium layer overlaid with a 40 nm palladium layer. The metal was deposited onto the clean SiO_2/Si substrates *via* shadow mask lithography with a

CV-8 Electron Beam Deposition System (Temescal). To fabricate the active layers, reflectin solutions were dropcast onto the electrodes, and the solvent was allowed to evaporate in ambient overnight. The use of low volume solutions yielded thin films with a thickness of ~0.2 μm to ~0.4 μm, while the use of high volume solutions yielded thicker films. The reflectin films were then mechanically scribed with a probe station needle to leave a rectangular reflectin square spanning each electrode pair.

3.3.3: Optical Microscopy

The completed devices were imaged before and after electrical measurements with an Axio Imager A1 Microscope (Carl Zeiss) outfitted with an Epiplan 20X, NA = 0.4 lens (Carl Zeiss). The image data was processed with AxioVision AC Release 4.5 (Carl Zeiss). The device dimensions (length and width) were extracted by analyzing these images.

3.3.4: Atomic Force Microscopy

The thicknesses of all reflectin films were measured with atomic force microscopy (AFM) by examining trenches scratched directly into the films. Iridium coated silicon probes (Asylum Research ASYELEC-01) were used to record the images. The films were examined *in situ* at elevated relative humidities with a MFP-3D AFM (Asylum Research) outfitted with a Humidity Sensing Cell (Asylum Research). The scans were rastered either at 0.17 Hz or at 1.0 Hz and normalized using polynomial subtraction for improved image quality. The thicknesses of the films were found to increase by ~40% upon going from dry conditions (< 50% relative humidity) to 90% relative humidity. The swollen thicknesses of the reflectin films under appropriate humidified conditions were reported for the device dimensions in all instances and were used for the relevant calculations. The swelling had no effect on the integrity of the films, as gauged by both atomic

force and optical microscopy. The AFM data and parameters were processed/extracted with the Gwyddion software package.

3.3.5: Two-Terminal Measurements

The current was recorded as a function of voltage at various relative humidities on a PM 5 Probe Station (Cascade Microtech) outfitted with a 4156C Semiconductor Parameter Analyzer (Agilent). The electrical measurements were performed in ambient atmosphere under controlled humidity conditions, with the humidity constantly monitored *via* a hygrometer (Fisher Scientific). The sweep rate was 0.2 V μs^{-1} and the hold time was 0.5 s. Measurements with palladium hydride electrodes were performed under a 5% hydrogen:95% argon atmosphere.

3.3.6: Three-Terminal Measurements

The current was recorded as a function of the source-drain voltage, at different gate voltages, in a humidified environment on a PM-5 Probe Station (Cascade Microtech) outfitted with a 4156C Semiconductor Parameter Analyzer (Agilent). The electrical measurements were performed under a 5% hydrogen:95% argon atmosphere, with the humidity carefully controlled and constantly monitored *via* a hygrometer (Fisher Scientific). The sweep rate was 0.2 V μs^{-1} and the hold time was 0.5 s.

3.4: Results and Discussion

We began our studies by heterologously expressing a histidine-tagged *Doryteuthis* (*Loligo*) *pealeii* reflectin A1 isoform in E. coli according to previously reported protocols.[20,21] We first extracted crude reflectin from E. coli inclusion bodies. The protein was then sequentially purified

by immobilized metal affinity chromatography under denaturing conditions and high performance liquid chromatography (HPLC). The identity of the purified protein was definitively confirmed by in-gel tryptic digestion and tandem mass spectrometry. Notably, the optimized expression and purification procedure yielded >800 mg of reflectin per liter of E. coli cell culture with a purity of over 99%. This high yield and excellent purity enabled the high throughput fabrication of reflectin-based devices.

For our measurements, we fabricated two-terminal bottom-contact devices according to the scheme shown in Figure 3.1. In brief, we deposited an array of palladium contacts onto the surface of clean silicon dioxide/silicon (SiO_2/Si) substrates via electron-beam evaporation through a shadow mask. Next, we dropcast aqueous reflectin solutions onto the electrodes. The solvent was then allowed to evaporate, and the excess protein was removed from the substrate via mechanical scribing. The resulting completed devices were subjected to physical and electrical characterization.
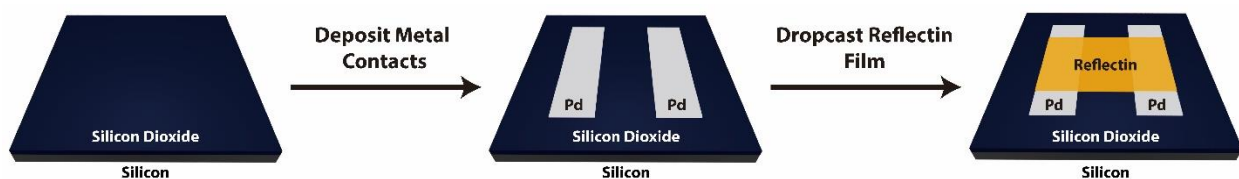
Figure 3.1: Illustration of the fabrication of two-terminal reflectin-based devices. Palladium contacts are first deposited onto the surface of a silicon dioxide/silicon (SiO_2/Si) substrate. Next, reflectin is dropcast directly onto the electrodes from aqueous solution. After drying, excess material is removed via mechanical scribing to furnish the completed device.

We first characterized our devices with both optical microscopy and atomic force microscopy (AFM). A typical optical image of a reflectin device is shown in Figure 3.2A. The optical image demonstrated that the film was uniform, with few apparent defects. A typical

corresponding AFM image is shown in Figure 3.2B. The image indicated that the surface topography of the reflectin film was relatively smooth and featureless with a root mean square (RMS) roughness of ~0.5 nm. The devices were now poised for electrical interrogation.
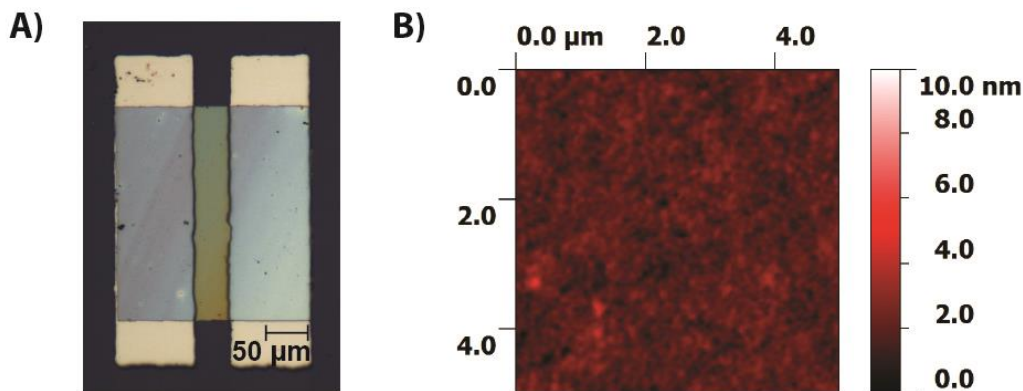
Figure 3.2: **(A)** A typical optical image of a device where a thin reflectin film bridges two palladium electrodes. **(B)** A representative AFM image of the reflectin film from **A**. The film is relatively smooth and featureless with an RMS roughness of ~0.5 nm.

We investigated the electrical properties of the reflectin films by recording current (I) as a function of voltage (V) at a relative humidity of 90%.[23] The I-V characteristics of a typical reflectin-based device, when contacted with palladium electrodes, are shown in Figure 3.3. This 0.24 μm-thick device featured a low current density of 0.7×10^{-2} A/cm^2 at 1.5 V, consistent with previous findings for ~1 to ~2 μm-thick reflectin films contacted with proton-blocking electrodes.[21] Subsequently, we converted the device's electron-conducting Pd contacts into proton-injecting PdH$_x$ contacts via exposure to hydrogen gas in situ (Figure 3.3A). As illustrated in Figure 3.3B, the current density of the device increased by nearly an order of magnitude to 5.9×10^{-2} A/cm^2 at 1.5 V, in agreement with literature precedent.[13,21] These measurements confirmed the presence of protonic conductivity for thin reflectin films.
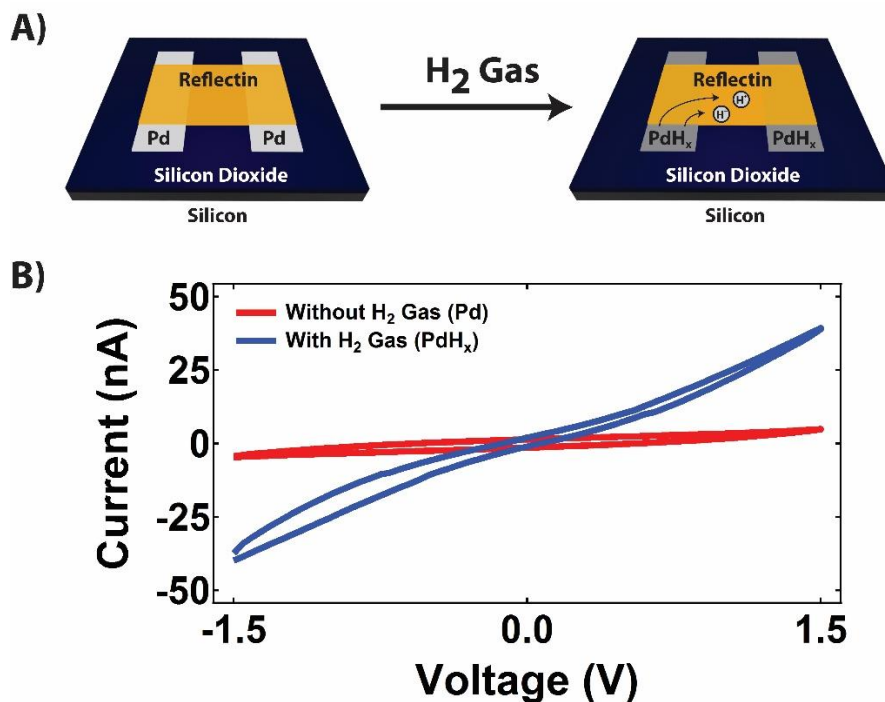
Figure 3.3: (A) An illustration of a two-terminal reflectin-based device, which undergoes in situ treatment with hydrogen (H_2) gas. The palladium electrodes are converted to palladium hydride electrodes, enabling the injection of protons into the film. **(B)** The current versus voltage characteristics of a reflectin film contacted with palladium (red) and palladium hydride (blue) electrodes. The device current increases by an order of magnitude upon switching from palladium to palladium hydride electrodes in situ. Both the forward and reverse scans are shown for each measurement. The measurements were performed at a relative humidity of 90%. The device had a length of 50 μm, a width of 280 μm, and a thickness of 0.24 μm.

We next studied the electrical properties of reflectin films featuring an average thickness of 0.30 ($\pm$0.06) μm in a three-terminal transistor configuration (Figure 3.4A). The I-V characteristics of a typical protonic transistor are shown in Figure 3.4B. We found that the protonic source-drain current (I_{SD}) in these devices, measured at different source-drain voltages (V_{SD}), was dictated by the applied gate voltage (V_{GS}). The protonic current decreased upon changing the V_{GS} from +10 V to 0 V to −10 V at a relative humidity of 90% (Figures 3.4A and 3.4B). This gating behavior was consistent with previous studies of maleic chitosan-based and reflectin-based protonic transistors.[13,14,21]
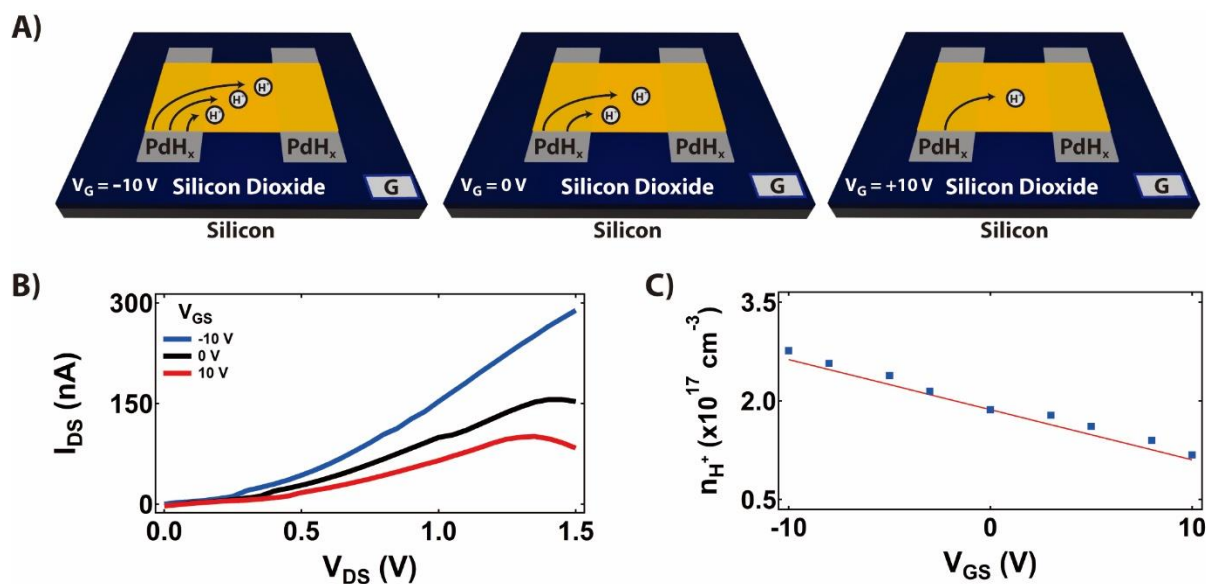
Figure 3.4: (A) Illustration of the protonic current for a protonic transistor under different applied gate voltages. The magnitude of the current decreases as the gate voltage (V_{GS}) is changed from −10 V (left) to 0 V (middle) to +10 V (right). **(B)** The source–drain current (I_{DS}) versus source–drain voltage (V_{DS}) characteristics of a reflectin-based protonic transistor obtained at $V_{GS} = -10$ V (blue), $V_{GS} = 0$ V (black), and $V_{GS} = +10$ V (red). I_{DS} decreases as V_{GS} is changed from a negative value to a positive value. The measurements were performed at a relative humidity of 90%. **(C)** A plot of the experimentally observed proton charge carrier density (n_{H+}) as a function of V_{GS} (blue squares). The data correspond to the I_{DS} versus V_{GS} characteristics in (B). The red line represents the calculated proton charge carrier density. There is good agreement between the experimental and calculated values of the proton charge carrier densities. The device had a length of 50 μm, a width of 280 μm, and a thickness of 0.35 μm.

We proceeded to calculate the proton mobility from the I-V characteristics of our transistors from thin reflectin films via established literature protocols.[13,14,21] We therefore extracted the conductivity from the transistors' I_{SD} vs. V_{SD} curves and used a linear fit of the dependence of this conductivity on V_{GS} to calculate the corresponding proton mobilities.[13,14,21] The average calculated value of $\mu_{H+} = 7.7$ (± 2.1) $\times 10^{-3}$ cm^2 V^{-1} s^{-1} for thin reflectin films was similar to the previously reported values of $\sim 7.3 \times 10^{-3}$ cm^2 V^{-1} s^{-1} for thick reflectin films,[21] $\sim 3 \times 10^{-3}$ cm^2 V^{-1} s^{-1} for dilute acids,[22] $\sim 3.9 \times 10^{-3}$ cm^2 V^{-1} s^{-1} for poly(3,4-ethylenedioxythiophene):poly(styrenesulfonate) (PEDOT:PSS) films,[23] and $\sim 4.9 \times 10^{-3}$ cm^2 V^{-1} s^{-1} for maleic chitosan nanofibers.[14]

We used the calculated mobilities and conductivities to evaluate the proton charge carrier density of the thin reflectin films according to established procedures.[13,14,21] For example, at a V_{GS} = 0 V, we found an average charge carrier density of n_{H+} = 2.5 ($\pm$1.1) $\times$ 10^{17} cm^{-3}. This value was similar to that previously reported for both thick reflectin films and other proton-conducting materials.[13,14,21] We then evaluated the charge carrier density of the films at different values of V_{GS}. Notably, the experimentally determined charge carrier density was in excellent agreement with the one theoretically predicted by the equation $n_{H+} = n_{H+}^{0} - V_{GS}C_{GS}/et$ (Figure 3.4C).

Finally, we calculated the I_{HIGH}/I_{LOW} ratios of protonic transistors from thin reflectin films. We found a ratio of 3.3 ($\pm$0.3) between the high current state at V_{GS} = $-$ 10 V and the low current state at V_{GS} = + 10 V. This I_{HIGH}/I_{LOW} ratio of 3.3 represented a 2-fold improvement over the value of ~1.6 previously found for thick reflectin films.[21] Although this ratio was certainly below values of >10^{6} reported for organic transistors,[24] it compared favorably to the best values found for protonic transistors under comparable conditions and in analogous configurations (Table 3.1).[12,13,21] These observations underscored the excellent performance of the thin reflectin film-based protonic transistors.

Device material	Estimated I_{HIGH}/I_{LOW} ratio	Approximate thickness (μm)	Reference
Reflectin A1 (thick films)	1.6[a]	~1-2	21
Mesoporous silica	2.9[b]	~0.1-0.2	12
Maleic chitosan	3.3[c]	~0.1	13
Reflectin A1 (thin films)	3.3[a]	~0.2-0.4	This work

[a]The value was estimated at V_{GS} = $-$10 V, V_{GS} = +10 V, and V_{DS} = 1.5 V.
[b]The value was estimated at V_{GS} = $-$1.0 V, V_{GS} = +1.0 V, and V_{DS} = 2.0 V.
[c]The value was estimated at V_{GS} = $-$15 V, V_{GS} = +15 V, and V_{DS} = 1.5 V.

Table 3.1: A comparison of the estimated I_{HIGH}/I_{LOW} ratios for protonic transistors from various materials. The devices were tested and characterized under comparable conditions and in analogous configurations. The approximate corresponding thicknesses for each type of device are also indicated.

3.5: Conclusion

In conclusion, we have electrically characterized protein-based protonic transistors from reflectin films with an average thickness of ∼0.30 μm. The figures of merit measured for these devices, including a mobility of $\mu_{H+} = 7.7\ (\pm2.1) \times 10^{-3}\ cm^2\ V^{-1}\ s^{-1}$ and a charge carrier density of $n_{H+} = 2.5\ (\pm1.1) \times 10^{17}\ cm^{-3}$, are comparable to previously reported values for reflectin films with a ∼1 to ∼2 μm thickness.[21] However, transistors from thin reflectin films feature a more than 2-fold improvement in their I_{HIGH}/I_{LOW} ratio relative to transistors from thick reflectin films. The measured ratio of 3.3 compares favorably to the best values reported for similar devices (Table 3.1). In their totality, our findings highlight the importance of the active layer geometry for optimum protonic transistor functionality.

3.6: Acknowledgements

3.7: References

1. R. M. Owens, G. G. Malliaras, *MRS Bull.* **2010**, *35*, 449–456.

2. M. Irimia-Vladu, N. S. Sariciftci, S. Bauer, *J. Mater. Chem.* **2011**, *21*, 1350–1361.

3. P. Meredith, C. J. Bettinger, M. Irimia-Vladu, A. B. Mostert, P. E. Schwenn, *Rep. Prog. Phys.* **2013**, *76*, 034501.

4. G. Tarabella, F. M. Mohammadi, N. Coppedè, F. Barbero, S. Iannotta, C. Santato, F. Cicoira, *Chem. Sci.* **2013**, *4*, 1395–1409.

5. J. Rivnay, R. M. Owens, G. G. Malliaras, *Chem. Mater.* **2014**, *26*, 679–685.

6. M. Berggren, A. Richter-Dahlfors, *Adv. Mater.* **2007**, *19*, 3201–3213.

7. G. Lanzani, *Nat. Mater.* **2014**, *13*, 775–776.

8. G. G. Malliaras, *Biochim. Biophys. Acta* **2013**, *1830*, 4286–4287.

9. K. Svennersten, K. C. Larsson, M. Berggren, A. Richter-Dahlfors, *Biochim. Biophys. Acta* **2011,** *1810*, 276–285.

10. V. F. Petrenko N. Maeno, *J. Phys. Colloq.* **1987**, *48*, C1-115–C1-119.

11. Z. G. Chiragwandi, O. Nur, M. Willander, N. Calander, *Appl. Phys. Lett.* **2003**, *83*, 5310–5312.

12. R. Fan, S. Huh, R. Yan, J. Arnold, P. Yang, *Nat. Mater.* **2008,** *7*, 303–307.

13. C. Zhong, Y. Deng, A. F. Roudsari, A. Kapetanovic, M. P. Anantram, M. Rolandi, *Nat. Commun.* **2011**, *2*, 476.

14. Y. Deng, E. Josberger, J. Jin, A. F. Rousdari, B. A. Helms, C. Zhong, M. P. Anantram, M. Rolandi, *Sci. Rep.* **2013**, *3*, 2481.

15. A. M. Deml, A. L. Bunge, M. A. Reznikov, A. Kolessov, R. P. O'Hayre, *J. Appl. Phys.* **2012**, *111*, 074511.

16. W. J. Crookes, L.-L. Ding, Q. L. Huang, J. R. Kimbell, J. Horwitz, M. J. McFall-Ngai, *Science* **2004**, *303*, 235–238.

17. R. M. Kramer, W. J. Crookes-Goodson, R. R. Naik, *Nat. Mater.* **2007**, *6*, 533–538.

18. A. R. Tao, D. G. DeMartini, M. Izumi, A. M. Sweeney, A. L. Holt, D. E. Morse, *Biomaterials* **2010**, *31*, 793–801.

19. M. Izumi, A. M. Sweeney, D. DeMartini, J. C. Weaver, M. L. Powers, A. Tao, T. V. Silvas, R. M. Kramer, W. J. Crookes-Goodson, L. M. Mäthger, R. R. Naik, R. T. Hanlon, D. E. Morse, *J. R. Soc. Interface* **2010**, *7,* 549–560.

20. L. Phan, W. G. WalkupIV, D. D. Ordinario, E. Karshalev, J.-M. Jocson, A. M. Burke, A. A. Gorodetsky, *Adv. Mater.* **2013**, *25*, 5621–5625.

21. D. D. Ordinario, L. Phan, W. G. Walkup IV, J. M. Jocson, E. Karshalev, N. Hüsken, and A. A. Gorodetsky, *Nat. Chem.* **2014**, *6*, 596–602.

22. S. Cukierman, *Biochim. Biophys. Acta, Bioenerg.* **2006**, *1757*, 876–885.

23. E. Stavrinidou, P. Leleux, H. Rajaona, D. Khodagholy, J. Rivnay, M. Lindau, S. Sanaur, G. G. Malliaras, *Adv. Mater.* **2013**, *25*, 4488–4493.

24. I. Kymissis, in *Organic Field Effect Transistors: Theory, Fabrication and Characterization, Integrated Circuits and Systems*, Springer, New York, **2009**.

CHAPTER 4   Production and Electrical Characterization of the Reflectin A2 Isoform From *Doryteuthis (Loligo) pealeii*

4.1: Abstract

Cephalopods have recently emerged as a source of inspiration for the development of novel functional materials. Within this context, a number of studies have explored structural proteins known as reflectins, which play a key role in cephalopod adaptive coloration in vivo and exhibit interesting properties in vitro. Herein, we report an improved high-yield strategy for the preparation and isolation of reflectins in quantities sufficient for materials applications. We first select the *Doryteuthis* (*Loligo*) *pealeii* reflectin A2 (RfA2) isoform as a "model" system and validate our approach for the expression and purification of this protein. We in turn fabricate RfA2-based twoterminal devices and employ both direct and alternating current measurements to demonstrate that RfA2 films conduct protons. Our findings underscore the potential of reflectins as functional materials and may allow a wider range of researchers to investigate their properties.

4.2: Introduction

Cephalopods (squid, octopuses, and cuttlefish) are well known for their sophisticated neurophysiology, complex behavior, and stunning camouflage displays.[1–6] Recently, these animals have drawn significant attention as sources of novel materials for optical systems,[7–10] biomedical technologies,[11–15] and bioelectronic devices.[16–20] Within this context, a number of literature reports have investigated the properties of unique structural proteins known as reflectins,[7–10,14,16–18,21–24]

which are found in cephalopod skin cells (i.e. leucophores, iridophores, and chromatophores).[25–30] In vivo, reflectins in general have been shown to play important roles in cephalopod adaptive coloration by serving as components of optically-active ultrastructures, including layered stacks of membrane-enclosed platelets in iridophores,[25,26] membrane-bound arrangements of spherical microparticles in leucophores,[27,28] and interconnected networks of pigment granules in chromatophores.[29,30] In vitro, the *Doryteuthis* (*Loligo*) *pealeii* reflectin A1 (RfA1) isoform has found applications in reconfigurable infrared camouflage coatings that are actuated by chemical and mechanical stimuli,[7,8] proton-conducting films with electrical figures of merit rivaling those of some artificial analogues,[16–18] and biocompatible substrates that support the proliferation and differentiation of neural stem cells.[14] Overall, reflectins' fascinating properties have provided a strong impetus for their continued exploration from both fundamental and applied perspectives.

Herein, we describe an improved methodology for the production of difficult-to-handle reflectins in quantities sufficient for materials applications. We first select the *Doryteuthis* (*Loligo*) *pealeii* reflectin A2 (RfA2) isoform as a "model" system for electrical characterization and validate a new high-yield strategy for the expression and purification of this precipitation-prone protein. We subsequently fabricate and characterize two-terminal devices for which RfA2 thin films constitute the active layer. We in turn interrogate RfA2-based devices featuring palladium and palladium hydride electrodes via direct current electrical measurements and RfA2-based devices featuring gold electrodes via alternating current electrical measurements. From our experiments, we glean that RfA2 is an effective proton-conducting material, with properties similar to those of RfA1. Overall, our findings underscore the potential of reflectins as functional materials and may allow a wider range of researchers to investigate their properties.

4.3: Experimental Section

4.3.1: Expression and Purification of Reflectin A2

Histidine-tagged wild type reflectin A2 (RfA2) was expressed and purified *via* a protocol that was modified from an analogous one previously reported for wild type reflectin A1 (RfA1)[31,32]. In brief, an *E. coli* codon optimized gene coding for histidine-tagged wild type RfA2 from *Doryteuthis (Loligo) pealeii* (Genbank: ACZ57765.1) was synthesized and cloned into the pJExpress414 vector (DNA2.0). The vector was transformed into BL21(DE3) cells (Novagen). RfA2 was expressed at 37 °C using Overnight Express Instant Terrific Broth (TB) media (Novagen) supplemented with 100 µg mL^{-1} Carbenicillin. RfA2 was insoluble when expressed at 37 °C and was sequestered in inclusion bodies. The inclusion bodies were then extracted by using BugBuster® (Novagen) according to the manufacturer's suggested protocols. The inclusion bodies were subsequently solubilized in denaturing buffer (pH 7.4, 50 mM sodium phosphate, 300 mM
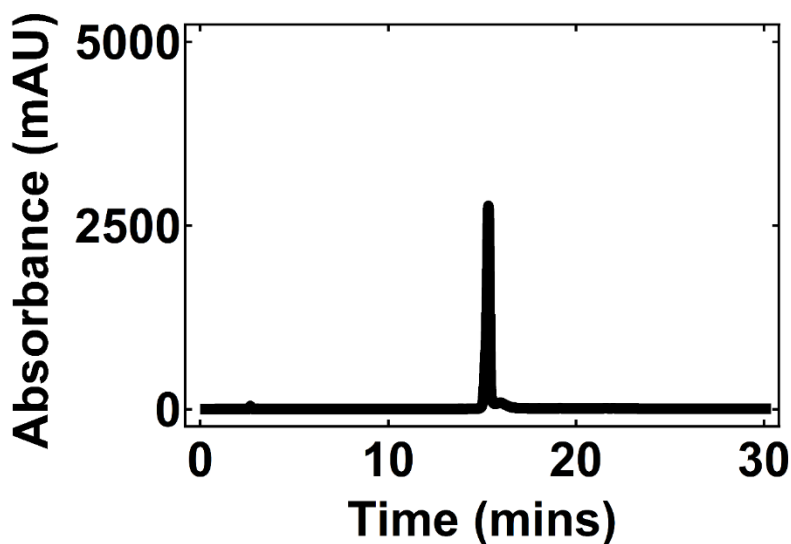
Figure 4.1: A typical analytical reverse phase HPLC chromatogram for RfA2 obtained after inclusion body filtration and concentration. The elution of the protein was monitored at a wavelength of 280 nm. The peak indicates excellent purity.

sodium chloride, 6 M guanidine hydrochloride) through repeated manual agitation and sequentially filtered through 5, 0.45, and 0.22 μm filters. The protein was next purified by high-performance liquid chromatography (HPLC) on an Agilent 1260 Infinity system using an Agilent reverse phase C18 column with a gradient evolved from 95% Buffer A:5% Buffer B to 5% Buffer A:95% Buffer B at a flow rate of 1 mL min-1 over 30 minutes (Buffer A: 99.9% H2O, 0.1% TFA; Buffer B: 95% acetonitrile, 4.9% H2O, 0.1% TFA) (Figure 4.1). The fractions containing RfA2 were pooled, flash frozen in liquid nitrogen, and lyophilized, yielding > 200 mg of pure RfA2 protein per liter of *E. coli* cell culture.

A2_reflectin (100%), 29,199.9 Da
A2 reflectin
19 exclusive unique peptides, 41 exclusive unique spectra, 264 total spectra, 195/236 amino acids (83% coverage)

MHHHHHHNRY   MMR **HRPMYSN**   **MYR** TGRK **YRG**   **VMEPMSRMTM**   **DFQGRYMDSQ**   **GRMVDPRYYD**   **YGRCHDYDRY**   **YGRSMFNYGP**
NMDGQRYGGW   **MDFPERYMDM**   **SGYQMDMHGR**   **WMDSQGRYCN**   **PMGHSWSNRQ**   **GYYPGSNYGR**   **NMFNPERYMD**   **MSGYQMDMQG**
RWMDMGGRHV   **NPFSHSMYGR**   **NMFNPSYFSN**   **RHMDNPERYM**   **DMSGYQMDMQ**   **GR** WMDTQGRY   MDPSWSNMYD   NYNSWY

Figure 4.2: A tryptic peptide sequence coverage map obtained from tandem mass spectrometry analysis of the trypsin-digested of the histidine-tagged RfA2 protein. Bolded amino acids with a yellow background correspond to amino acids comprising tryptic peptides. Bolded amino acids with a green background correspond to oxidized amino acids comprising tryptic peptides. The total sequence coverage of ~ 83 % confirmed the purified protein's identity as RfA2 from *Doryteuthis pealeii*.

4.3.2: Characterization of Reflectin A2

Wild type RfA2 was characterized according to a general protocol, which was adopted from the literature[31-34]. Throughout the purification process, purified and unpurified reflectin samples were analyzed by sodium dodecyl sulfate polyacrylamide gel electrophoresis (SDS-PAGE) and GelCode Blue Staining (Thermo) using an Invitrogen XCell *SureLock* Mini using NuPAGE Novex 4-12% Bis-Tris gels, with NuPAGE MOPS as the running buffer under reducing conditions. Stained protein bands were routinely subjected to in-gel tryptic digestion, as confirmation of protein identity[31-33]. After digestion, the peptides were separated on a reverse phase C18 chromatography column and analyzed by mass spectrometry either on a Synapt G2

instrument (Waters) outfitted with an electrospray ionization source or on an EASY-nLC system (Proxeon Biosystems, now Thermo Scientific) connected to a hybrid LTQ-FT spectrometer (Thermo Scientific) equipped with a nanoelectrospray ion source (Proxeon Biosystems, now Thermo Scientific)[31,34]. The resulting sequence coverages routinely exceeded > 80 % for RfA2 (Figure 4.2).

4.3.3: Fabrication of Reflectin A2-based Devices

The two-terminal devices were fabricated using a protocol modified from established procedures[32]. In brief, silicon dioxide/silicon or glass substrates (International Wafer Service, Inc.) were first cleaned in Piranha solution (1:3 hydrogen peroxide to sulfuric acid) and washed thoroughly. To fabricate devices for two-terminal direct current measurements, arrays of paired electrodes consisting of a 4 nm chromium adhesion layer overlaid with a 40 nm palladium layer were electron-beam evaporated onto SiO$_2$/Si substrates through a shadow mask. The dimensions of the palladium paired electrodes were 100 μm wide by 400 μm long, with an inter-electrode separation of 50 μm. To fabricate devices for two-terminal alternating current measurements, arrays of paired electrodes consisting of a 4 nm chromium adhesion layer overlaid with a 40 nm gold layer were electron-beam evaporated onto glass substrates through a shadow mask. The dimensions of the gold paired electrodes were 2.5 cm wide by 3 cm long with an inter-electrode separation of 100 μm. For all devices, aqueous solutions containing HPLC-purified RfA2 were prepared and subsequently dropcast onto the electrodes. The resulting films were dried in ambient conditions, and the excess material was scribed away mechanically, leaving the desired completed devices. To convert electron-injecting palladium (Pd) electrodes to proton-injecting palladium

hydride (PdH_x) electrodes, the devices were exposed to a 5% hydrogen/95% argon atmosphere both before and during the electrical measurements.

4.3.4: Physical Characterization of Reflectin A2-based Devices

The devices were characterized with optical and atomic force microscopy, as previously described[31,32]. The dimensions of the reflectin films were determined from analysis of optical images obtained with a Zeiss Axio Imager A1 Microscope. The thicknesses of both dry and humidified reflectin films were determined from the analysis of topographical scans obtained with an Asylum Research MFP-3D Atomic Force microscope outfitted with an Asylum Research Humidity Sensing Cell.

4.3.5: Electrical Characterization of Reflectin A2-based Devices

The completed devices were characterized electrically in two different configurations according to established procedures[32]. The direct current measurements were performed on a Cascade Microtech PM-5 Probe Station outfitted with an Agilent 4156C Semiconductor Parameter Analyzer, with the current was recorded as a function of voltage at a scan rate of ~ 0.6 V/s. The direct current measurements for palladium-contacted and palladium hydride-contacted devices were performed under 100% argon and 5% hydrogen/95% argon atmospheres, respectively. The alternating current measurements were performed with a 4294A Impedance Analyzer (Agilent) at various frequencies with a constant applied voltage of 500 mV. The alternating current measurements for gold-contacted devices were performed under a 100% argon atmosphere. All electrical experiments were performed at an 80% relative humidity, which was monitored with a Fisher Scientific hygrometer.
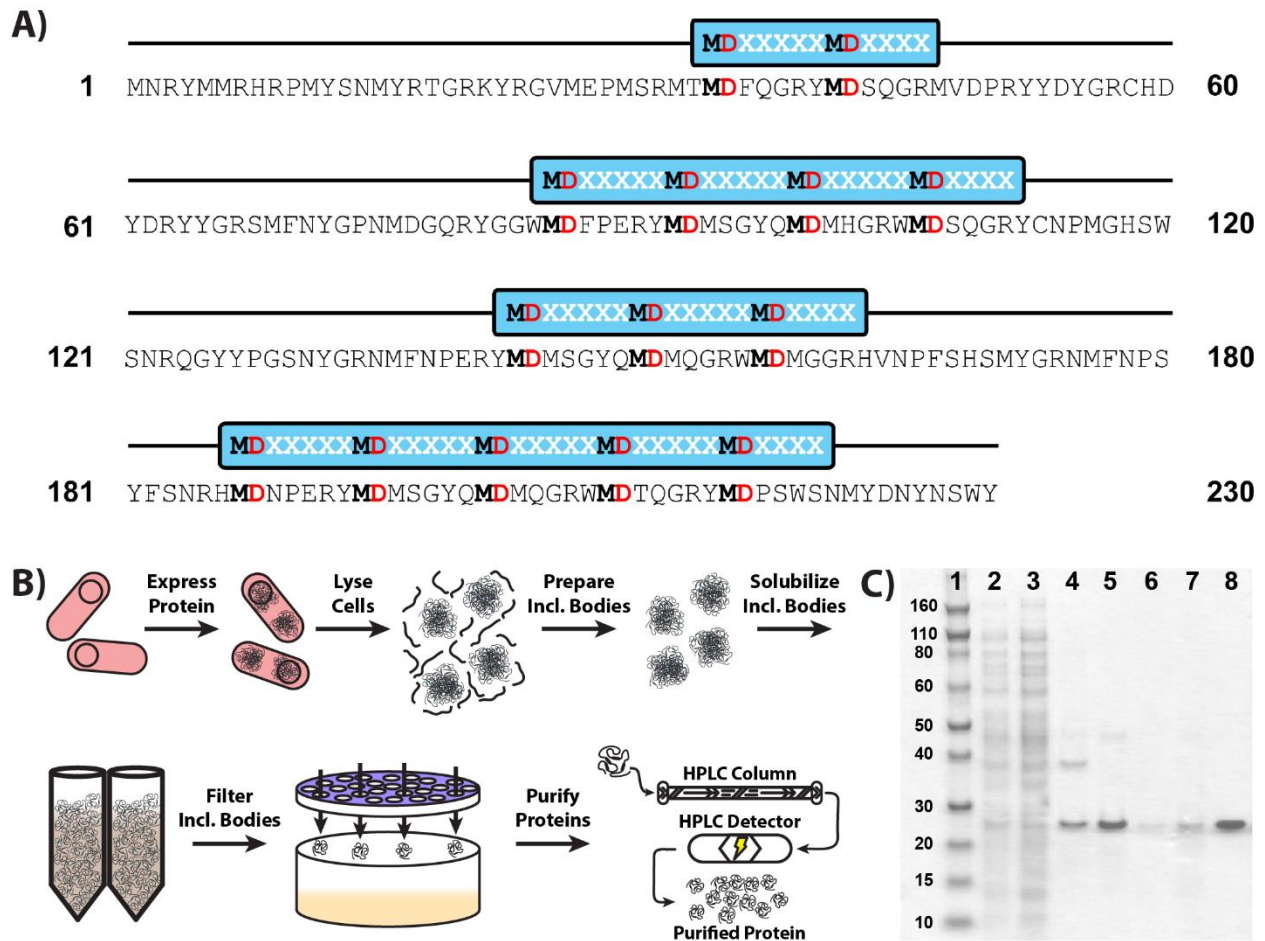
Figure 4.3: (A) Illustration of the primary sequence of *Doryteuthis* (*Loligo*) *pealeii* reflectin A2. The conserved sequence motifs of the form (M/F–D–X_5)(M–D–X_5)$_n$(M–D–$X_{3/4}$) are indicated above the sequence in light blue. The conserved aspartic acid and methionine residues present in the subdomains are indicated in bolded red and bolded black, respectively. **(B)** Illustration of the expression and purification of RfA2. The procedure entails protein expression, cell lysis, inclusion body preparation, inclusion body solubilization, inclusion body filtration, and protein purification via high performance liquid chromatography. **(C)** Analysis of the expression and purification of RfA2 via sodium dodecyl sulfate polyacrylamide gel electrophoresis (SDS-PAGE). The stain indicates the total protein. The individual lanes correspond to: lane 1, 10–160 kDa molecular weight standards; lane 2, total protein; lane 3, soluble protein; lane 4, insoluble protein; lane 5, solubilized inclusion bodies; lane 6, filtered inclusion bodies; lane 7, concentrated filtered inclusion bodies; lane 8, HPLC eluate.

4.4: Results and Discussion

Having previously demonstrated that *Doryteuthis* (*Loligo*) *pealeii* reflectin A1 is an excellent proton conductor,[16–18] we sought to extend these studies and explore the electrical functionality of other reflectins. For our experiments, we specifically selected *Doryteuthis* (*Loligo*)

pealeii reflectin A2 (Figure 4.3A) due to its key biological role in the dynamic optical functionality of iridophores[23,26] and its similarity to reflectins from other squid species (with the exception of reflectin B1). Indeed, RfA2 from D. pealeii features a >60% pair-wise amino acid sequence identity with the majority of isolated reflectins from *E. scolopes*,[21] *D. opalescens*,[26] and *L. forbesi*,[35] and much like its homologues, this reflectin variant contains multiple characteristic $(M/F–D–X_5)(M–D–X_5)_n(M–D–X_{3/4})$ sequence motifs and large percentages of both aromatic and charged amino acids (Figure 4.3A).[23,26] Furthermore, although the biochemical characterization of RfA2 has been reported,[23,24,26] the protein has not been studied as a functional material to date and possesses completely unexplored electrical properties. Given the aforementioned considerations, we viewed RfA2 as a judicious "model" reflectin for electrical characterization and further investigation.

We began our studies by developing and implementing an improved strategy for the production of RfA2 in high yield (Figure 4.3B), with each step of the revised procedure monitored via gel electrophoresis (Figure 4.3C). First, we used protocols validated for RfA1 to heterologously express histidine-tagged RfA2 in E. coli,[7,16] finding that the protein was sequestered within intracellular inclusion bodies (as reported for RfA1). The inclusion bodies were then prepared/isolated through several rounds of non-ionic detergent extraction and centrifugation. Subsequently, the nearly pure RfA2 (from the inclusion bodies) was solubilized through repeated manual agitation. Here, when attempting to purify the protein via immobilized metal ion affinity chromatography (IMAC), we found that even under denaturing conditions, RfA2 was prone to irreversible self-assembly into larger aggregates and/or spontaneous precipitation (as reported for some reflectins).[9,10,22,24] Our standard protocol[7,16] thus furnished relatively small amounts of material, which were appropriate for basic characterization but not adequate for high throughput

device fabrication. Consequently, rather than relying upon a time-consuming, expensive, and difficult IMAC step, we revised our procedure and simply filtered the RfA2 solutions to remove any insoluble debris and/or precipitates. We in turn isolated the desired protein from the filtrate via high performance liquid chromatography (HPLC), obtaining typical estimated purities of >95% (Figure 4.1). Finally, we confirmed the identity of the protein via in-gel tryptic digestion and tandem mass spectrometry, obtaining typical sequence coverages of >80% (Figure 4.2). Notably, due to the use of histidine-tagged RfA2, we were able to directly compare the efficacy of the previously reported[7,16] and current procedures, discovering that our new streamlined strategy not only avoided a challenging column chromatography step but also improved the yield by well over an order of magnitude to >200 mg of pure protein per liter of cell culture.

With our desired material in hand, we proceeded to fabricate two-terminal bottom contact devices according to the scheme illustrated in Figure 4.4A.[16–18] First, we prepared arrayed palladium or gold metal contacts on either silicon dioxide/silicon or glass substrates, respectively, *via* electron beam physical vapor deposition through a shadow mask. Next, we dropcast aqueous solutions of RfA2 directly onto the electrode arrays. We then allowed the residual solvent to evaporate, prior to removing excess material through mechanical scribing. These arrayed devices enabled high throughput physical and electrical characterization of RfA2 films.

We next characterized our RfA2-based devices with optical microscopy and atomic force microscopy (AFM).[16–18] The optical microscopy experiments indicated that the RfA2 active layers contained few apparent defects (a representative image for a palladium-contacted device is shown in Figure 4.4B). The AFM experiments indicated that the RfA2 films were relatively uniform with root mean square (RMS) roughnesses of >3 nm (a representative image is shown in Figure 4.4C).

The physical characterization experiments confirmed the integrity of our films and facilitated interpretation of the electrical measurements.
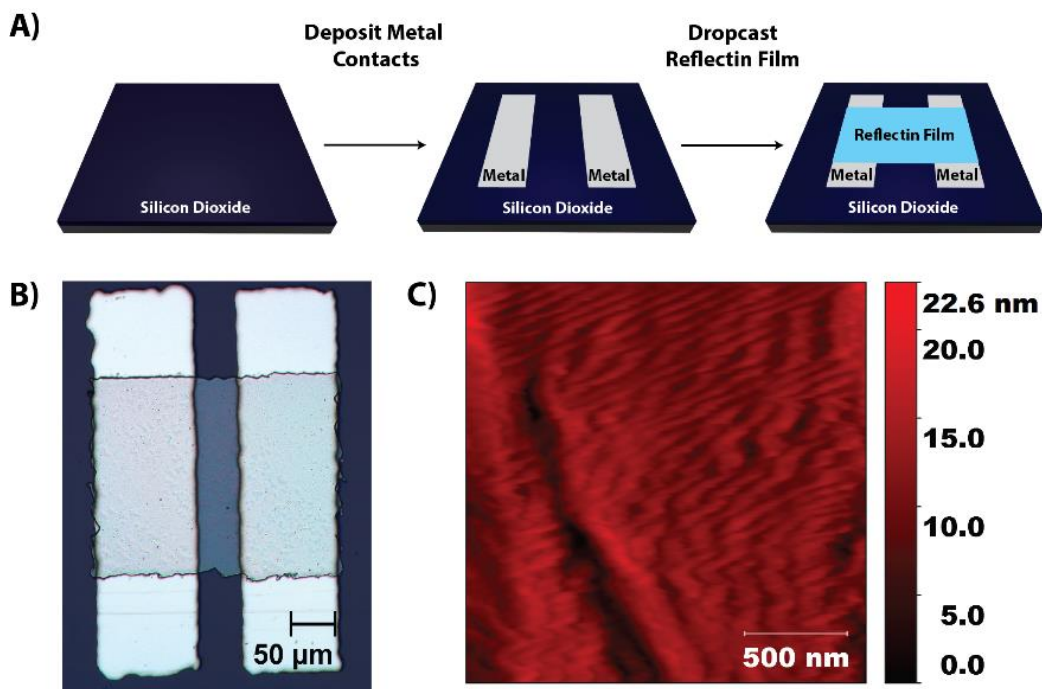
Figure 4.4: (A) General scheme for the fabrication of RfA2-based devices. **(B)** A representative optical image of a completed device for which an RfA2 film bridges two palladium electrodes. **(C)** A representative atomic force microscopy (AFM) image of an RfA2 film.

We subsequently investigated the electrical properties of RfA2 films contacted by proton-blocking palladium and proton-injecting palladium hydride electrodes (Figure 4.5A). Thus, we first recorded current (I) as a function of voltage (V) at a relative humidity (RH) of 80% for palladium-contacted devices (a representative measurement is shown in Figure 4.5B). From the I–V characteristics, we extracted an average current density of $7.3 \pm 4.5 \times 10^{-4}$ A cm^{-2} at 1.5 V across 6 independent palladium-contacted devices. We in turn formed proton-transparent palladium hydride contacts via exposure of the palladium contacts to hydrogen gas in situ (Figure 4.5A),[16–20,36] prior to again recording current as a function of voltage at an RH of 80% (a

representative measurement is shown in Figure 4.5B). From the I–V characteristics, we extracted

an average current density of $1.8 \pm 0.6 \times 10^{-2}$ A cm^{-2} at 1.5 V across 6 independent palladium

hydride-contacted devices. Here, we found that the characteristics displayed hysteresis between

the forward and reverse scans and that the observed current density increased by more than an

order of magnitude upon conversion of the contacts from proton-blocking to proton-injecting (in

close agreement with literature precedent for RfA1[16–18] and derivatized chitosan[19,20]). Interestingly,

the current density found for RfA2 was lower than the current density of $\sim 2.6 \times 10^{-2}$ A cm^{-2}

previously found for RfA1 at an RH = 80%.[16] This difference could be rationalized by analyzing

the two proteins' histidine-tagged amino acid sequences (Figure 4.6); relative to RfA1, RfA2
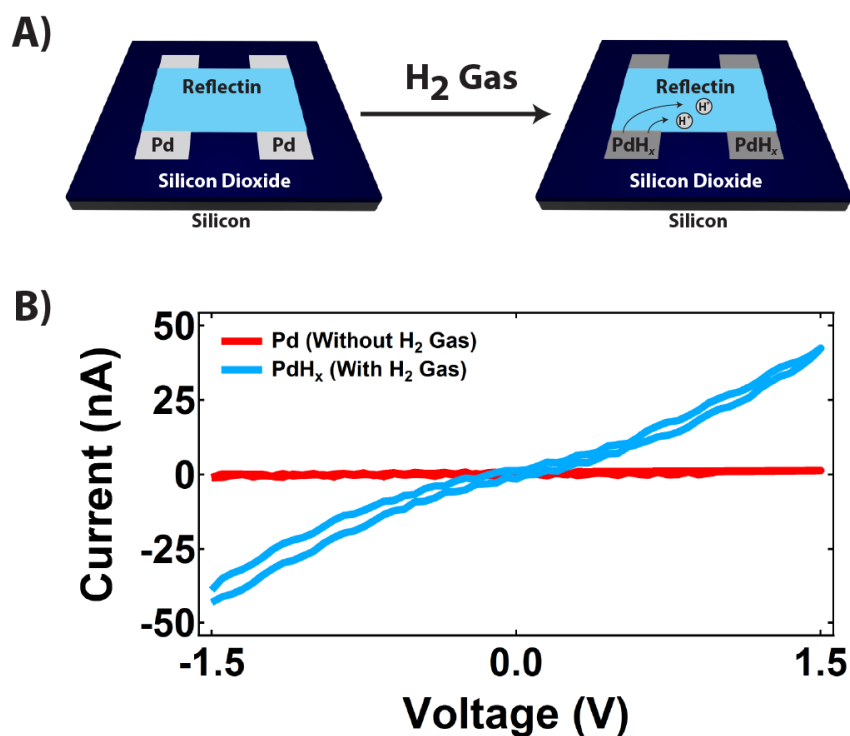
Figure 4.5: (A) An illustration of an RfA2-based two-terminal device before and after in situ treatment with hydrogen (H$_2$) gas. The palladium (Pd) electrodes are converted to palladium hydride (PdH$_x$) electrodes in the presence of H$_2$, enabling the injection of protons into the film. **(B)** The current versus voltage characteristics of an RfA2 film contacted with palladium (red) and palladium hydride (blue) electrodes. The magnitude of the current increases by more than an order of magnitude upon moving from proton-blocking to proton-injecting electrodes. Both the forward and reverse scans are shown for each measurement.

possesses a small but significant decrease in its percentage of charged amino acids (which are crucial for proton transport)[16] and thus might be expected to function less effectively as a proton conductor. Altogether, our observations provided strong evidence that RfA2 was a proton-conducting material.

```
A2    -MHHHHHHNRYMMRHRPMYSNMYRTGRKYRGVMEPMSRMTMDFQGRYMDSQGRMVDPRYY
A1    MAHHHHHHNRYLNRQR-LY-NMYRN--KYRGVMEPMSRMTMDFQGRYMDSQGRMVDPRYY

A2    D-YGRCHDYDRYYGRSMFNYGPNMDGQRYGGWMDFPERYMDMSGYQMDMHGRWMDSQGRY
A1    DYYGRMHDHDRYYGRSMFNQGHSMDSQRYGGWMDNPERYMDMSGYQMDMQGRWMDAQGRF

A2    CNPMGHSWSNRQGYYPG-----SNYGRNMFN------------PERYMDMSGYQMDMQG
A1    NNPFGQMWHGRQGHYPGYMSSHSMYGRNMYNPYHSHYASRHFDSPERWMDMSGYQMDMQG

A2    RWMDMGGRHVNPFSHSMYGRNMFNP--SYFSNRHMDNPERYMDMSGYQMDMQGRWMDTQG
A1    RWMDNYGRYVNPFNHHMYGRNMCYPYGNHYYNRHMEHPERYMDMSGYQMDMQGRWMDTHG

A2    RYMDP-----------------------------------SWSNMYDNY-------
A1    RHCNPFGQMWHNRHGYYPGHPHGRNMFQPERWMDMSGYQMDMQGRWMDNYGRYVNPFSHN

A2    ----------------------------------NSW-------------------
A1    YGRHMNYPGGHYNYHHGRYMNHPERHMDMSSYQMDMHGRWMDNQGRYIDNFDRNYYDYHM

A2    Y
A1    Y
```

Figure 4.6: A sequence alignment of histidine-tagged reflectin A2 and histidine-tagged reflectin A1[31,32] from *D. pealeii.* The alignment was generated by using the MUSCLE software[42,43]. The charged amino acids (D, E, H, K, R) are highlighted in yellow, and they constitute 27.5% of the sequence for RfA2 and 30.3% of the sequence RfA1.

To gain additional insight into the electrical properties of RfA2, we used electrochemical impedance spectroscopy to interrogate RfA2 films contacted by gold electrodes in the presence of water (H_2O) and deuterium oxide (D_2O) vapor (Figure 4.7A). Thus, we first recorded Nyquist plots of the imaginary versus the real parts of the impedance at an RH of 80% for devices in the presence of H_2O (a representative measurement is shown in Figure 4.7B). By fitting our curves with a simple equivalent circuit that accounted for the bulk impedance and capacitive effects at the electrodes,[16] we extracted an average conductivity of $7.4 \pm 2.0 \times 10^{-5}$ S cm^{-1} across 5 independent devices in the presence of H_2O. We in turn altered the environment from H_2O to D_2O vapor in situ (Figure

4.7A), prior to again recording the imaginary versus the real parts of the impedance at an RH of 80% (a representative measurement is shown in Figure 4.7B). From fits of this data, we extracted an average conductivity of $4.3 \pm 1.1 \times 10^{-5}$ S cm^{-1} across 5 independent devices in the presence of D_2O. Here, we found that our plots displayed a semicircle in the high-frequency region and an inclined spur in the low-frequency region, in line with both literature precedent for RfA1[16] and expectations for ion-conducting materials contacted by blocking electrodes.[37–41] Importantly, we also noted a clear kinetic isotope effect for the RfA2 films, with a decrease of ~40% in their average conductivity upon moving from H_2O to D_2O vapor. Together, our observations provided additional compelling evidence that RfA2 was a proton-conducting material.
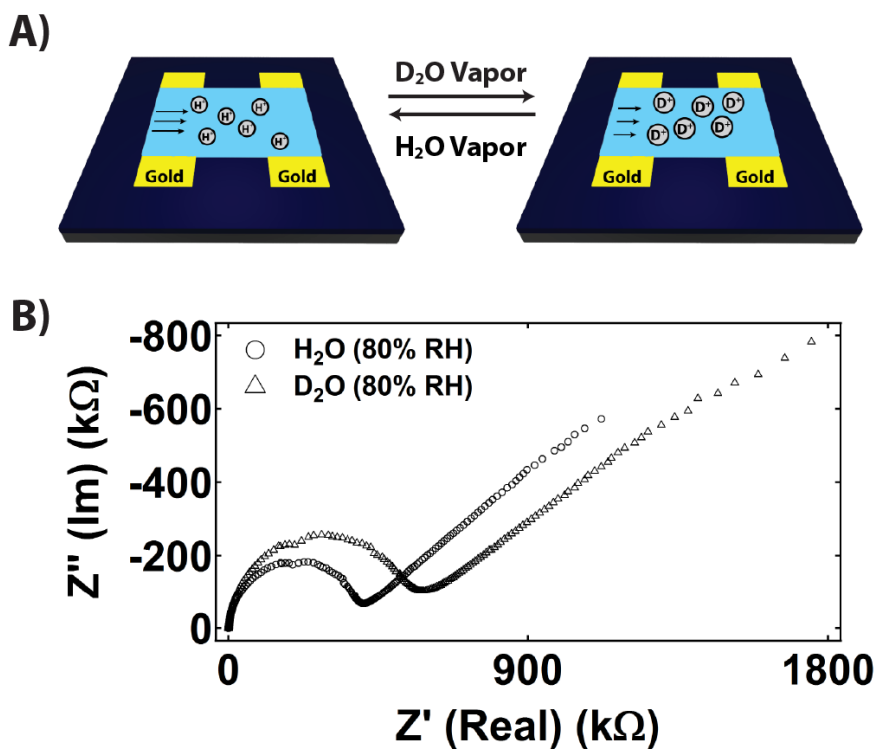
Figure 4.7: (A) An illustration of a two-terminal RfA2-based device in the presence of water (H_2O) vapor and deuterium oxide (D_2O) vapor. **(B)** A representative Nyquist plot of the imaginary versus the real parts of the impedance for an RfA2-based two-terminal device in the presence of H_2O (open circles) and D_2O (open triangles). There is a change in the effective film resistance upon moving from H_2O to D_2O, demonstrating the kinetic isotope effect for the RfA2 film.

4.5: Conclusion

In conclusion, we have demonstrated an improved methodology for the production of reflectins in quantities sufficient for materials applications, and our findings constitute a significant advance for several reasons. First, our straightforward protocol omits a challenging chromatography step and enables the expression and purification of potentially difficult-to-handle reflectins in high yield, as demonstrated for the RfA2 "model" system. The presented strategy should be broadly applicable for the production of arbitrary reflectin variants (and perhaps even unrelated proteins) that are sequestered within inclusion bodies (for example, we have included the gel electrophoresis data for RfA1 produced via our protocol in Figure 4.8). Furthermore, our methodology has enabled the exploration of RfA2's electrical functionality for the first time, adding to the limited body of knowledge currently available for reflectins' materials properties. Based on the sequence similarity between various reflectins and the demonstrated electrical functionality of both RfA1 and RfA2, we cautiously postulate that protonic conductivity may be a general property of these proteins (although our hypothesis certainly warrants additional investigation). Finally, due to its relatively short amino acid sequence (when compared to RfA1), RfA2 may hold value as a platform for establishing relationships between structure and in vitro function for the reflectin family of proteins. Altogether, our observations highlight the potential of reflectins as functional materials and may afford new opportunities for the study of their multi-faceted properties.
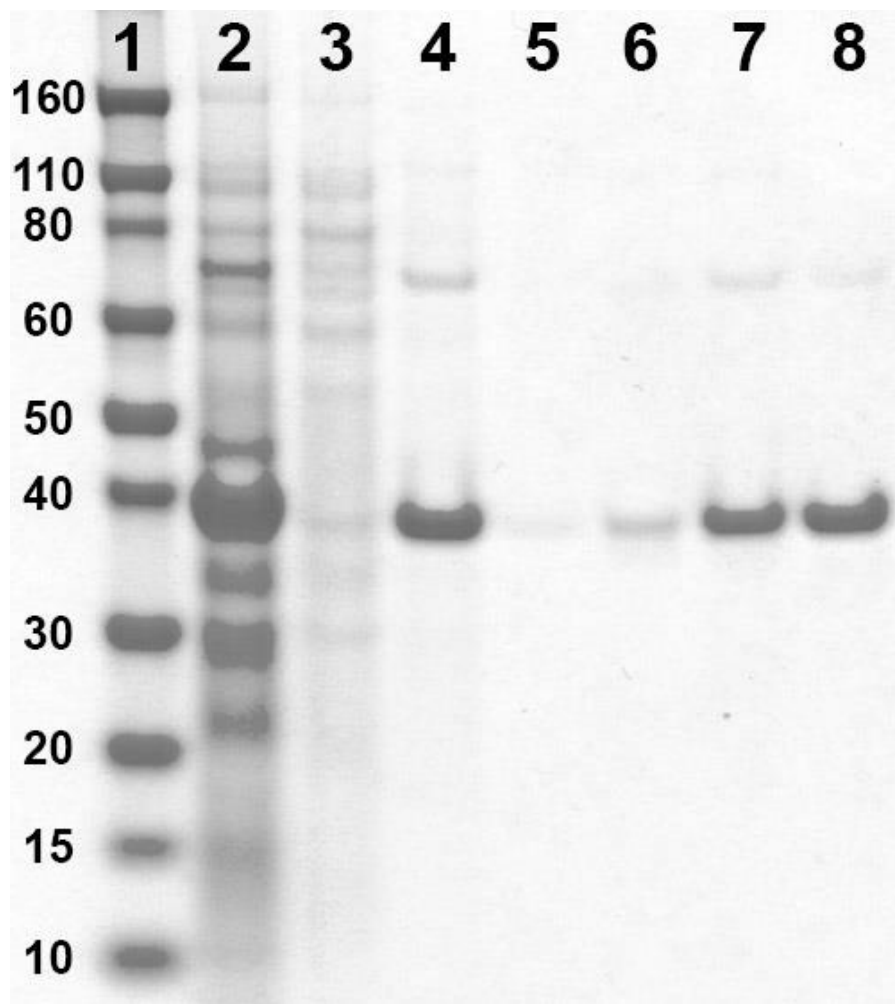
Figure 4.8: Analysis of the expression and purification of histidine-tagged RfA1[31,32] *via* sodium dodecyl sulfate polyacrylamide gel electrophoresis (SDS-PAGE). The overall procedure was identical to the one described for RfA2 above. The stain indicates the total protein. The individual lanes correspond to: lane 1, 10-160 kDa molecular weight standards; lane 2, total protein; lane 3, soluble protein; lane 4, insoluble protein; lane 5, solubilized inclusion bodies; lane 6, filtered inclusion bodies; lane 7, concentrated filtered inclusion bodies; lane 8, HPLC eluate. After HPLC purification, RfA1 produced via this method was indistinguishable from the one produced via the previously reported protocols[31,32].

4.6: Acknowledgements

directed and supervised research which forms the basis for the material in the chapter. Author Contributions: D. D. O. and A. A. G. conceptualized and designed the experiments; D. D. O., L. P., W. G. W. IV, Y. V. D., E. M. L., and M. N. performed the research; L. P. and W. G. W. IV designed and cloned the genes; L. P., E. M. L., J. K., and M. N. expressed and purified the protein; D. D. O., I. K., and A. A. G. analyzed the data; and D. D. O. and A. A. G. wrote the paper.

4.7: References

1. N. J. Abbott, R. Williamson, L. Maddock, in *Cephalopod Neurobiology: Neuroscience Studies in Squid, Octopus, and Cuttlefish*, Oxford University Press, Oxford, **1995**.

2. L. Borrelli, G. Fiorito, in *Learning and Memory: A Comprehensive Reference*, ed. J. H. Byrne, Academic Press, Oxford, **2008**, ch. 1.31, pp. 605–627.

3. R. T. Hanlon, J. B. Messenger, in *Cephalopod Behaviour*, Cambridge University Press, United Kingdom, **1998**.

4. L. M. Mäthger, E. J. Denton, N. J. Marshall, R. T. Hanlon, *J. R. Soc., Interface* **2009**, *6*, 149–163.

5. R. T. Hanlon, C.-C. Chiao, L. M. Mäthger, K. C. Buresch, A. Barbosa, J. J. Allen, L. Siemann, C. Chubb, in *Animal Camouflage: Mechanisms and Functions*, ed. M. Stevens and S. Merilaita, Cambridge University Press, Cambridge, **2011**, ch. 9, pp. 145–163.

6. G. Kaufman, C. Orlt, Kings of Camouflage, Producers. *Cuttlefish: The Brainy Bunch* [Television Broadcast], Public Broadcasting Service (PBS), **2011**.

7. L. Phan, W. G. Walkup IV, D. D. Ordinario, E. Karshalev, J.-M. Jocson, A. M. Burke, A. A. Gorodetsky, *Adv. Mater.* **2013**, *25*, 5621–5625.

8. L. Phan, D. D. Ordinario, E. Karshalev, W. G. Walkup IV, M. Shenk, A. A. Gorodetsky, *J. Mater. Chem. C* **2015**, *3*, 6493–6498.

9. R. M. Kramer, W. J. Crookes-Goodson, R. R. Naik, *Nat. Mater.* **2007**, *6*, 533–538.

10. G. Qin, P. B. Dennis, Y. Zhang, X. Hu, J. E. Bressner, Z. Sun, W. J. Crookes-Goodson, R. R. Naik, F. G. Omenetto, D. L. Kaplan, *J. Polym. Sci., Part B: Polym. Phys.* **2013**, *51*, 254–264.

11. J. Jin, V. Reese, R. Coler, D. Carter, M. Rolandi, *Adv. Healthcare Mater.* **2014**, *3*, 349–353.

12. P. Hassanzadeh, M. Kharaziha, M. Nikkhah, S. Shin, J. Jin, S. He, W. Sun, C. Zhong, M. Dokmeci, A. Khademhosseini, M. Rolandi, *J. Mater. Chem. B* **2013**, *1*, 4217–4224.

13. A. Cooper, C. Zhong, Y. Kinoshita, R. Morrison, M. Rolandi, M. Zhang, *J. Mater. Chem.* **2012**, *22*, 3105–3109.

14. L. Phan, R. Kautz, J. Arulmoli, I. H. Kim, D. T. T. Le, M. A. Shenk, M. M. Pathak, L. A. Flanagan, F. Tombola, A. A. Gorodetsky, *ACS Appl. Mater. Interfaces* **2016**, *8*, 278–284.

15. Y. J. Kim, W. Wu, S. E. Chun, J. Whitacre, C. J. Bettinger, *Proc. Natl. Acad. Sci. U. S. A.* **2013**, *110*, 20912–20917.

16. D. D. Ordinario, L. Phan, W. G. Walkup IV, J.-M. Jocson, E. Karshalev, N. Hüsken, A. A. Gorodetsky, *Nat. Chem.* **2014**, *6*, 596–602.

17. D. D. Ordinario, L. Phan, J.-M. Jocson, T. Nguyen, A. A. Gorodetsky, *APL Mater.* **2015**, *3*, 014907.

18. D. D. Ordinario, L. Phan, Y. Van Dyke, T. Nguyen, A. G. Smith, M. Nguyen, N. M. Mofid, M. K. Dao, A. A. Gorodetsky, *Chem. Mater.* **2016**, *28*, 3703–3710.

19. C. Zhong, Y. Deng, A. F. Roudsari, A. Kapetanovic, M. P. Anantram, M. Rolandi, *Nat. Commun.* **2011**, *2*, 476.

20. Y. Deng, E. Josberger, J. Jin, A. F. Rousdari, B. A. Helms, C. Zhong, M. P. Anantram, M. Rolandi, *Sci. Rep.* **2013**, *3*, 2481.

21. W. J. Crookes, L. L. Ding, Q. L. Huang, J. R. Kimbell, J. Horwitz, M. J. McFall-Ngai, *Science* **2004**, *303*, 235–238.

22. A. R. Tao, D. G. DeMartini, M. Izumi, A. M. Sweeney, A. L. Holt, D. E. Morse, *Biomaterials* **2010**, *31*, 793–801.

23. M. Izumi, A. M. Sweeney, D. G. DeMartini, J. C. Weaver, M. L. Powers, A. R. Tao, T. V. Silvas, R. M. Kramer, W. J. Crookes-Goodson, L. M. Mäthger, R. R. Naik, R. T. Hanlon, D. E. Morse, *J. R. Soc., Interface* **2010**, 7, 549–560.

24. R. Levenson, C. Bracken, N. Bush, D. E. Morse, *J. Biol. Chem.* **2016**, 291, 4058–4068.

25. D. G. DeMartini, D. V. Krogstad, D. E. Morse, *Proc. Natl. Acad. Sci. U. S. A.* **2013**, *110*, 2552–2556.

26. D. G. DeMartini, M. Izumi, A. T. Weaver, E. Pandolfi, D. E. Morse, *J. Biol. Chem.* **2015**, *290*, 15238–15249.

27. D. G. DeMartini, A. Ghoshal, E. Pandolfi, A. T. Weaver, M. Baum, D. E. Morse, J. *Exp. Biol.* **2013**, *216*, 3733–3741.

28. L. Mäthger, S. L. Senft, M. Gao, S. Karaveli, G. R. R. Bell, R. Zia, A. M. Kuzirian, P. B. Dennis, W. J. Crookes-Goodson, R. R. Naik, G. W. Kattawar, R. T. Hanlon, *Adv. Funct. Mater.* **2013**, *23*, 3980–3989.

29. L. F. Deravi, A. P. Magyar, S. P. Sheehy, G. R. R. Bell, L. M. Mäthger, S. L. Senft, T. J. Wardill, W. S. Lane, A. M. Kuzirian, R. T. Hanlon, E. L. Hu, K. K. Parker, *J. R. Soc., Interface* **2014**, *11*, 20130942.

30. J. B. Messenger, *Biol. Rev. Cambridge Philos. Soc.* **2001**, *76*, 473–528.

31. L. Phan, W. G. Walkup IV, D. D. Ordinario, E. Karshalev, J.-M. Jocson, A. M. Burke, A. A. Gorodetsky, *Adv. Mater.* 2013, **25**, 5621–5625.

32. D. D. Ordinario, L. Phan, W. G. Walkup IV, J.-M. Jocson, E. Karshalev, N. Hüsken, A. Gorodetsky, *Nat. Chem.* 2014, **6**, 596–602.

33. A. Kalli, S. Hess, *Proteomics* 2012, **12**, 21–31.

34. A. Shevchenko, H. Tomas, J. Havlis, J. V. Olsen, M. Mann, *Nat. Protoc.* 2006, **1**, 2856–2860.

35. J. L. Weiss, N. A. Evans, T. Ahmed, J. D. J. Wrigley, S. Khan, C. Wright, J. N. Keen, A. Holzenburg, J. B. C. Findlay, *Biochim. Biophys. Acta, Biomembr.* **2005**, *1668*, 164–174.

36. H. Morgan, R. Pethig, G. T. Stevens, *J. Phys. E: Sci. Instrum.* **1986**, *19*, 80–82.

37. E. Barsoukov, J. R. Macdonald, in *Impedance Spectroscopy: Theory, Experiment and Applications, 2nd ed.*, Wiley, Hoboken, **2005**.

38. X.-Z. Yuan, C. Song, H. Wang, J. Zhang, in *Electrochemical Impedance Spectroscopy in PEM Fuel Cells: Fundamentals and Applications*, Springer, New York, **2012**.

39. R. A. Huggins, *Ionics* **2002**, *8*, 300–313.

40. Z. Xie, C. Song, B. Andreaus, T. Navessin, Z. Shi, J. Zhang, S. Holdcroft, *J. Electrochem. Soc.* **2006**, *153*, 173–178.

41. T. Soboleva, Z. Xie, Z. Shi, E. Tsang, T. Navessin, S. Holdcroft, *J. Electroanal. Chem.* **2008**, *622*, 145–152.

42. R. C. Edgar, *Nucleic Acids Res.* **2004**, *32*, 1792 – 1797.

43. R. C. Edgar, *BMC Bioinf.* **2004**, *5*, 113.

CHAPTER 5   Photochemical Doping of Protonic Transistors From Reflectin

5.1: Abstract

The field of bioelectronics has the potential to revolutionize both fundamental biology and personalized medicine. As such, much research effort has been devoted to the development of devices and materials that are intrinsically compatible with biological systems. Within this context, several recent studies have focused on protonic transistors from naturally occurring materials, such as squid-derived polysaccharides and proteins. Herein, we report the rational design, fabrication, and characterization of two- and three-terminal protonic devices, for which the active material consists of a protein-based proton conductor doped with a small molecular photoacid. We electrically interrogate these devices both in the absence and presence of illumination, demonstrating that an exogenous photophysical stimulus selectively enhances their electrical properties. Our findings hold significance for understanding and controlling proton transport not only in bioelectronic platforms but also across a wide range of voltage-regulated proton-conducting materials and device platforms.

5.2: Introduction

Organic bioelectronics, an emerging field focused on the integration of biological and electronic systems, has the potential to revolutionize both fundamental biology and personalized medicine.[1-8] Within this area, protonic transistors from naturally occurring materials (such as

squid-derived polysaccharides and proteins) have garnered attention as an exciting new class of devices.[9-13] Relative to their traditional inorganic counterparts, protonic transistors from biological materials offer a number of advantages, including straightforward fabrication, ease of chemical functionalization, favorable mechanical properties, enhanced sensitivity, and intrinsic biocompatibility.[1-12] Moreover, given the crucial and ubiquitous role of proton translocation in biological processes,[14-18] these devices appear particularly well-suited for the direct and sensitive transduction of biochemical events into electrical signals. Consequently, protonic transistors, of which there have been very few examples reported to date,[19-22] hold great promise for transformative bioelectronics applications and constitute highly relevant targets for further research and development.

The electrical functionality of protonic transistors is similar to that of classic field effect transistors (FETs) from inorganic materials.[9-13] Indeed, for these devices, the source-drain current (I_{DS}) at different source-drain voltages (V_{DS}) is determined by the proton charge carrier density in the active channel and modulated via the application of a gate voltage (V_{GS}).[9-13] Given this operating principle, proton conduction in the active layer of the prototypical device shown in Figure 5.1A can be described in a manner similar to electron and hole conduction in inorganic semiconductors; such parallels were initially suggested more than 50 years ago by Eigen and de Maeyer[23] and recently expanded upon by the Rolandi Group.[10, 13] Within the context of this proposed model, the devices' active layer contains proton-donating functional groups, which release free protons as the charge carriers, and a network of hydrogen-bonded water molecules, which permeates the active layer[9, 10] and facilitates proton transport via the Grotthuss mechanism (Figure 5.1B).[24-26] The energetics associated with charge transport in the active layer are in turn calculated from the Gibbs–Helmholtz equation and represented by a straightforward diagram
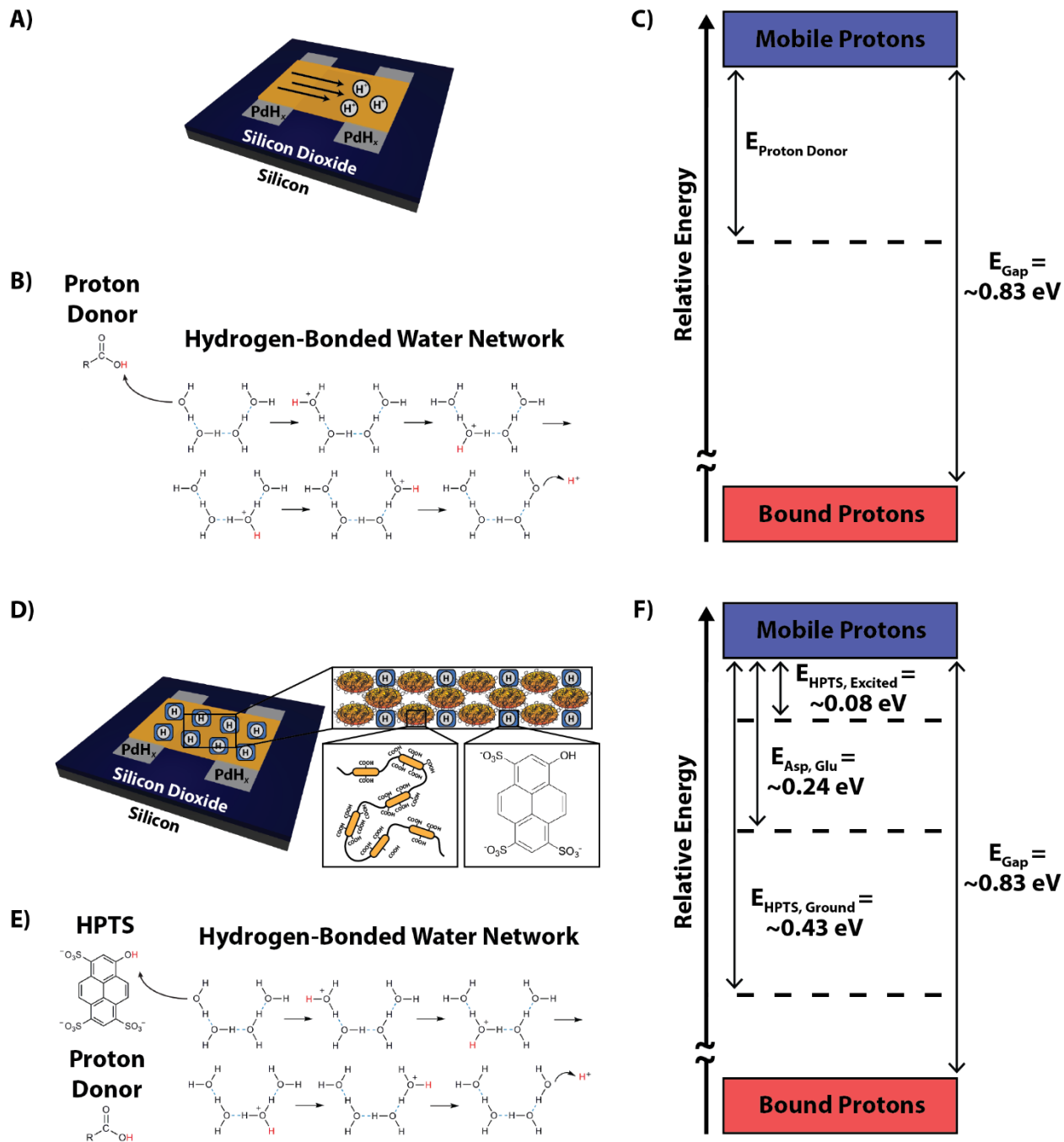
Figure 5.1: **(A)** A schematic of a prototypical protonic transistor. **(B)** An illustration of the translocation of a mobile proton (red) along a chain of hydrogen-bonded water molecules. The mobile proton originates from ionizable chemical groups. **(C)** An illustration of the energy diagram for a prototypical protonic device. The bound and mobile protons are separated by an energy gap of 0.83 eV and proton donors possess effective energies within this gap. **(D)** A schematic of a protonic transistor from reflectin (orange) and HPTS (blue). **(E)** An illustration of proton translocation along a chain of hydrogen-bonded water molecules in an HPTS-doped reflectin-based device. The mobile proton (red) may originate from the HPTS' hydroxy group or from the carboxyl groups of reflectin's aspartic or glutamic acid residues ($E_{Asp,Glu} = \sim 0.24$ eV). **(F)** An illustration of the energy diagram for an HPTS-doped reflectin-based device. HPTS serves as a proton trap in its ground state ($E_{HPTS,Ground} = \sim 0.43$ eV) and as a proton donor in its excited state ($E_{HPTS,Excited} = \sim 0.08$ eV).

(Figure 5.1C).[10, 13] In the energy diagram, the bound protons of water molecules and mobile protons in flux between hydrogen bonds are separated by an energy gap of $E_{Gap} = 0.83$ eV, as calculated from the dissociation constant of water K_w (Figure 5.1C).[10] Furthermore, the active material's proton-donating functional groups serve as dopants and possess effective energies within the gap that are dictated by their individual acid dissociation constants K_a (Figure 5.1C). In its totality, the above conceptual framework makes it possible to understand, engineer, and rationally manipulate the behavior of protonic transistors.

Herein, we demonstrate the modulation of the electrical properties of two- and three-terminal protonic devices via exogenous triggering of a photochemical reaction. We first design devices for which the active layer consists of a protein-based proton conductor doped with a small molecular photoacid. We subsequently fabricate two-terminal variants of such devices and electrically interrogate them both in the absence and presence of illumination, observing an increase in current due to selective excitation of the incorporated dopant. We in turn study the behavior of analogous three-terminal devices (protonic transistors) and show that their charge carrier density is controlled with both applied voltages and photochemical stimuli. Our findings hold relevance for understanding and controlling proton transport in a variety of voltage-regulated proton-conducting materials and device platforms.

5.3: Experimental Section

5.3.1: Preparation of Wild-Type and Mutant Reflectins

Wild-type reflectin A1 and mutant reflectin A1, which features a "randomized" amino acid sequence, were expressed and purified according to a general established protocol.[11, 12] In brief,

the pJExpress414 expression vectors containing either wild-type or mutant reflectin were transformed into BL21(DE3) cells (Novagen). The desired reflectin variant was expressed at 37 °C using Overnight Express Instant Terrific Broth (TB) media (Novagen) supplemented with 100 μg mL^{-1} Carbenicillin. The protein was completely insoluble when expressed at 37 °C and was sequestered in inclusion bodies prepared using Novagen BugBuster according to the manufacturer's suggested protocol. The inclusion bodies were then solubilized in denaturing buffer (pH 7.4, 50 mM sodium phosphate, 300 mM sodium chloride, 6 M guanidine hydrochloride) and purified under denaturing conditions on HisPur Cobalt Resin (Thermo Scientific) immobilized metal affinity chromatography (IMAC) gravity columns according to the manufacturer's protocols. The protein was eluted by using denaturing buffer supplemented with 250 mM imidazole. The fractions containing reflectin were pooled and concentrated on Millipore Amicon Concentrators before further purification with high-performance liquid chromatography (HPLC) on an Agilent 1260 Infinity system using an Agilent reverse phase C18 column with a gradient evolved from 95% Buffer A:5% Buffer B to 5% Buffer A:95% Buffer B at a flow rate of 1 mL min^{-1} over 30 min (Buffer A: 99.9% H$_2$O, 0.1% TFA; Buffer B: 95% acetonitrile, 4.9% H$_2$O, 0.1% TFA). The pure reflectin fractions were pooled, flash frozen in liquid nitrogen, and lyophilized. The identity of the purified protein was confirmed by in-gel tryptic digestion and tandem mass spectrometry on a Thermo Orbitrap instrument outfitted with an electrospray ionization source. The protein concentrations and yields were quantified via the Bradford protein assay with bovine serum albumin (BSA) as a standard (BioRad).

5.3.2: Fabrication of Reflectin-Based Devices

The two-terminal devices and transistors were fabricated by a protocol modified from established procedures.[11, 12] In brief, SiO$_2$/Si substrates (International Wafer Service, Inc.) were

first cleaned in Piranha solution (1:3 hydrogen peroxide to sulfuric acid) and washed thoroughly. Subsequently, arrays of paired electrodes consisting of a 4 nm chromium adhesion layer overlaid with a 40 nm palladium layer were electron-beam evaporated onto the clean substrates through a shadow mask. The paired electrodes possessed dimensions of 100 μm by 400 μm, as well as a separation of 50 μm. Aqueous solutions containing HPLC-purified wild-type or mutant reflectin A1 and proton donors (either HPLC-purified HPTS or MPTS) were then prepared. Solutions of either 900 μM wild-type reflectin; 900 μM wild-type reflectin and 100 μM HPTS; 900 μM wild-type reflectin and 100 μM MPTS; or 900 μM mutant reflectin and 100 μM HPTS were in turn cast onto the electrodes. The resulting films were dried in ambient atmosphere, and the excess material was scribed away mechanically, leaving a completed device. To form proton-injecting PdH_x electrodes that would not be readily depleted of protons, the devices were exposed to a 5% hydrogen/95% argon atmosphere both before and during the electrical measurements.[9-12, 27, 28]

5.3.3: Physical Characterization of Reflectin-Based Devices

The devices were characterized with optical and atomic force microscopy, as previously described,[11, 12] and with fluorescence microscopy. The length and width of the reflectin films were determined from analysis of optical images obtained with a Zeiss Axio Imager A1m Microscope outfitted with an X-Cite 120 Light Source. The thicknesses of both dry and humidified reflectin films were extracted from the analysis of topographical scans obtained with an Asylum Research MFP-3D Atomic Force Microscope outfitted with an Asylum Research Humidity Sensing Cell. The presence and distribution of HPTS in the reflectin films was determined from analysis of fluorescence images obtained on a Leica DM4000-B Microscope outfitted with a Lumecor Light Engine Sola 6-LCR-SB Light Source and an LED 405 Filter Cube, which was equipped with a

bandpass excitation filter (center wavelength of 405 nm and fwhm wavelength of 60 nm) and a bandpass emission filter (center wavelength of 470 nm and fwhm wavelength of 40 nm).

5.3.4: Electrical Characterization of Reflectin-Based Devices

The completed devices were electrically characterized in two different configurations by modifying a previously described procedure.[11, 12] The electrical experiments were performed on a Cascade Microtech PM-5 Probe Station outfitted with an Agilent 4156C Semiconductor Parameter Analyzer. The scan rate was ~ 0.6 V s^{-1} for the measurements. All experiments were performed under a 5% hydrogen/95% argon atmosphere and 90% relative humidity (which was constantly monitored with a Fisher Scientific hygrometer). The presence of hydrogen gas ensured that the palladium hydride electrodes were not depleted of protons during the experiments.[9-12, 27, 28] For the two-terminal measurements, the current was recorded as a function of voltage either without illumination, with illumination from a HDE Corp. blue laser light source (413 nm peak wavelength, 50 mW power, ~ 0.2 W/cm^2 power density), or with illumination from a Shenzhen Ezoneda Technology Co. red laser light source (657 nm peak wavelength, 5 mW power, ~ 0.2 W/cm^2 power density). For the three-terminal measurements, the source-drain current was recorded as a function of the source-drain voltage at various applied gate voltages either without illumination or with illumination from the blue laser light source. All experiments were performed at a consistent laser intensity.

5.3.5: Analysis of the Electrical Data

The figures of merit for reflectin devices were extracted from analysis of the current versus voltage characteristics by following standard literature procedures.[9-12] For the two-terminal devices, the reported current densities were calculated by dividing the measured current by the

cross-sectional area of the reflectin films (width multiplied by the thickness). For the three-terminal devices, the gate capacitance per unit area C_{GS} was first calculated according to Equation #1:

$$C_{GS} = \frac{\varepsilon}{t_{ox}} \quad (1)$$

where ε and t_{ox} are the permittivity and thickness of the gate oxide, respectively. In turn, the conductivity of reflectin for each V_{GS} was calculated from the slope of the I_{DS} versus V_{DS} curves in the low bias regime. Next the proton mobility μ_{H^+} was obtained by fitting a plot of the conductivity as a function of V_{GS} with Equation #2:

$$\mu_{H^+} = \frac{\partial \sigma}{\partial V_{GS}} \cdot \frac{t}{C_{GS}} \quad (2)$$

where $\frac{\partial \sigma}{\partial V_{GS}}$ is the slope of the linear fit, t is the thickness of the reflectin film, and C_{GS} is the gate capacitance per unit area. The proton mobility was then used to calculate the proton concentration n_{H^+} from Equation #3:

$$n_{H^+} = \frac{\sigma_{H^+}}{\mu_{H^+} \cdot e} \quad (3)$$

where σ_{H^+} is the conductivity evaluated at an arbitrary value of V_{GS}, e is the elementary charge, and μ_{H^+} is the proton mobility. The theoretically predicted proton concentration at different V_{GS} values was determined according to Equation #4:

$$n_{H^+} = n_{H^+}^o - \frac{C_{GS} \cdot V_{GS}}{e \cdot t} \quad (4)$$

where n_{H^+} is the theoretically predicted proton concentration at an arbitrary gate bias, $n_{H^+}^o$ is the experimentally observed proton concentration at $V_{GS} = 0$ V, C_{GS} is the gate capacitance per unit area, e is the elementary charge, and t is the film thickness.

5.4: Results and Discussion

We began our experiments by rationally designing bioelectronic devices that featured a photochemical dopant within their proton-conducting active layers (Figure 5.1D). As the conductive biomaterial for our devices, we selected the cephalopod structural protein reflectin.[29-34] This protein represented a judicious choice due to its controllable self-assembly behavior,[11, 12, 30, 31, 33, 34] robustness under harsh conditions,[12, 33] compatibility with other biological systems,[35] and excellent proton transport properties.[11, 12] As the dopant for our devices, we selected the well-known photoacid 8-hydroxypyrene-1,3,6-trisulfonic acid (HPTS), for which photoexcitation makes the proton on its 8-hydroxy group more labile.[36-44] This molecule represented a judicious choice because it has been used to investigate proton generation and transport in Nafion fuel cell membranes,[41] microcrystalline cellulose powders,[42] poly(ethylene glycol) solutions,[43] and fibrillar bovine bovine serum albumin mats.[44] Here, for our device design, free protons would originate from some of the reflectins' charged amino acids and/or the HPTS' hydroxy groups, and then would translocate along a network of hydrogen-bonded water molecules (Figure 5.1E). Although the carboxyl side chains of reflectin's aspartic acid ($pK_a = 3.9$) and glutamic acid ($pK_a = 4.3$) residues would possess fixed energies of $E_{Asp,Glu} = \sim 0.24$ eV,[11] the HPTS' 8-hydroxy groups would possess variable energies of $E_{HPTS,Ground} = \sim 0.43$ eV and $E_{HPTS,Excited} = \sim 0.08$ eV in the molecules' ground ($pK_a = \sim 7.3$) and excited ($pK_a = \sim 1.3$) states, respectively (Figure 5.1F).[36-44]

Therefore, in their ground states, the HPTS molecules would behave as traps, which do not readily donate protons, and in their excited states, the HPTS molecules would behave as dopants, which contribute freely diffusing protons to the hydrogen-bonded water network. Consequently, we expected selective photoexcitation of HPTS to modulate the free charge carrier density and control the electrical properties of doped protonic devices in both two- and three-terminal configurations.
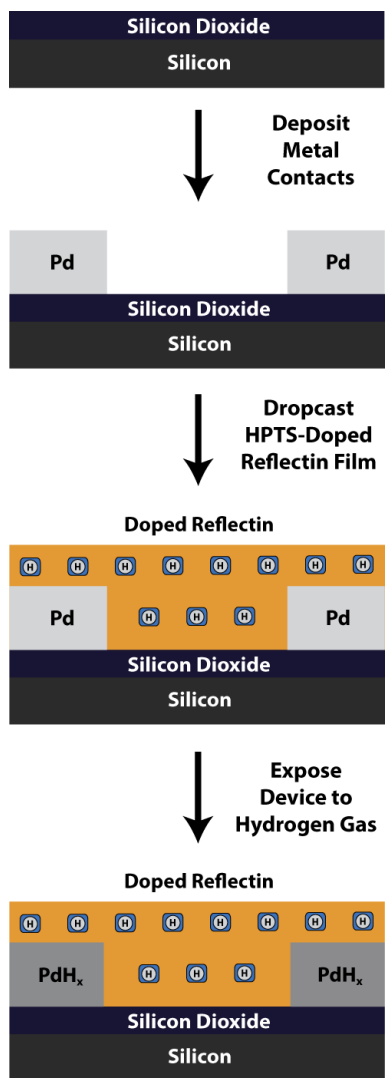
Figure 5.2: Overview of the fabrication process for doped reflectin-based devices. To prepare the devices, palladium contacts are first deposited onto the surface of a silicon dioxide/silicon (SiO_2/Si) substrate. Next, HPTS-doped reflectin is dropcast directly onto the electrodes from aqueous solution. After drying, excess material is removed via mechanical scribing. The palladium contacts are in turn converted to and maintained as proton-injecting palladium hydride contacts through continuous *in situ* exposure to hydrogen gas before and during electrical measurements.
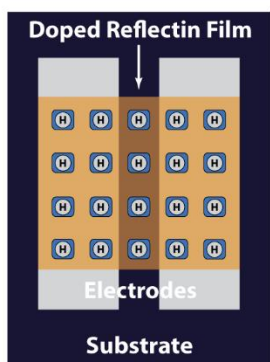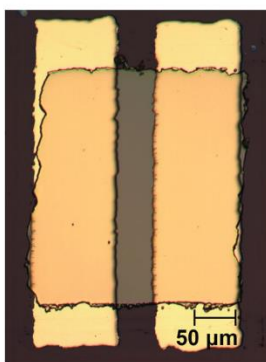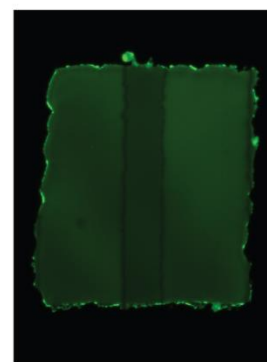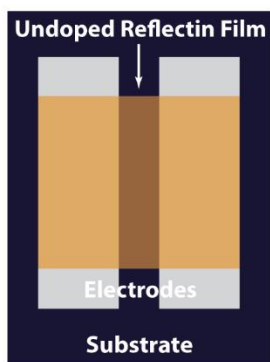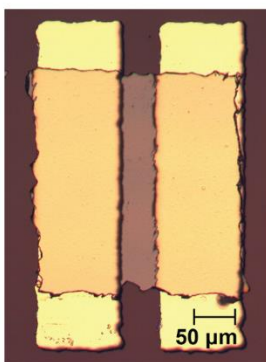
Figure 5.3: (A) A schematic of a two-terminal device where an HPTS-doped reflectin film bridges two electrodes. **(B)** A typical optical microscopy image of a device-integrated HPTS-doped reflectin film. **(C)** A typical fluorescence microscopy image of a device-integrated HPTS-doped reflectin film. **(D)** A schematic of a two terminal device where an undoped reflectin film bridges two electrodes. **(E)** A typical optical microscopy image of a device-integrated undoped reflectin film. **(F)** A typical fluorescence microscopy image of a device-integrated undoped reflectin film.

We proceeded to fabricate the designed protonic devices, for which the active material consisted of a reflectin variant doped with a small molecule, according to the scheme in Figure 5.2. We initially examined these device's constituent HPTS-doped reflectin films with optical and fluorescence microscopy, comparing them to undoped reflectin films. The optical microscopy images demonstrated that both types of films were uniform with few apparent defects (Figure 5.3). However, the fluorescence microscopy images revealed the presence of blue-green fluorescence, which we associated with HPTS, only for the doped reflectin films (the pristine reflectin films

were indistinguishable from the background) (Figure 5.3). Overall, these measurements suggested that the doped reflectin films closely resembled their undoped counterparts but contained uniformly distributed HPTS.
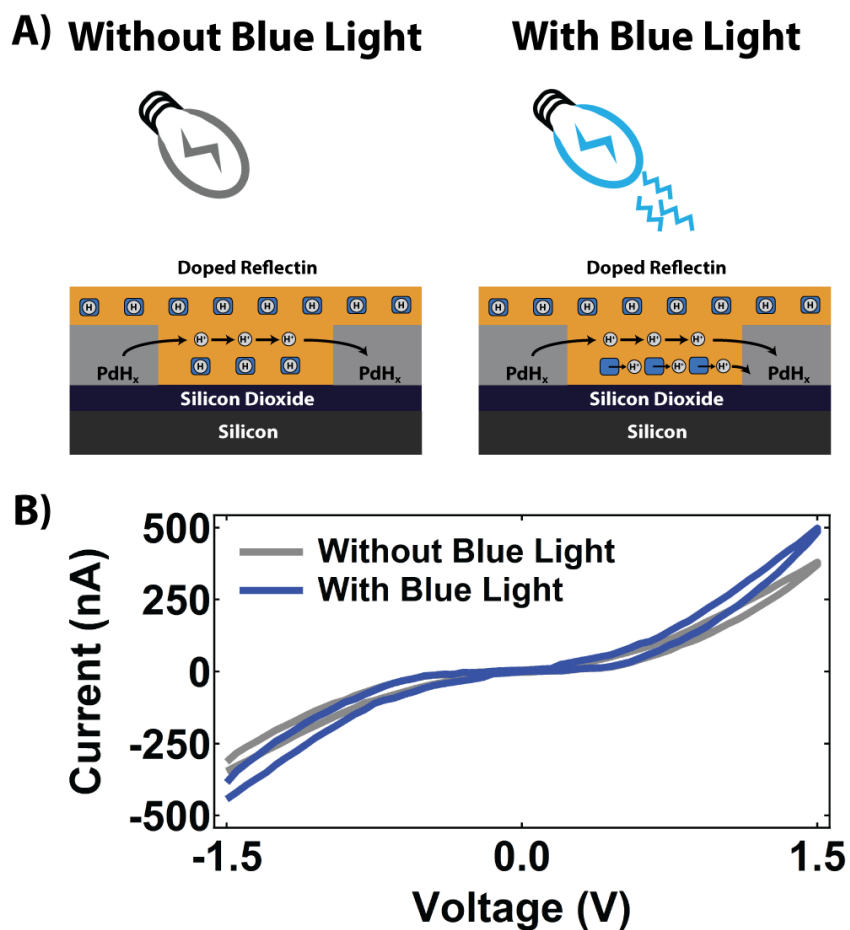
Figure 5.4: (A) Schematic of a two-terminal device from an HPTS-doped reflectin film. Illumination of the device with blue light photoexcites HPTS and induces the release of protons into the film. **(B)** The current versus voltage characteristics of a typical device from an HPTS-doped reflectin film without (gray) and with (blue) blue light illumination. Both the forward and reverse scans are shown.

We initially characterized the electrical properties of two-terminal devices fabricated from HPTS-doped reflectin films without and with blue light illumination (Figure 5.4A). Here, we irradiated HPTS at a wavelength of 413 nm, which is near both its peak absorbance wavelength of 405 nm and pH-independent isosbestic point of 415 nm.[36-40] Such irradiation is well-known to

photoexcite HPTS, thereby substantially lowering the pK_a and making the hydroxy proton more labile.[36-44] As an example, the current–voltage characteristics for a representative HPTS-doped reflectin device are shown in Figure 5.4B. In the absence of blue light, we measured a current density of 6.40×10^{-2} A cm^{-2} at 1.5 V, but in the presence of blue light, we observed a noticeable ~ 31% increase in the current density to 8.39×10^{-2} A cm^{-2} at 1.5 V (Figure 5.4B). Regardless of illumination, the electrical characteristics exhibited hysteresis between the forward and reverse
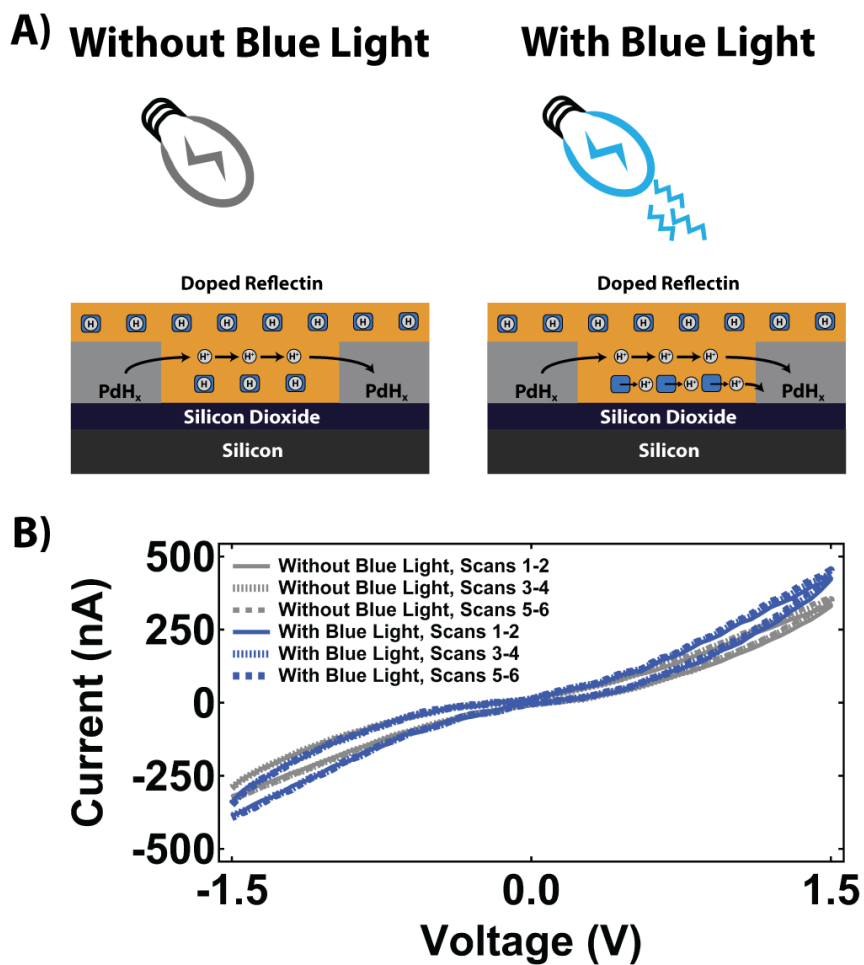
Figure 5.5: (A) An illustration of a two-terminal HPTS-doped reflectin-based device without and with blue light illumination. Illumination of the device with blue light photoexcites HPTS and induces the release of protons into the film. **(B)** The current versus voltage characteristics of a typical device from an HPTS doped reflectin film without (gray) and with (blue) blue light illumination. Without blue light illumination, the electrical properties of the device show very little variability ($\leq$ ~3%) over 6 consecutive scans (the gray solid, dashed, and dotted lines are almost identical). With blue light illumination, the electrical properties of the device also show very little variability ($\leq$ ~3%) over an additional 6 consecutive scans (the blue solid, dashed, and dotted lines are almost identical).

scan directions (as reported for biological proton conductors)[9-12] and changed very little over multiple repeated scan cycles (as shown in Figure 5.5). These experiments led us to postulate that illumination of the doped films was triggering the release of labile protons and thereby leading to a concomitant increase in the protonic current.
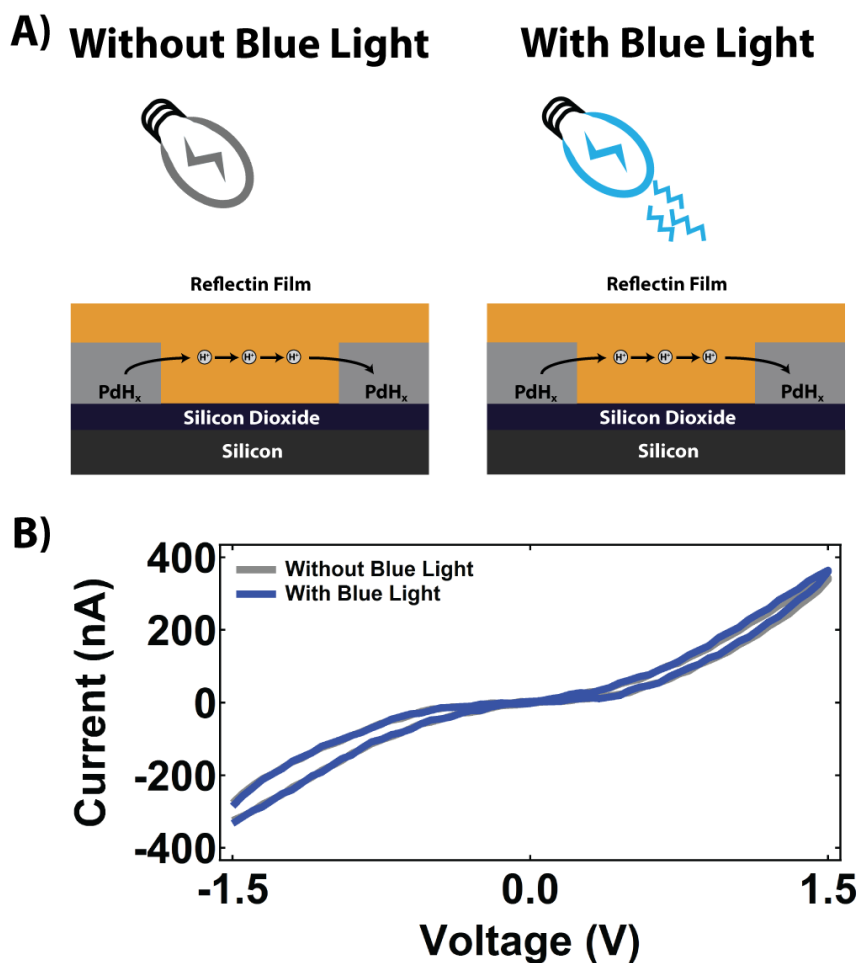
Figure 5.6: (A) An illustration of a two-terminal undoped reflectin-based device without and with blue light illumination. Illumination of the device with blue light has no effect on the charge carrier concentration in the film. **(B)** The current versus voltage characteristics of a typical device from an undoped reflectin film without (gray) and with (blue) blue light illumination. Both the forward and reverse scans are shown.

Next, we investigated the electrical properties of two-terminal devices fabricated from undoped (lacking HPTS) reflectin films without and with blue light illumination (Figure 5.6A). As

an example, the current–voltage characteristics for a representative undoped reflectin device are shown in Figure 5.6B. In the absence of blue light, we measured a current density of 8.84×10^{-2} A cm^{-2} at 1.5 V, and in the presence of blue light, we observed a slight $\sim 4\%$ decrease in the current density to 8.50×10^{-2} A cm^{-2} at 1.5 V (Figure 5.6B). This control suggested that the presence of HPTS was associated with the light-induced increase in protonic current observed for our devices.
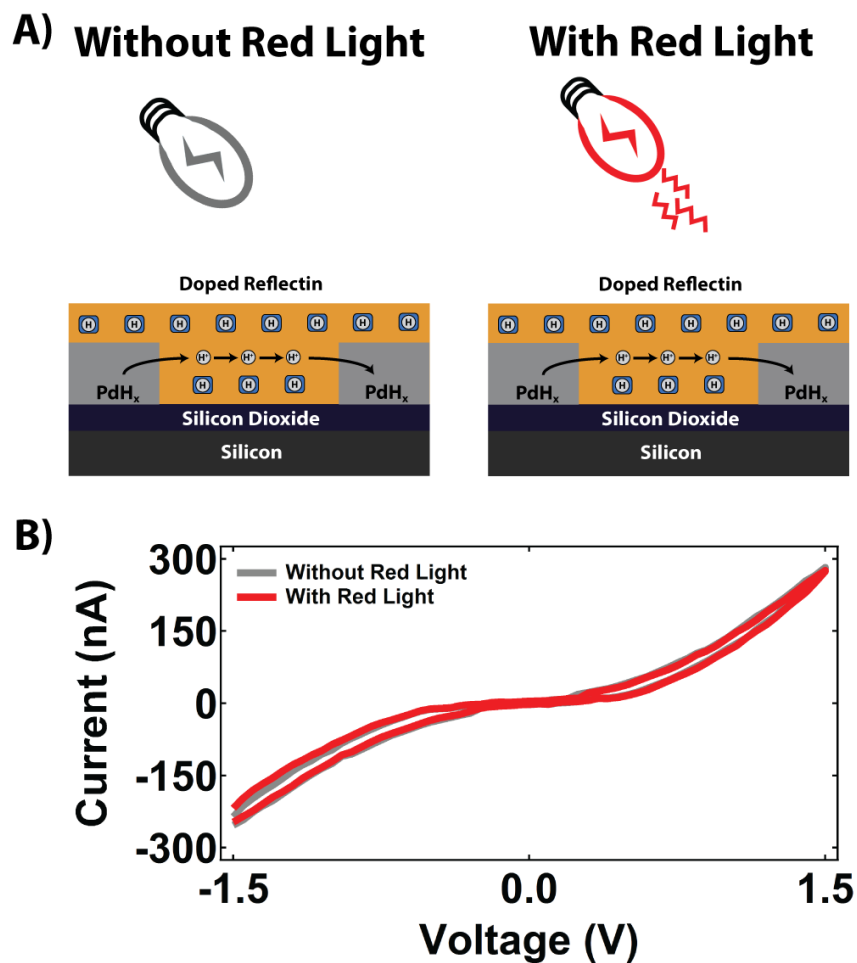
Figure 5.7: **(A)** An illustration of a two-terminal HPTS-doped reflectin-based device without and with red light illumination. Illumination of the device with red light has no effect on the charge carrier concentration in the film. **(B)** The current versus voltage characteristics of a typical device from an undoped reflectin film without (gray) and with (red) red light illumination. Both the forward and reverse scans are shown.

We subsequently studied the electrical properties of two-terminal devices fabricated from HPTS-doped reflectin films without and with red light illumination (Figure 5.7A). Here, we chose a peak wavelength of 657 nm, which was well outside the absorption window of HPTS and would not promote the molecule to its excited state (or affect its pK_a). As an example, the current–voltage characteristics for a representative HPTS-doped reflectin device are shown in Figure 5.7B. In the absence of red light, we measured a current density of 6.44×10^{-2} A cm^{-2} at 1.5 V, and in the presence of red light, we measured a slight ∼ 2% decrease in the current density to 6.31×10^{-2} A cm^{-2} at 1.5 V (Figure 5.7B). This observation indicated that just the presence of HPTS in its ground state (due to the lack of an appropriate stimulus) was not sufficient to induce a protonic current increase in our devices.

We in turn interrogated the electrical properties of two-terminal devices fabricated from reflectin films doped with 8-methoxypyrene-1,3,6-trisulfonic acid (MPTS), both without and with blue light illumination (Figure 5.8A). MPTS is a derivative of HPTS with a methoxy group in place of the hydroxy group, so this molecule, while physically and structurally similar to HPTS, cannot release protons upon photoexcitation.[41, 42, 45] As an example, the current–voltage characteristics for a representative MPTS-doped reflectin device are shown in Figure 5.8B. In the absence of blue light, we measured a current density of 6.70×10^{-2} A cm^{-2} at 1.5 V, but in the presence of blue light, we measured a marginal ∼ 2% increase in the current density to 6.84×10^{-2} A cm^{-2} at 1.5 V (Figure 5.8B). This observation constituted compelling evidence that a specific photochemical reaction was directly responsible for the protonic current increase in our devices.

As an additional demonstration, we investigated the electrical properties of two-terminal devices from an HPTS-doped reflectin mutant without and with blue light illumination (Figure 5.9A). For these studies, we selected a reflectin mutant with a "randomized" amino acid sequence,
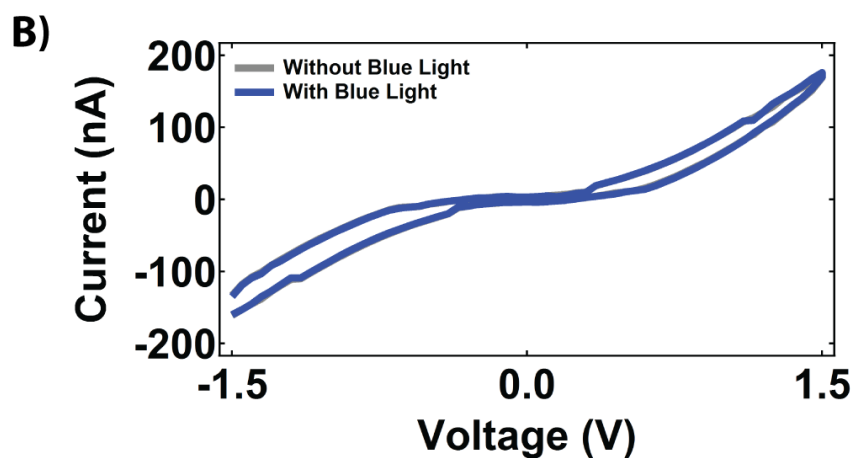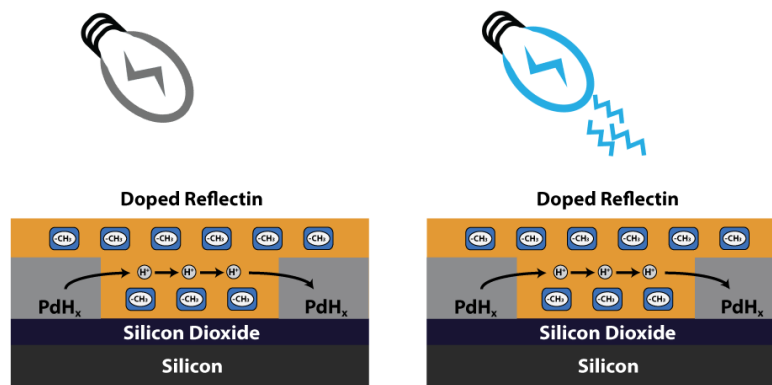
Figure 5.8: **(A)** An illustration of a two-terminal MPTS-doped reflectin-based device without and with blue light illumination. Illumination of the device with blue light has no effect on the charge carrier concentration in the film. **(B)** The current versus voltage characteristics of a typical device from an MPTS-doped reflectin film without (gray) and with (blue) blue light illumination. Both the forward and reverse scans are shown.

which our previous experiments had shown to conduct protons but less effectively than wild-type reflectin.[11] Here, we sought to investigate whether the conductivity of even this relatively poor proton conductor could be augmented with an exogenous photophysical stimulus. As an example, the current–voltage characteristics for a representative HPTS-doped reflectin mutant device are shown in Figure 5.9B. In the absence of blue light, we measured a current density of 1.64×10^{-2} A cm^{-2} at 1.5 V, but in the presence of blue light, we measured a significant $\sim 23\%$ increase in the current density to 2.03×10^{-2} A cm^{-2} at 1.5 V (Figure 5.9B). This experiment served as an

important positive control and further strengthened our assertion that a photochemical reaction accounted for the protonic current increase in our devices.
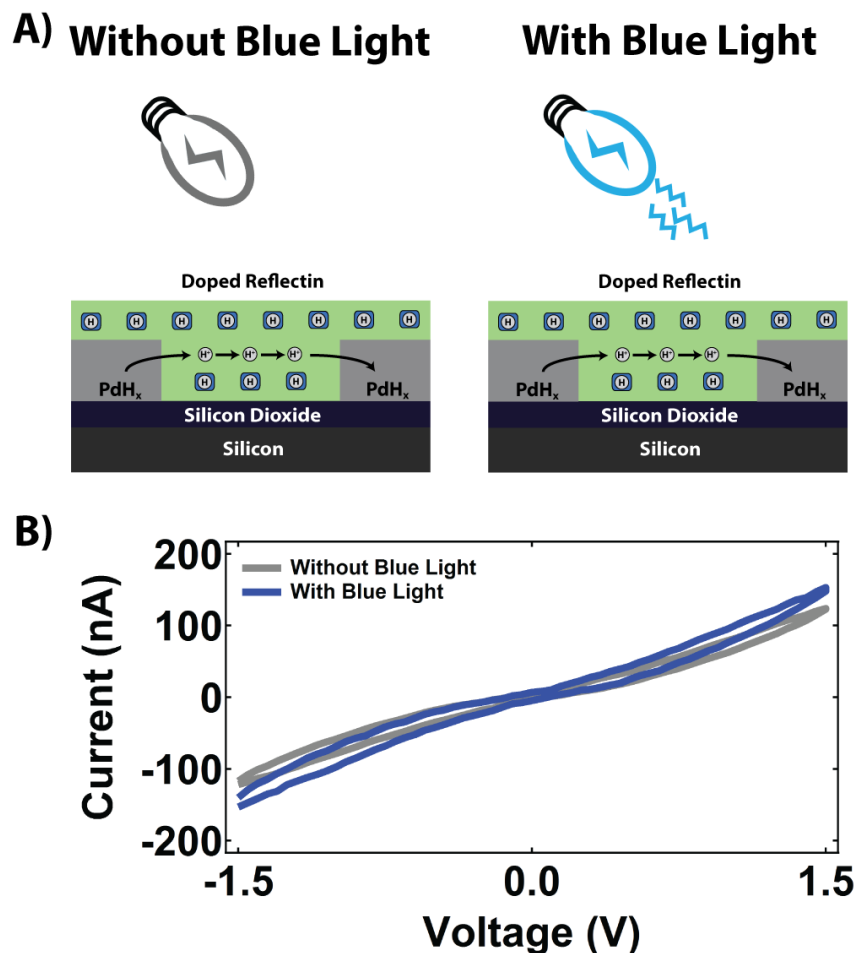
Figure 5.9: (A) An illustration of a two-terminal HPTS-doped reflectin mutant-based device without and with blue light illumination. Illumination of the device with blue light photoexcites HPTS and induces the release of protons into the film. **(B)** The current versus voltage characteristics of a typical device from an HPTS-doped reflectin mutant film without (gray) and with (blue) blue light illumination. Both the forward and reverse scans are shown.

The results of the photochemical doping experiments are summarized in Figure 5.10 (note that a minimum of eight independent two-terminal devices were tested under each set of conditions). Upon illumination with blue light, we observed average current increases of ~ 26 (± 7) % and ~ 23 (± 7) %, for the devices fabricated from HPTS-doped wild-type reflectin films

and from HPTS-doped mutant reflectin films, respectively. In contrast, when illuminated with red light, devices from HPTS-doped wild-type reflectin exhibited an average current decrease of ∼ 1 (±3) %, and when illuminated with blue light, devices from undoped reflectin exhibited an average current decrease of ∼ 3 (±5) %. Finally, blue light illumination did not appreciably affect the current for devices from MPTS-doped reflectin. Overall, these findings definitively demonstrated our ability to selectively augment the electrical properties of reflectin-based protonic devices with a photochemical reaction.
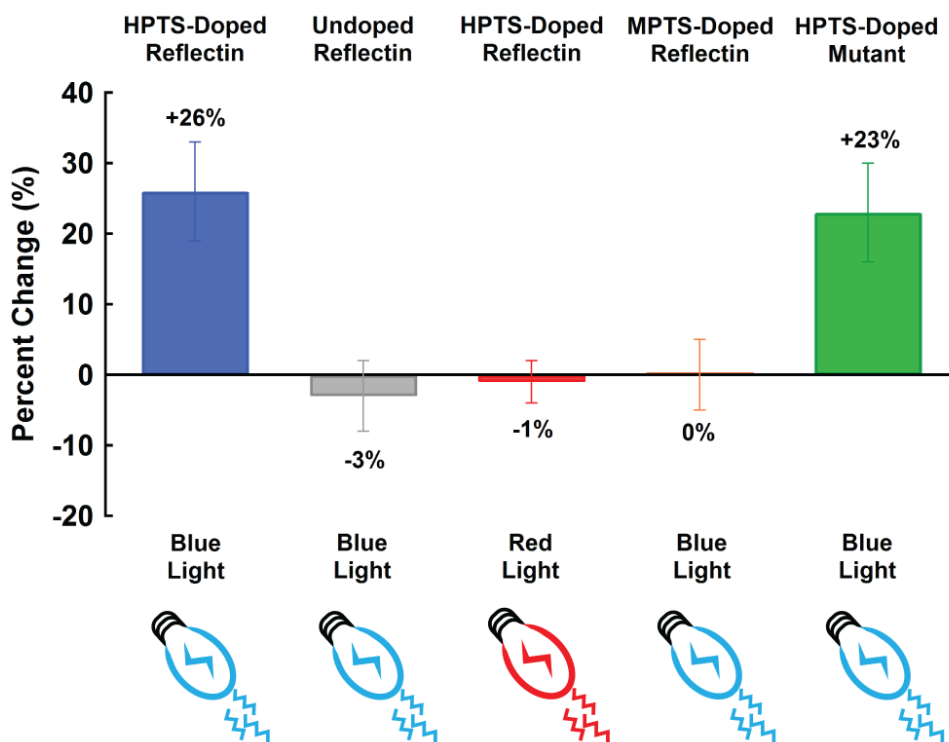
Figure 5.10: Summary of the change in current density for reflectin-based devices under various conditions. A plot of the percent change in current density observed for devices from HPTS-doped wild-type reflectin under blue light (blue), undoped wild-type reflectin under blue light (gray), HPTS-doped wild-type reflectin under red light (red), MPTS-doped wild-type reflectin under blue light (orange), and HPTS-doped "randomized" mutant reflectin under blue light (green). The error bars correspond to the standard deviation obtained from measurements on a minimum of eight independent devices.
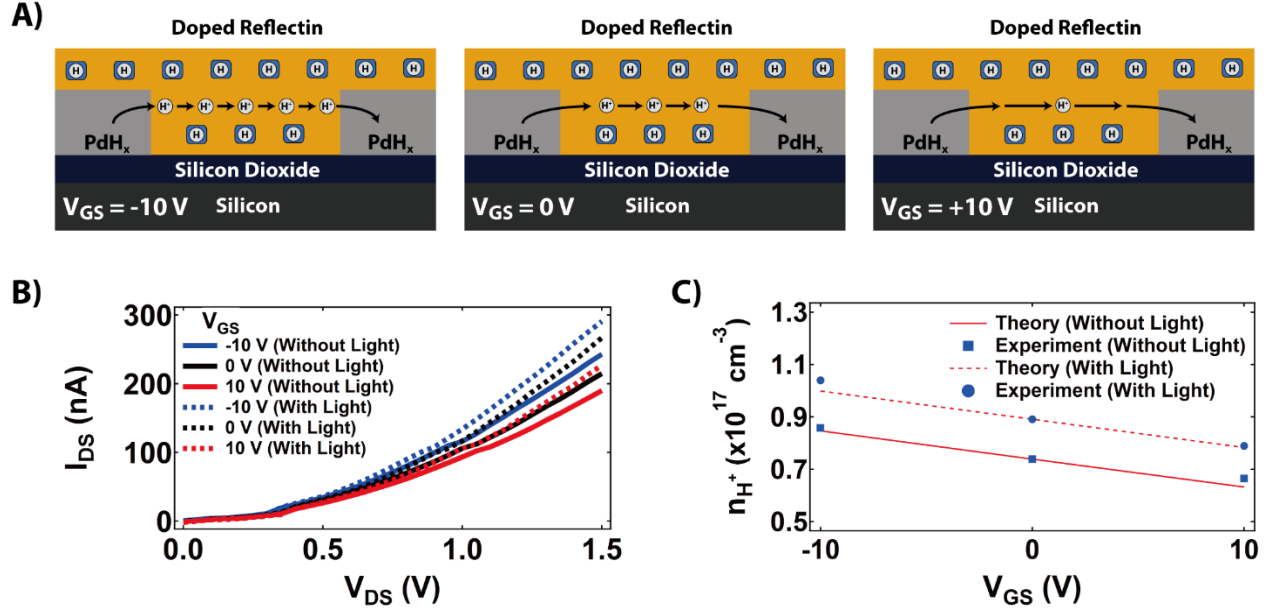
Figure 5.11: **(A)** Schematic of the change in protonic current for an HPTS-doped protonic transistor under different applied gate voltages. **(B)** The source–drain current (I_{DS}) versus source–drain voltage (V_{DS}) characteristics of an HPTS-doped reflectin-based protonic transistor obtained at $V_{GS} = -10$ V (blue), $V_{GS} = 0$ V (black), and $V_{GS} = +10$ V (red), both without (solid lines) and with (dashed lines) blue light illumination. Note that I_{DS} decreases as V_{GS} is changed from a negative value to a positive value both without and with illumination. **(C)** A plot of the experimentally observed proton charge carrier density (n_{H+}) as a function of V_{GS} both without (blue squares) and with (blue dots) blue light illumination. The corresponding theoretically calculated values are indicated by the dashed and solid red lines.

Having validated the photochemical doping strategy for two-terminal devices, we shifted our focus and characterized the electrical properties of three-terminal devices (protonic transistors) from HPTS-doped reflectin films in the absence of illumination. As a specific example, the I_{DS} versus V_{DS} characteristics obtained at different V_{GS} for a representative transistor are shown in Figure 5.11A. As expected for such devices, we found that the application of a negative V_{GS} induced the injection of protons into the channel, increasing the I_{DS}, and that the application of a positive V_{GS} depleted the channel of protons, decreasing the I_{DS} (Figure 5.11B).[11, 12] From measurements on five independent devices, we calculated a mobility of $\mu_{H+} = 4.2$ (± 1.0) $\times 10^{-3}$ cm^2 V^{-1} s^{-1} and a free proton concentration of $n_{H+} = 7.5$ (± 0.7) $\times 10^{16}$ cm^{-3} at $V_{GS} = 0$; these figures of merit were quite similar to values of $\mu_{H+} = 7.3$ (± 2.8) $\times 10^{-3}$ cm^2 V^{-1} s^{-1} and $n_{H+} = 10.6$ (± 6.1)

$\times 10^{16}$ cm^{-3} at $V_{GS} = 0$ previously reported for transistors from undoped reflectin films.[11, 12] Moreover, the experimentally observed proton concentrations at different gate voltages were in good agreement with the values theoretically predicted by the equation $n_{H+} = n_{H+}^0 - V_{GS}C_{GS}/et$ (Figure 5.11C).[9-12] Overall, protonic transistors from HPTS-doped reflectin films showed very similar performance to previously reported protonic transistors from undoped reflectin films.[11, 12]

We proceeded to photophysically modulate the electrical properties of protonic transistors from HPTS-doped reflectin films. As shown for the representative transistor in Figure 5.11B, we recorded an obvious blue light-induced increase in the source-drain current measured at any specific gate voltage. From measurements on five independent devices, we again calculated a mobility of $\mu_{H+} = 3.6$ (± 1.1) $\times 10^{-3}$ cm^2 V^{-1} s^{-1} and a free proton concentration of $n_{H+} = 10.8$ (± 3.3) $\times 10^{16}$ cm^{-3} at $V_{GS} = 0$ under blue light. Relative to the values found for our devices in the absence of blue light, the mobility decreased slightly by ~13% but the proton concentration increased significantly by ~45% (between the average values from five independent devices). These observations confirmed that the changes in the *I–V* characteristics of our protonic transistors were primarily due to an increase in the free charge carrier (proton) concentration, as might be expected from the model used to rationalize the functionality of doped protonic devices (Figure 5.1).

5.5: Conclusion

In conclusion, we have designed and implemented an advantageous strategy for the modulation of the electrical properties of both two- and three-terminal protonic devices with an exogenous photochemical stimulus, and our findings are significant for a number of reasons. First, the applied stimulus is mild and the presented doping methodology is straightforward. Our

approach therefore requires no tedious chemical modification of the proton-conducting material or extensive optimization of the device geometry and fabrication procedures. Second, our experiments reveal that protonic devices are sensitive to even subtle changes in their local charge carrier (proton) concentration. This sensitivity underscores their potential for interfacing with a broad range of voltage- or light-activated proton-transporting biomolecules, such as voltage-gated proton channels and bacterial rhodopsins.[15, 16] Third, our study constitutes one of the rare examples of protonic transistors reported in the literature.[9-12, 19-22] Indeed, the reported findings constitute a general strategy for controlling proton flow in such devices via two independent stimuli (applied voltage and light). Fourth, our measurements provide strong additional validation for the conceptual framework and model used to explain and rationalize conductivity in protonic transistors, as initially suggested more than 50 years ago.[10, 13, 23] Our observations thus reaffirm and enhance the state-of-the-art fundamental understanding of the operating mechanism of these devices, which is certain to aid efforts aimed at improving their performance. Finally, the presented general methodology possesses few limitations and should be broadly applicable for a wide range of materials and technologies that leverage proton transport.[46-49] One can envision using an analogous general approach to improve and better understand the performance of electrolyzers, sensors, batteries, and fuel cells.[46-49] Altogether, the findings reported here highlight the potential of voltage-regulated protonic devices as platforms for the fundamental study of proton transport and underscore their promise for applications in the next generation of bioelectronics technologies.

Chem. Mater. **2016**, *28*, 3703. The co-authors listed in this publication directed and supervised research which forms the basis for the material in the chapter. Author Contributions: D. D. O. and A. A. G. conceptualized and designed the experiments; D. D. O., L. P., Y. V. D., T. N., A. G. S., M. N., N. M. M., and M. K. D. performed the research; L. P. expressed and purified the protein, D. D. O. and A. A. G. analyzed the data; and D. D. O. and A. A. G. wrote the paper.

5.7: References

1. M. Berggren, A. Richter-Dahlfors, *Adv. Mater.* **2007**, *19*, 3201– 3213.

2. R. M. Owens, G. G. Malliaras, *MRS Bull.* **2010**, *35*, 449– 456.

3. K. Svennersten, K. C. Larsson, M. Berggren, A. Richter-Dahlfors, *Biochim. Biophys. Acta, Gen. Subj.* **2011**, *1810*, 276– 285.

4. G. G. Malliaras, *Biochim. Biophys. Acta, Gen. Subj.* **2013**, *1830*, 4286– 4287.

5. J. Rivnay, R. M. Owens, G. G. Malliaras, *Chem. Mater.* **2014**, 26, 679– 685.

6. S. Park, Y. J. Kang, S. Majd, *Adv. Mater.* **2015**, *27*, 7583– 7619.

7. K. Manoli, M. Magliulo, M. Y. Mulla, M. S. M. Singh, L. Sabbatini, G. Palazzo, L. Torsi, *Angew. Chem., Int. Ed.* **2015**, *54*, 12562– 12576.

8. X. Strakosas, M. Bongo, R. M. Owens, *J. Appl. Polym. Sci.* **2015**, *132*, 41735/1– 41735/14.

9. C. Zhong, Y. Deng, A. F. Roudsari, A. Kapetanovic, M. P. Anantram, M. Rolandi, M. *Nat. Commun.* **2011**, *2*, 1489/1– 1489/5.

10. Y. Deng, E. Josberger, J. Jin, A. F. Roudsari, B. A. Helms, C. Zhong, M. P. Anantram, M. Rolandi, M. *Sci. Rep.* **2013**, *3*, 2481/1– 2481/9.

11. D. D. Ordinario, L. Phan, W. G. Walkup IV, J-M. Jocson, E. Karshalev, N. Hüsken, A. A. Gorodetsky, *Nat. Chem.* **2014**, *6*, 596– 602.

12. D. D. Ordinario, L. Phan, J-M. Jocson, T. Nguyen, A. A. Gorodetsky, *APL Mater.* **2015**, *3*, 014907/1– 014907/5.

13. Z. Hemmatian, T. Miyake, Y. Deng, E. E. Josberger, S. Keene, R. Kautz, C. Zhong, J. Jin, M. Rolandi, *J. Mater. Chem. C* **2015**, *3*, 6407– 6412.

14. B. Alberts, A. Johnson, J. Lewis, M. Ratt, K. Roberts, P. Walter, in *Molecular Biology of the Cell, 4th ed.*, Garland Science, New York, **2002**.

15. T. E. DeCoursey, *Physiol. Rev.* **2003**, *83*, 475– 579.

16. O. P. Ernst, D. T. Lodowski, M. Elstner, P. Hegemann, L. S. Brown, H. Kandori, *Chem. Rev.* **2014**, *114*, 126– 163.

17. J. P. Hosler, S. Ferguson-Miller, D. A. Mills, *Annu. Rev. Biochem.* **2006**, *75*, 165– 187.

18. C. A. Wraight, *Biochim. Biophys. Acta, Bioenerg.* **2006**, *1757*, 886– 912.

19. V. F. Petrenko, N. Maeno, *J. Phys. Colloq.* **1987**, *48*, C1-115– C1-119.

20. Z. G. Chiragwandi, O. Nur, M. Willander, N. Calander, *Appl. Phys. Lett.* **2003**, *83*, 5310– 5312.

21. R. Fan, S. Huh, R. Yan, J. Arnold, P. Yang, *Nat. Mater.* **2008**, *7*, 303– 307.

22. A. M. Deml, A. L. Bunge, M. A. Reznikov, A. Kolessov, R. P. O'Hayre, *J. Appl. Phys.* **2012**, *111*, 074511/1– 074511/8.

23. M. Eigen, L. de Maeyer, *Proc. R. Soc. London, Ser. A* **1958**, *247*, 505– 533.

24. C. J. T. de Grotthuss, *Ann. Chim.* **1806**, *58*, 54– 73.

25. N. Agmon, *Chem. Phys. Lett.* **1995**, *244*, 456– 462.

26. S. Cukierman, *Biochim. Biophys. Acta, Bioenerg.* **2006**, *1757*, 876– 885.

27. E. E. Josberger, Y. Deng, W. Sun, R. Kautz, M. Rolandi, *Adv. Mater.* **2014**, *26*, 4986– 4990.

28. T. Miyake, E. E. Josberger, S. Keene, Y. Deng, M. Rolandi, *APL Mater.* **2015**, *3*, 014906/1– 014906/6.

29. W. J. Crookes, L. L. Ding, Q. L. Huang, J. R. Kimbell, J. Horowitz, M. J. McFall-Ngai, *Science* **2004**, *303*, 235– 238.

30. R. M. Kramer, W. J. Crookes-Goodson, R. R. Naik, *Nat. Mater.* **2007**, *6*, 533– 538.

31. A. R. Tao, D. G. DeMartini, M. Izumi, A. M. Sweeney, A. L. Holt, D. E. Morse, *Biomaterials* **2010**, *31*, 793– 801.

32. D. G. DeMartini, M. Izumi, A. T. Weaver, E. Pandolfi, D. E. Morse, *J. Biol. Chem.* **2015**, *290*, 15238– 15249.

33. L. Phan, W. G. Walkup IV, D. D. Ordinario, E. Karshalev, J-M. Jocson, A. Burke, A. A. Gorodetsky, *Adv. Mater.* **2013**, *25*, 5621– 5625.

34. L. Phan, D. D. Ordinario, E. Karshalev, W. G. Walkup IV, M. A. Shenk, A. A. Gorodetsky, *J. Mater. Chem. C* **2015**, *3*, 6493– 6498.

35. L. Phan, R. Kautz, J. Arulmoli, I. H. Kim, D. T. T. Le, M. A. Shenk, M. M. Pathak, L. Flanagan, F. Tombola, A. A. Gorodetsky, *ACS Appl. Mater. Interfaces* **2016**, *8*, 278– 284.

36. O. S. Wolfbeis, E. Fürlinger, H. Kroneis, H. Marsoner, H. *Fresenius' Z. Anal. Chem.* **1983**, *314*, 119– 124.

37. Y. Avnir, Y. Barenholz, *Anal. Biochem.* **2005**, *347*, 34– 41.

38. R. Barnadas-Rodrıguez, J. Estelrich, *J. Photochem. Photobiol., A* **2008**, *198*, 262– 267.

39. J. R. Lakowicz, in *Principles of Fluorescence Spectroscopy, 3rd ed.*, Springer Science + Business Media, New York, **2006**.

40. I. Johnson, M. T. Z. Spence, in *The Molecular Probes Handbook – A Guide to Fluorescent Probes and Labeling Technologies, 11th ed.*, Life Technologies, Inc., Eugene, OR, **2010**.

41. D. B. Spry, A. Goun, K. Glusac, D. E. Moilanen, M. D. Fayer, *J. Am. Chem. Soc.* **2007**, *129*, 8122– 8130.

42. N. Amdursky, R. Simkovitch, D. Huppert, *J. Phys. Chem. B* **2014**, *118*, 13859– 13869.

43. S. Haghighat, S. Ostresh, J. M. Dawlaty, *J. Phys. Chem. B* **2016**, *120*, 1002– 1007.

44. N. Amdursky, X. Wang, P. Meredith, D. D. C. Bradley, M. M. Stevens, *Adv. Mater.* **2016**, *28*, 2692– 2698.

45. M. Kriechbaum, O. S. Wolfbeis, E. Koller, *Chem. Phys. Lipids* **1987**, *44*, 19– 29.

46. P. Colomban, in *Proton Conductors: Solids, Membranes and Gels – Materials and Devices*, Cambridge University Press, Cambridge, U.K., **1992**.

47. K.-D. Kreuer, *Chem. Mater.* **1996**, *8*, 610– 641.

48. K.-D. Kreuer, S. J. Paddison, E. Spohr, M. Schuster, *Chem. Rev.* **2004**, *104*, 4637– 4678.

49. E. Fabbri, D. Pergolesi, E. Traversa, *Chem. Soc. Rev.* **2010**, *39*, 4355– 4369.

CHAPTER 6   Protochromic Devices From Reflectin

6.1: Abstract

Cephalopods possess remarkable camouflage capabilities, which are enabled by their complex innervated skin architectures and advanced controlling nervous systems. As such, cephalopod skin constitutes an exciting source of inspiration for biomimetic camouflage technologies. Herein, we emulate aspects of optically-active ultrastructures found in squid skin cells and design color-changing bioelectronic devices, which consist of a proton-transporting active layer contacted by a proton-conducting actuating electrode. We observe and quantify distinct shifts in the reflectance and coloration of our devices, which we attribute to changes in thickness induced by the direct electrical injection/extraction of protons. Our findings may hold relevance for developing novel color-changing technologies, understanding ion-transporting biological systems, and engineering improved bioelectronic platforms.

6.2: Introduction

Cephalopods, such as the squid *Doryteuthis (Loligo) pealeii*, have captured the imaginations of scientists and the general public due to their advanced vertebrate-like neurophysiology and unrivaled ability to blend into nearly any environment.[1-6] These animals' camouflage capabilities are enabled by a sophisticated skin structure, wherein multiple different cell types (leucophores, chromatophores, and/or iridophores) perform distinct optical functions but work in concert to control the skin's overall appearance.[4,5] For example, the skin of *D. pealeii* contains iridophores, which modulate the reflection of light, and chromatophores, which modulate

the transmission of light.[7-9] Interestingly, both of these cell types are hierarchically controlled by a network of nerve fibers, which directly interfaces the cells with the central nervous system.[10,11] This sophisticated architecture enables longfin inshore squid skin to effectively serve as a bioelectronic display with capabilities that are enviable from the perspective of manmade dynamic camouflage systems.[5] Given such functionality, cephalopod skin in general has emerged as a tremendous source of inspiration for camouflage devices from both artificial and naturally-occurring materials.[12-17]

As targets for replication in bioelectronic camouflage devices, cephalopod iridophores are particularly interesting because their ultrastructure facilitates the transduction of chemical signals
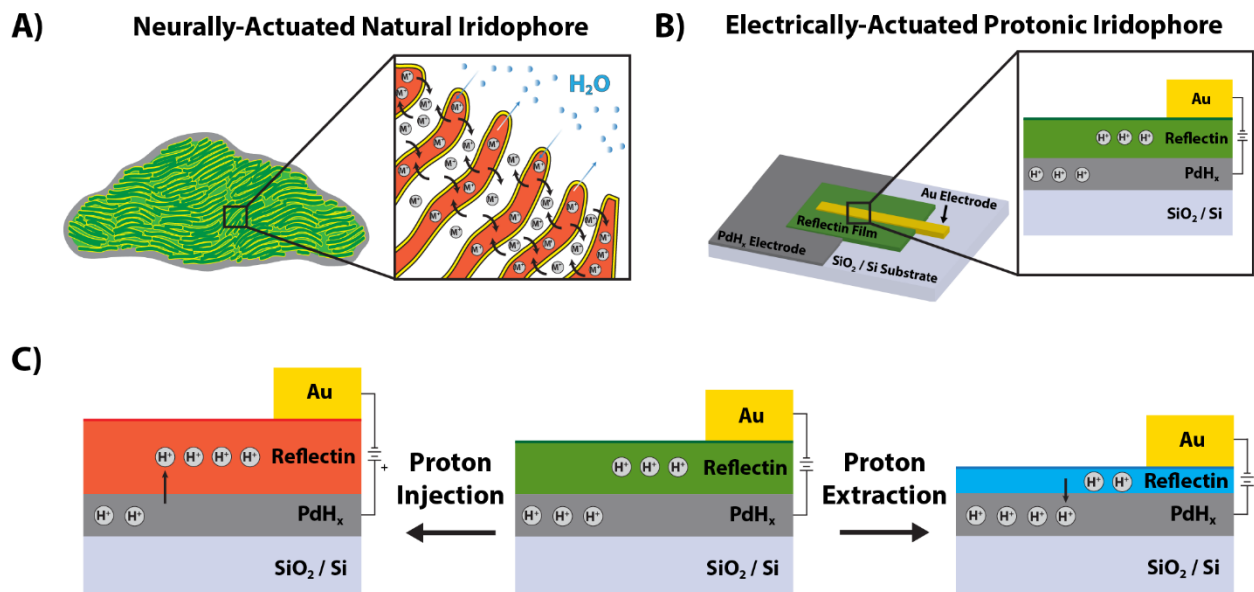
Figure 6.1: **(A)** A simplified, general schematic of a neurally-activated natural iridophore. The color of the iridophore is determined by its constituent Bragg reflector-like structures, which consist of alternating membrane-enclosed reflectin platelets and deep invaginations into the cellular interior. **(B)** A simplified, general schematic of an electrically-actuated protonic iridophore. This protonic device consists of a proton-injecting PdH_x actuation electrode (in analogy to an ion-permeable membrane), a proton-conducting RfA1 active layer (in analogy to a single iridophore platelet) and an ion-blocking Au electrode (as a stable reference). **(C)** A schematic of the effect of direct proton injection and extraction on the thickness and reflectance of a device-integrated RfA1 active layer (center). The injection of protons leads to an increase in thickness and a red shift in reflectance for the RfA1 layer (left), while the extraction of protons leads to a decrease in thickness and a blue shift in reflectance for the RfA1 layer (right).

106

into mechanical and optical effects.[18,19] To illustrate this point, a schematic of a squid iridophore is shown in Figure 6.1A. The cell's plasma membrane folds into a periodic arrangement, wherein membrane-enclosed platelets from proteins called reflectins alternate with deep invaginations into the cellular interior.[18-30] This structure effectively constitutes a biological Bragg reflector comprised of layers from high and low refractive index materials.[18,19] The reflector is activated via a neurally-controlled signaling cascade that leads to phosphorylation and then condensation of the reflectin proteins (Figure 6.1A).[18,19] The accompanying flux of ions across the cell membrane and subsequent expulsion of water into the invaginations change the size, spacing, and refractive index of the platelets, modulating the reflector's optical properties (Figure 6.1A).[18,19] This rapid and fully reversible process affords exquisite control over the wavelength of light reflected by the iridophores, allowing the cells to tune their coloration across the entire visible spectrum.[18,19]

Herein, we present a new class of cephalopod-inspired protochromic devices with optical characteristics that are electrically controlled. We first draw inspiration from the ultrastructures of squid iridophores and design device architectures featuring a proton-transporting reflectin A1 (RfA1) active layer contacted by a proton-conducting palladium hydride (PdH_x) actuating electrode. We subsequently fabricate such devices and optically characterize them both without and with applied electrical biases. We observe and quantify distinct shifts in the reflectance and coloration of our devices, which we attribute to changes in thickness induced by the direct electrical injection or extraction of protons. Our findings may hold relevance for developing novel color-changing technologies, understanding ion-transporting biological systems, and engineering improved bioelectronic platforms.

6.3: Experimental Section

6.3.1: Production of Wild-Type and Mutant Reflectins

Wild-type reflectin A1 and mutant reflectin A1 (in which the aspartic acid and glutamic acid residues were substituted with alanines) were expressed, purified, and characterized according to a general established protocol.[26-28] In brief, the pJExpress414 expression vectors containing either the wild type or mutant reflectin were transformed into BL21(DE3) cells (Novagen). The reflectins were expressed at 37 °C using Overnight Express Instant Terrific Broth (TB) media (Novagen) supplemented with 100 μg mL^{-1} Carbenicillin. The reflectins were completely insoluble when expressed at 37 °C and were sequestered in inclusion bodies prepared using Novagen BugBuster® according to the manufacturer's suggested protocol. The inclusion bodies were then solubilized in denaturing buffer (pH 7.4, 50 mM Sodium Phosphate, 300 mM NaCl, 6M guanidine hydrochloride) and purified under denaturing conditions on HisPur Cobalt Resin (Thermo Scientific) immobilized metal affinity chromatography (IMAC) gravity columns according to the manufacturer's protocols. The protein was eluted by using denaturing buffer supplemented with 250 mM imidazole. The fractions containing reflectin were pooled and concentrated on Millipore Amicon Concentrators before further purification with high-performance liquid chromatography (HPLC) on an Agilent 1260 Infinity system using an Agilent reverse phase C18 column with a gradient evolved from 95% Buffer A:5% Buffer B to 5% Buffer A:95% Buffer B at a flow rate of 1 mL min^{-1} over 30 minutes (Buffer A: 99.9% H_2O, 0.1% TFA; Buffer B: 95% acetonitrile, 4.9% H_2O, 0.1% TFA). The pure reflectin fractions were pooled, flash frozen in liquid nitrogen, and lyophilized. The identity of the purified proteins was confirmed by in-gel tryptic digestion and tandem mass spectrometry on a Thermo Orbitrap instrument outfitted with an electrospray ionization source. The protein concentrations and yields were quantified via the Bradford protein assay with bovine serum albumin (BSA) as a standard (BioRad).

6.3.2: Fabrication of Reflectin-Based Devices

The two-terminal devices were fabricated in a sandwich configuration by drawing upon preciously-reported procedures.[26-28] In brief, SiO$_2$/Si substrates (International Wafer Service, Inc.) were first cleaned in Piranha solution (1:3 hydrogen peroxide to sulfuric acid) and washed thoroughly. Subsequently, contacts consisting of a 4 nm chromium adhesion layer overlaid with a 40 nm palladium layer were electron-beam evaporated using a Temescal FC-2000 Bell Jar Deposition System onto the clean substrates through a shadow mask. Next, a film of either wild-type RfA1 or mutant RfA1 was coated evenly between the palladium contact and the substrate surface. Subsequently, a 40 nm gold contact was deposited over the substrate surface and the RfA1 film, partially overlapping areas where the RfA1 film contacted the palladium contact. To prevent degradation of the RfA1 film during, the gold top contact was deposited via a layered strategy, i.e. 1 nm, 2 nm, 3 nm, 4 nm, and 5 nm layers of gold were first deposited sequentially, followed by 25 nm of gold in 5 nm increments. To further mitigate the possibility of film degradation, the film was allowed to cool for 5 minutes after the deposition of each layer, and the temperature of the evaporation chamber was kept below 30° C at all times. Finally, to form proton-injecting PdH$_x$ electrodes the devices were exposed to a 5% hydrogen/95% argon atmosphere in situ.

6.3.3: Physical Characterization of Reflectin-based Devices

The thicknesses of the RfA1 films were determined from the analysis of topographical scans obtained with an Asylum Research MFP-3D Atomic Force microscope. The AFM data was analyzed with the Gwyddion software package. The topological scans were rastered at 0.50 Hz and normalized using polynomial subtraction for improved image quality.

6.3.4: Imaging of Reflectin-Based Devices

The devices were imaged with a D800 camera (Nikon) equipped with a 105 mm f/2.8 AF-S Micro-Nikkor (Nikon). The images were captured with an exposure time of 1/25 second, aperture setting of f/11, and ISO of 1600.

6.3.5: Spectroscopic Characterization of Reflectin-Based Devices

The device-integrated RfA1 films were characterized with optical microscopy and reflectance measurements both with and without applied voltages (see below). The optical images were obtained with a Craic Technologies 20/20 PV™ UV-visible-NIR Microspectrophotometer (outfitted with a Zeiss Ultrafluar 10X lens, NA = 0.2) and processed with the manufacturer's ImageUV software. The reflectance spectra were measured both with and without applied voltages with a Craic Technologies 20/20 PV™ UV-visible-NIR Microspectrophotometer outfitted with a tungsten halogen white light source (effective wavelength range of $\lambda = 350$ nm to $\lambda = 1700$ nm). During the measurements, the devices were housed in a custom built enclosure, which maintained the relative humidity at 90 %. The reflectance data were acquired normal to the substrate surface and were referenced to a Thorlabs 25.4 mm Protected Aluminum Mirror (unless otherwise noted).

6.3.6: Electrical Characterization of Reflectin-based Devices

The devices were characterized by using a 2400 Series SourceMeter Source Measure Unit (SMU) (Keithley Instruments). For the electrical measurements, the current as a function of time was recorded after application of either negative voltages of -1.5 V or positive voltages of +1.5 V. During the measurements, the devices were housed in a custom built enclosure, which maintained the relative humidity at 90 %.

6.3.7: Analysis of the Current-Voltage Data

The charge extracted from or injected into the RfA1 films was calculated from the initial current spike according to the methods of Rolandi and co-workers[31,32] by using the following equation:

$$Q = \int_{t=0}^{t=t_{spike}} I_o dt \quad (1)$$

where Q is the total amount of charge in Coulombs, t_{spike} is the time in seconds, and I_o is the measured current in Amps. The total charge Q was in turn converted to the total proton concentration per unit volume (protons cm^{-3}).

6.3.8: Estimation of Reflectin Film Thickness

The thicknesses of the RfA1 films were estimated by using thin-film interference theory.[33] First, we calculated the refractive index of hydrated RfA1 films according to the method of Sackmann and co-workers[34] by using the following equation:

$$n_F = n_M \sqrt{1 + \frac{3\frac{h_o}{h}}{\left(\frac{n_o^2 + 2n_M^2}{n_o^2 - n_M^2}\right) - \frac{h_o}{h}}} \quad (2)$$

where n_F is the refractive index of the hydrated film, n_o is the refractive index of the pure solute, n_M is the refractive index of the pure solvent, h_o is the dry film thickness at low relative humidity, and h is the layer thickness at increased relative humidity. Next, we calculated the film thicknesses by using the following equation (which reasonably approximates the optical properties of our films at near-normal incidence):

$$2 \cdot n_F \cdot d = m \cdot \lambda \quad (3)$$

where d is the thickness, n_F is the refractive index, m is an integer, and λ is the peak wavelength.

6.4: Results and Discussion

In an initial step towards emulating the iridophores' highly-evolved natural architecture, we rationally designed color-changing bioelectronic devices, such as the one illustrated in Figure 6.1B, which could be actuated by ionic fluxes originating not from a squid's central nervous system but from an external electronic circuit. For our approach, we were conceptually encouraged by 1) prior demonstrations that the neurally-controlled influx/efflux of ions alters the dimensions and optical properties of single iridophore platelets[18] and 2) the report that acetic acid-induced injection of protons into RfA1-based coatings modulates their thickness and reflectance *in vitro*.[16] Furthermore, our device design leveraged recent advances in bioprotonics, wherein PdH_x electrodes exchange protons with cephalopod-derived proton conductors, such as maleic chitosan and RfA1 (note that the chemical injection of protons via acid vapor, while highly effective, is impractical for interfacing with external electronics).[26-29,31,32,35-38] Thus, in lieu of a single protein-based platelet, our device incorporated a thin film of RfA1 as the color-changing active component, and in lieu of a surrounding ion-permeable membrane, our device incorporated a PdH_x electrode as the electrically-conducting actuating component (the ion-blocking gold electrode functioned as a stable reference) (Figure 6.1B). For this device, we expected that applied voltages would induce proton exchange between the PdH_x electrode and the RfA1 active layer, thereby leading to protonation/deprotonation of RfA1's amino acids (note that RfA1 possesses a pI of ~ 9)[19,23-25] and likely altering electrostatic interactions within the film's interior. Specifically, under a positive applied voltage, the injection of protons would increase the net positive charge and swell the film, leading to a red-shift in reflectance, and under a negative applied voltage, the extraction of protons
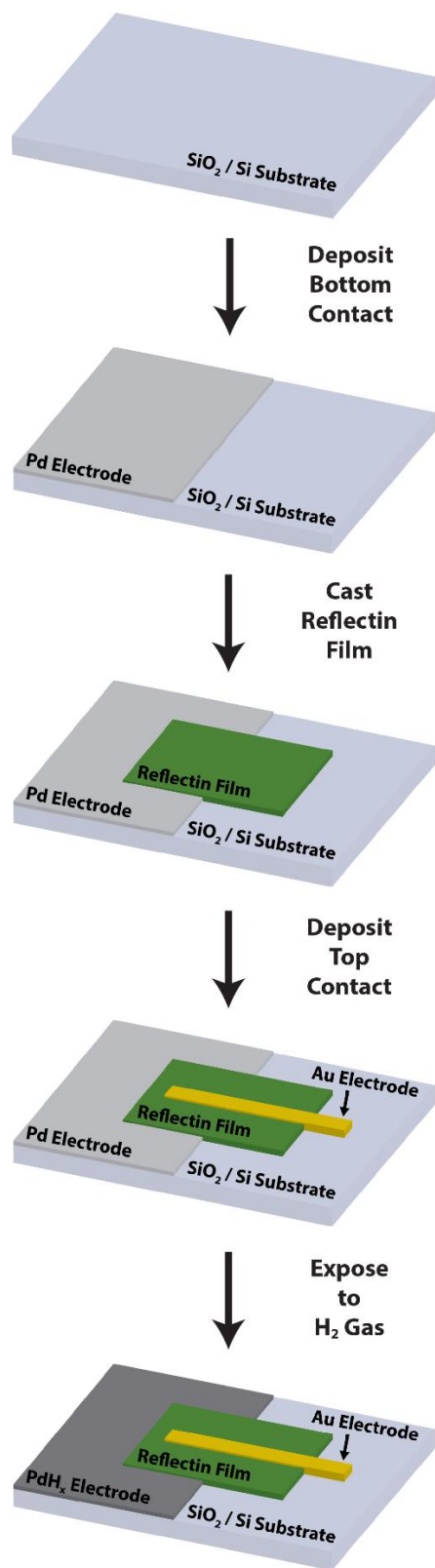
Figure 6.2: The general fabrication scheme for a protochromic device with a PdH_x/RfA1/Au architecture. The strategy consists of the deposition of a Pd bottom contact, the casting of an RfA1 film, the deposition of an Au top contact, and exposure to H_2 gas.

would decrease the positive charge and condense the film, leading to a blue-shift in reflectance (Figure 6.1C). The resulting stimuli-responsive protochromic devices would effectively constitute highly simplified protonic iridophores, with optical functionality roughly analogous to that of the natural system.

We began our experiments by fabricating the desired color-changing bioelectronic devices according to the scheme in Figure 6.2 (see the experimental section for additional details). In our approach, we adapted protocols previously validated for the fabrication of RfA1-based protonic devices.[26-29] First, as the bottom electrode, we deposited a chromium (Cr) adhesion layer followed by a palladium (Pd) layer onto a silicon dioxide/silicon (SiO_2/Si) substrate via electron-beam evaporation. Next, as the active layer, we cast a film of RfA1 onto a portion of the Pd-modified surface, scribing away excess material when necessary. In turn, as the top electrode, we deposited an Au layer directly onto the Pd- and RfA1-modified surface, again via electron-beam evaporation (note that a layered, low-temperature deposition strategy mitigated damage to the protein film, yielding pristine devices like the one shown in Figure 6.3). Finally, for the electrical measurements, we converted the electron-injecting Pd contacts to proton-injecting PdH_x contacts through exposure to hydrogen gas in situ.[26-29,31,32,36-38] The overall procedure furnished devices with a sandwich-type PdH_x/RfA1/Au architecture.
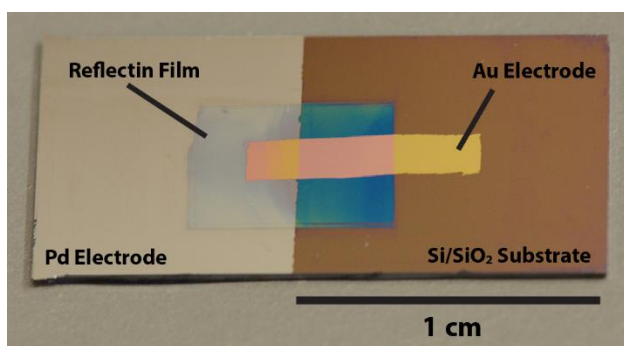
Figure 6.3. A photograph of a representative device, where an RfA1 film is sandwiched between a palladium bottom contact and a gold top contact.
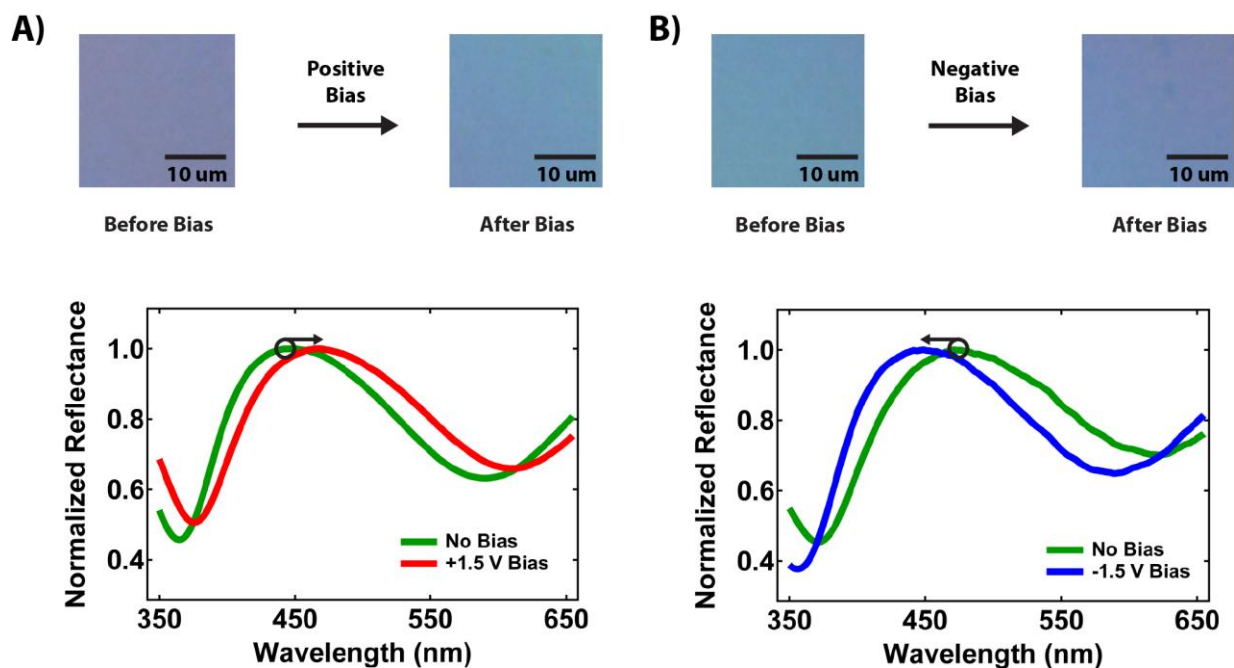
Figure 6.4: (**A**) Top: Optical images of a device-integrated RfA1 film before (left) and after (right) the application of a positive voltage. Note the change in the film color from violet to blue. Bottom: The reflectance spectra for a device-integrated RfA1 film before (green curve) and after (red curve) the application of a positive voltage, demonstrating a red-shift. (**B**) Top: Optical images of a device-integrated RfA1 film before (left) and after (right) the application of a negative voltage. Note the change in the film color from blue to violet. Bottom: The reflectance spectra for a device-integrated RfA1 film before (green curve) and after (blue curve) the application of a negative voltage, demonstrating a blue-shift.

With the desired devices in hand, we first evaluated the optical properties of their constituent RfA1 films without actuation. The optical microscopy images and corresponding reflectance spectra for two hydrated RfA1 films are shown in Figure 6.4A and Figure 6.4B in the absence of an applied voltage (green traces). From the reflectance spectras' peak wavelengths of 448 nm and 471 nm, we calculated expected hydrated thicknesses of 303 nm for the film in Figure 6.4A and 319 nm for the film in Figure 6.4B (see the experimental section for Calculation Details). In turn, we used atomic force microscopy (AFM) to measure the dry thicknesses of the two films and obtained values of 201 nm and 248 nm, which corresponded to approximate hydrated thicknesses of 281 nm for the film in Figure 6.4A and 347 nm for the film in Figure 6.4B (when accounting for swelling). Based on the agreement between the calculated and measured

thicknesses, we inferred that the reflectance and coloration of our device-integrated RfA1 films were dictated largely by thin film interference, in agreement with previous reports for reflectin-based coatings in vitro.[16,17]
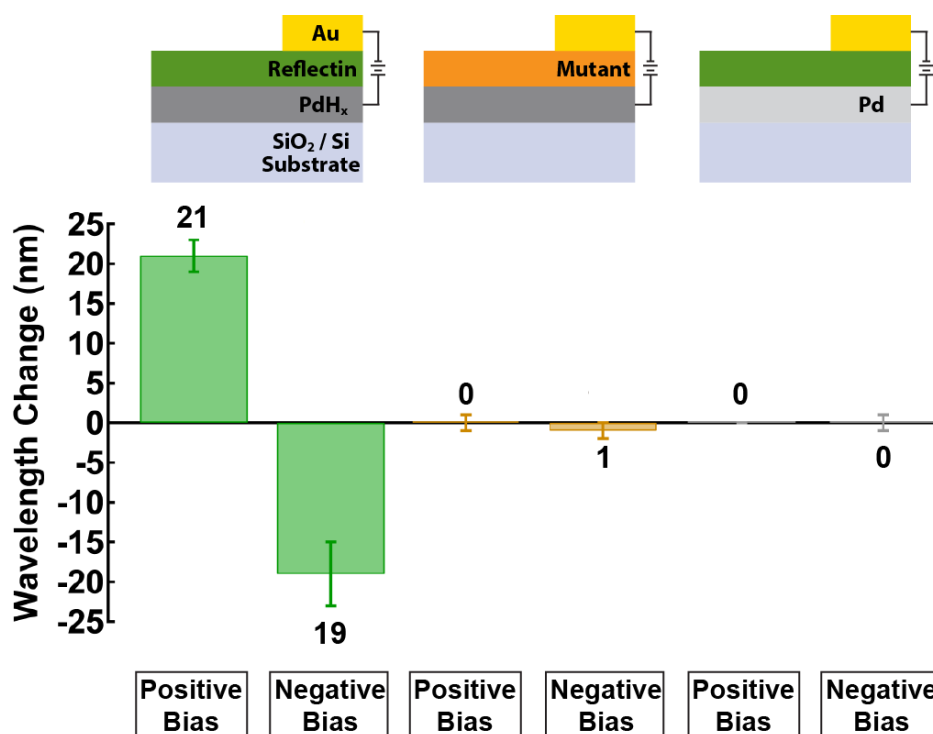
Figure 6.5: The average change in the peak reflectance wavelength for devices with PdH$_x$/RfA1/Au (left), PdH$_x$/m-RfA1/Au (middle), and Pd/RfA1/Au (right) architectures under both negative and positive applied biases. The error bars correspond to the standard deviations obtained for a minimum of 5 measurements.

We proceeded to investigate the effect of electrical actuation on the reflectance and coloration of our device-integrated RfA1 films. After application of a positive voltage for a representative film, we observed a distinct change in film coloration from violet to blue and an accompanying ~ 19 nm red shift in the peak reflectance (Figure 6.4A); note that the measurements were readily reproducible, as evidenced by an average shift of ~ 21 ± (2) nm across 7 independent devices (Figure 6.5). Assuming no substantial change in the refractive index, we estimated that the thickness of the device-integrated film in Figure 6.4A increased by 12 nm from 303 nm to 315 nm.

In contrast, after application of a negative voltage for a representative film, we observed a distinct change in the film coloration from blue to violet and an accompanying ~ 23 nm blue shift in the peak reflectance (Figure 6.4B); note that the measurements were again readily reproducible, as evidenced by an average shift of ~ 19 ± (4) nm across 7 independent devices (Figure 6.5). Assuming no substantial change in the refractive index, we estimated that the thickness of the device-integrated film in Figure 6.4B decreased by 16 nm from 319 nm to 303 nm. Based on our measurements, we postulated that the observed changes in reflectance and coloration likely resulted from swelling or condensation of the RfA1 layers, as induced by the direct electrical injection (positive voltages) or extraction (negative voltages) of protons, respectively.

Figure 6.6. **(A)** A schematic of a device with a PdH$_x$/m-RfA1/Au architecture before and after application of a positive voltage. The active layer is not capable of transporting protons. **(B)** The representative reflectance spectra for a device-integrated m-RfA1 film with palladium hydride and gold contacts before (green curve) and after (red curve) the application of a positive voltage. The spectra are nearly identical. **(C)** A schematic of a device with a PdH$_x$/m-RfA1/Au architecture before and after application of a negative voltage. The active layer is not capable of transporting protons. **(D)** The representative reflectance spectra for a device-integrated m-RfA1 film with palladium hydride and gold contacts before (green curve) and after (blue curve) the application of a negative voltage. The spectra are nearly identical.

In an initial key control experiment, we verified the importance of the proton-transporting RfA1 active layer for the functionality of our devices. For this purpose, we used a mutant RfA1 variant (m-RfA1) for which the proton-donating aspartic acid and glutamic acid residues were substituted with alanines, making the mutant a far less effective proton conductor than wild-type RfA1.[26] Thus, we fabricated and tested analogues of our devices with a PdH_x/m-RfA1/Au architecture, for which the reflectance spectra both without and with applied voltages are shown in Figure 6.6. Regardless of the voltage, we found only negligible changes in the films' reflectance, with a red shift of $0 \pm (1)$ nm in the peak wavelength across 5 devices for positive voltages and a blue shift of $1 \pm (1)$ nm in the peak wavelength across 5 devices for negative voltages (Figure 6.5). These measurements indicated that the effective transport of protons through the active layer was necessary for the observed shifts in reflectance and coloration.
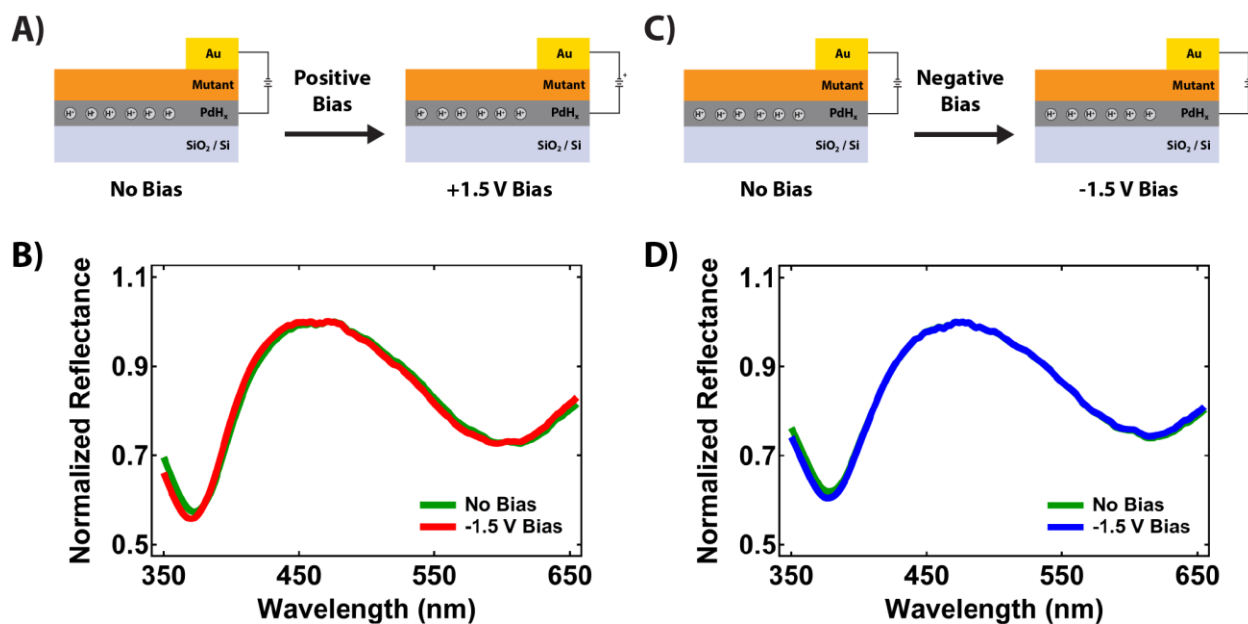

Figure 6.7. (A) A schematic of a device with a Pd/RfA1/Au architecture before and after application of a positive voltage. The electrode is not capable of injecting protons into the device. **(B)** The representative reflectance spectra for a device-integrated RfA1 film with palladium and gold contacts before (green curve) and after (red curve) the application of a positive voltage. The spectra are nearly identical. **(C)** A sche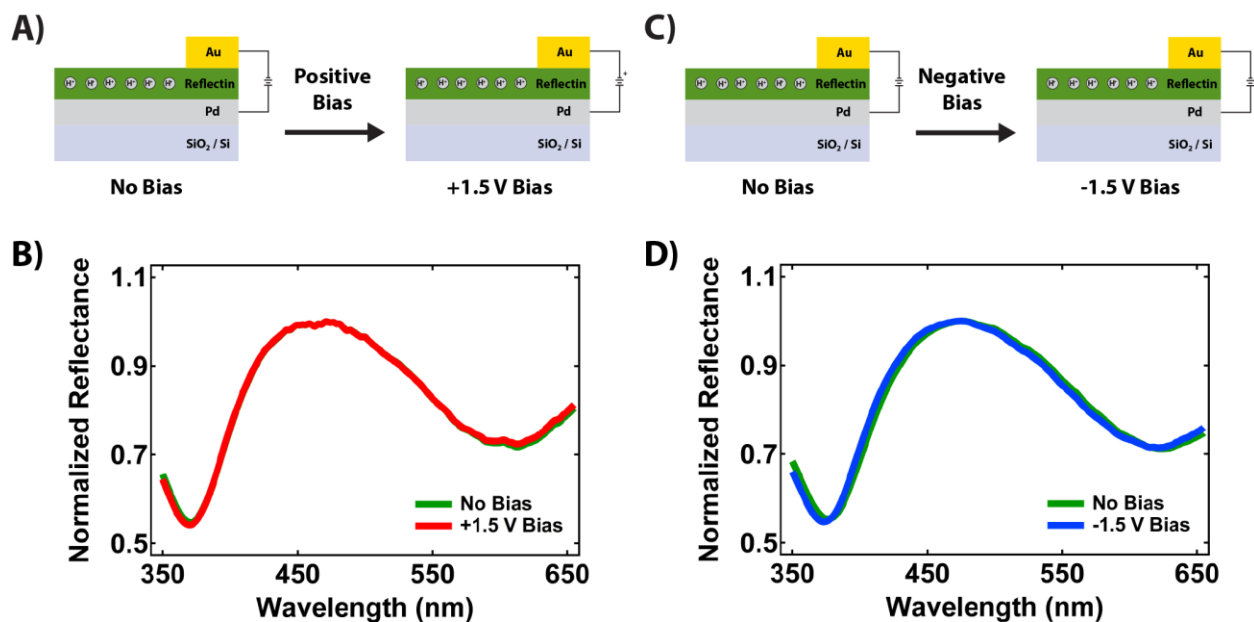matic of a device with a Pd/RfA1/Au architecture before and after application of a negative voltage. The electrode is not capable of injecting protons into the device. **(D)** The representative reflectance spectra for a device-integrated RfA1 film with palladium and gold contacts before (green curve) and after (blue curve) the application of a negative voltage. The spectra are nearly identical.

In another key control experiment, we verified the importance of proton injection/extraction for the functionality of our devices. For this purpose, we used Pd electrodes that had not been exposed to hydrogen gas, making them incapable of proton exchange as electrical contacts.[27,36] Thus, we fabricated and tested analogues of our devices with a Pd/RfA1/Au architecture, for which the reflectance spectra both without and with applied voltages are shown in Figure 6.7. Regardless of the voltage, we again found no change in the films' reflectance spectra, with a red shift of $0 \pm (0)$ nm in the peak wavelength across 5 devices for positive voltages and a blue shift of $0 \pm (1)$ nm in the peak wavelength across 5 devices for negative voltages (Figure 6.5). These measurements confirmed that the effective exchange of protons between the electrodes and active layer was required for the observed shifts in reflectance and coloration.
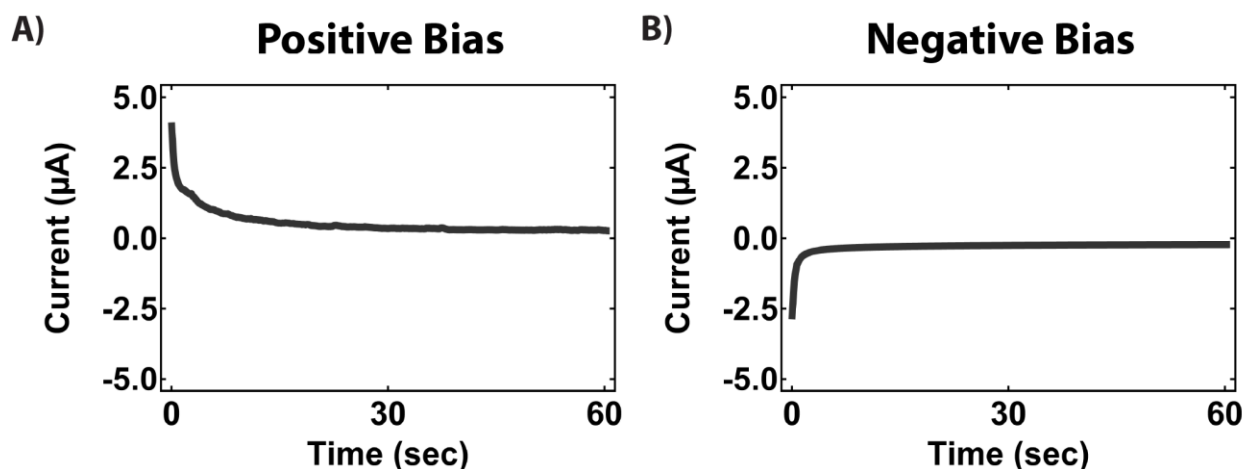
Figure 6.8. Temporal evolution of the current vs. voltage characteristics recorded for a device with a PdH$_x$/RfA1/Au architecture under A) a positive and B) a negative applied voltage.

Finally, we directly quantified the proton flux that accompanied the changes in the reflectance and coloration of the device-integrated RfA1 films. As examples, the current (I) versus time (t) curves recorded for PdH$_x$/RfA1/Au devices upon electrical actuation are shown in Figure 6.8. After the application of a positive voltage, we observed a time-dependent evolution of the

current, with the initial spike due to a rapid interfacial influx of protons into the RfA1 layer from the PdH_x electrode and the eventual decay likely due to quasi-steady-state diffusional proton transport (Figure 6.8). From integration of the spike in the I-t curves, we calculated that the total injected charge carrier density was $n_{H+} = 13.9 \pm 1 \times 10^{17}$ protons/cm^3 across 5 devices (see the experimental section for calculation details).[31,32] In analogous fashion, after the application of a negative voltage, we again observed a time-dependent evolution of the current, with the initial spike due to a rapid interfacial efflux of protons from the RfA1 layer into the PdH_x electrode and the eventual plateau likely due to slow quasi-steady-state diffusional proton transport (Figure 6.8). From integration of the spike in the I-t curves, we calculated that the total extracted charge carrier density was $n_{H+} = 8.6 \pm 1 \times 10^{17}$ protons/cm^3 across 4 devices (see the experimental section for Calculation Details).[31,32] Interestingly, the extracted proton concentration was similar, albeit not identical, to the values of $n_{H+} = \sim 1 - 3 \times 10^{17}$ protons/cm^3 previously obtained from the I-V characteristics of RfA1-based protonic transistors (note that the difference between the values likely arose from the distinct device configurations and interrogation strategies).[26-28] Altogether, our analysis further corroborated the notion that proton exchange between the PdH_x electrode and RfA1 active layers directly accounted for the observed shifts in reflectance and coloration.

6.5: Conclusion

In summary, we have rationally designed and characterized highly simplified protonic iridophores, for which the optical properties are modulated via an electrically-induced influx/efflux of protons, and our observations hold significance for several reasons. First, our measurements represent the only demonstration of the direct electrical triggering of reflectance and coloration changes for individual reflectin films. Given that reflectin-based coatings have been

previously actuated through mechanical and chemical means, the reported results highlight the reflectins' potential as adaptive optical materials and represent an initial step towards multi-layer camouflage devices that respond to multiple exogenous stimuli. Second, our measurements lend additional support (albeit indirectly and within an in vitro context) for the mechanism proposed to explain iridophore activation within squid skin, wherein the trans-membrane flux of ions plays a prominent role. Through the use of electrodes that inject/extract other cations, the described strategy could prove valuable for understanding how distinct charged species affect the condensation behavior and optical properties of reflectin platelets. Third, our experiments suggest that reflectin-based devices are well positioned for the sensitive spectroelectrochemical monitoring of ion (proton) fluxes, at both the local and global levels. Due to the intrinsic biocompatibility of reflectin, the described strategy may thus afford new opportunities for the interrogation of ion signaling pathways in device-interfaced living cells or ion-transporting biomolecules. Finally, our simplified devices effectively constitute model organic-inorganic interfaces, which facilitate the direct monitoring of proton injection/extraction. The overall approach may be suitable for the study of interfacial ion transport, as relevant for the operating mechanism of various bioelectronic platforms. Altogether, our observations may hold relevance for designing advanced bioinspired camouflage technologies, understanding the function of ion-transporting biological systems, and engineering improved bioelectronic devices.

6.6: Acknowledgements

E. S., and A. A. G. conceptualized and designed the experiments; D. D. O., E. M. L., and L. P. performed the research; M. N., J. P. L., and M. J. A. helped prepare material for experiments, D. D. O. and A. A. G. analyzed the data; and D. D. O., P. E. S., and A. A. G. wrote the paper.

6.7: References

1. N. J. Abbott, R. Williamson, L. Maddock, in *Cephalopod Neurobiology: Neuroscience Studies in Squid, Octopus, and Cuttlefish*, Oxford University Press, Oxford, **1995**.

2. R. T. Hanlon, J. B. Messenger, in *Cephalopod Behaviour*, Cambridge University Press, United Kingdom, **1998**.

3. G. Kaufman, C. Orlt, *Kings of Camouflage*, Producers. "Cuttlefish: The Brainy Bunch" [Television Broadcast], Public Broadcasting Service (PBS), **2011**.

4. L. M. Mäthger, E. J. Denton, N. J. Marshall, R. T. Hanlon, *J. R. Soc. Interface* **2009**, *6*, 149.

5. E. Kreit, L. M. Mäthger, R. T. Hanlon, P. B. Dennis, R. R. Naik, E. Forsythe, J. Heikenfeld, *J. R. Soc. Interface* **2013**, *10*, 20120601.

6. L. Phan, R. Kautz, E. M. Leung, K. L. Naughton, Y. Van Dyke, A. A. Gorodetsky, *Chem. Mater.* Accepted.

7. R. T. Hanlon, *Malacologia* **1982**, *23*, 89.

8. L. M. Mäthger, R. T, Hanlon, *Cell Tissue Res.* **2007**, *329*, 179.

9. R. A. Cloney, S. L. Brocco, *Am. Zool.* **1983**, *23*, 581–592.

10. J. B. Messenger, *Biol. Rev. Cambridge Philos Soc.* **2001**, *76*, 473.

11. T. J. Wardill, P. T. Gonzalez-Bellido, R. J. Crook, R. T. Hanlon, *Proc. R. Soc. B* **2012**, *279*, 4243.

12. C. Yu, Y. Li, X. Zhang, X. Huang, V. Malyarchuk, S. Wang, Y. Shi, L. Gao, Y. Su, Y. Zhang, H. Xu, R. T. Hanlon, Y. Huang, J. A. Rogers, *Proc. Natl. Acad. Sci. U. S. A.* **2014**, 111, 12998.

13. S. Zheng, D. Zhang, W. Huang, Z. Wang, S. G. Freire, X. Yu, A. T. Smith, E. Y. Huang, H. Nguon, L. Sun, *Nat. Commun.* **2016**, *7*, 11802.

14. Q. Wang, G. R. Gossweiler, S. L. Craig, X. Zhao, *Nat. Commun.* **2014**, *5*, 4899.

15. R. M. Kramer, W. J. Crookes-Goodson, R. R. Naik, *Nat. Mater.* **2007**, *6*, 533.

16. L. Phan, W. G. Walkup IV, D. D. Ordinario, E. Karshalev, J-M. Jocson, A. M. Burke, A. A. Gorodetsky, *Adv. Mater.* **2013**, *25*, 5621.

17. L. Phan, D. D. Ordinario, E. Karshalev, W. G. Walkup IV, M. A. Shenk, A. A. Gorodetsky, *J. Mater. Chem. C* **2015**, *3*, 6493.

18. D. G. DeMartini, D. V. Krogstad, D. E. Morse, *Proc. Natl. Acad. Sci. USA* **2013**, *110*, 2552.

19. D. G. DeMartini, M. Izumi, A. T. Weaver, E. Pandolfi, D. E. Morse, *J. Biol. Chem.* **2015**, *290*, 15238.

20. G. Qin, P. B. Dennis, Y. Zhang, X. Hu, J. E. Bressner, Z. Sun, W. J. Crookes-Goodson, R. R. Naik, F. G. Omenetto, D. L. Kaplan, *J. Polym. Sci., Part B: Polym. Phys.* **2013**, *51*, 254.

21. L. Phan, R. Kautz, J. Arulmoli, I. H. Kim, D. T. T. Le, M. A. Shenk, M. M. Pathak, L. A. Flanagan, F. Tombola, A. A. Gorodetsky, *ACS Appl. Mater. Interfaces* **2016**, *8*, 278.

22. W. J. Crookes, L. L. Ding, Q. L. Huang, J. R. Kimbell, J. Horwitz, M. J. McFall-Ngai, *Science* **2004**, *303*, 235.

23. A. R. Tao, D. G. DeMartini, M. Izumi, A. M. Sweeney, A. L. Holt, D. E. Morse, *Biomaterials* **2010**, *31*, 793.

24. M. Izumi, A. M. Sweeney, D. G. DeMartini, J. C. Weaver, M. L. Powers, A. R. Tao, T. V. Silvas, R. M. Kramer, W. J. Crookes-Goodson, L. M. Mäthger, R. R. Naik, R. T. Hanlon, D. E. Morse, *J. R. Soc. Interface* **2010**, *7*, 549.

25. R. Levenson, C. Bracken, N. Bush, D. E. Morse, *J. Biol. Chem.* **2016**, *291*, 4058.

26. D. D. Ordinario, L. Phan, W. G. Walkup IV, J-M. Jocson, E. Karshalev, N. Hüsken, A. A. Gorodetsky, *Nat. Chem.* **2014**, *6*, 596.

27. D. D. Ordinario, L. Phan, J-M. Jocson, T. Nguyen, A. A. Gorodetsky, *APL Mater*. **2015**, *3*, 014907.

28. D. D. Ordinario, L. Phan, Y. Van Dyke, T. Nguyen, A. G. Smith, M. Nguyen, N. M. Mofid, M. K. Dao, A. A. Gorodetsky, *Chem. Mater.* **2016**, *28*, 3703.

29. D. D. Ordinario, L. Phan, W. G. Walkup IV, Y. Van Dyke, E. M. Leung, M. Nguyen, A. G. Smith, J. Kerr, M. Naeim, I. Kymissis, A. A. Gorodetsky, *RSC Adv*. **2016**, *6*, 57103.

30. K. L. Naughton, L. Phan, E. M. Leung, R. Kautz, Q. Lin, Y. Van Dyke, B. Marmiroli, B. Sartori, A. Arvai, S. Li, M. E. Pique, M. Naeim, J. P. Kerr, M. J. Aquino, V. A. Roberts, E. D. Getzoff, C. Zhu, S. Bernstorff, A. A. Gorodetsky, *Adv. Mater*. **2016,** doi: 10.1002/adma.201601666.

31. E. Josberger, Y. Deng, W. Sun, R. Kautz, M. Rolandi, *Adv. Mater*. **2014**, *26*, 4986.

32. T. Miyake, E. Josberger, S. Keene, Y. Deng, M. Rolandi, *APL Mater.* **2015**, *3*, 014906.

33. A. Lipson, S. G. Lipson, H. Lipson, in *Optical Physics*, 4th ed.; Cambridge University Press: Cambridge, **2010**.

34. G. Mathe, A. Albersdörfer, K. R. Neumaier, E. Sackmann, *Langmuir* **1999**, *15*, 8726.

35. Z. Hemmatian, T. Miyake, Y. Deng, E. Josberger, S. Keene, R. Kautz, C. Zhong, J. Jin, M. Rolandi, *J. Mater. Chem. C* **2015**, *3*, 6407.

36. C. Zhong, Y. Deng, A. F. Roudsari, A. Kapetanovic, M. P. Anantram, M. Rolandi, *Nat. Commun*. **2011**, *2*, 476.

37. Y. Deng, E. Josberger, J. Jin, A. F. Rousdari, B. A. Helms, C. Zhong, M. P. Anantram, M. Rolandi, *Sci. Rep*. **2013**, *3*, 2481.

38. Y. Deng, B. Helms, M. Rolandi, *J. Polym. Sci., Part A: Polym. Chem.* **2015**, *53*, 211.

CHAPTER 7   Summary and Conclusions

In conclusion, we have demonstrated the fabrication, characterization, and application of various protonic devices based on the cephalopod protein reflectin. Our findings are significant for a number of reasons. First, we discovered and characterized novel electrical properties for the reflectin protein. To do this, we developed techniques and methods for characterizing the electrical properties of the reflectin protein. Our findings indicated that reflectin was a highly-efficient proton-conducting material. Second, we demonstrated the first example of a protein-based protonic transistor and developed strategies for optimizing their performance. Our protonic transistors possess figures of merit and performance which compare favorably to the best values reported for similar devices. Third, we developed methods for the production of reflectins in quantities significant for materials applications. Our straightforward protocol, which allowed for the characterization of the RfA2 isoform and the subsequent demonstration of RfA2-based protonic devices, and should also be broadly applicable for the production of arbitrary reflectin variants and, potentially, other unrelated proteins. Fourth, we designed and implemented a strategy for the modulation of the electrical properties of protonic devices with an exogeneous photochemical stimulus. Our method, which features a mild applied stimulus and a straightforward doping methodology, possesses few limitations and should be broadly applicable for a wide range of materials and technologies that leverage proton transport. Finally, we designed highly-simplified protonic iridophores, for which the optical properties are modulated via an electrically-induced influx/efflux of protons. These devices effectively constitute model organic-inorganic interfaces, and our overall approach may be suitable for the study of interfacial ion transport and relevant for the operating mechanism of various bioelectronic platforms. Altogether, the work described in this dissertation highlights the effectiveness of reflectin films as a proton-conducting material, the

potential of reflectin-based, voltage-regulated protonic devices as platforms for the fundamental study of proton transport and ion-transporting biological systems, the promise of future bioelectronics applications for reflectin-based devices, and the potential for advanced bioinspired camouflage technologies.